



Peter Augustin, Dipl.-Ing. Bsc.

Novel Biochemical Aspects of Flavoprotein-Mediated Electron Transport in Human Mitochondria

DISSERTATION

zur Erlangung des akademischen Grades

Doktor der technischen Wissenschaften

eingereicht an der

Technischen Universität Graz

Betreuer

Univ.-Prof. Dr. rer. nat. Peter Macheroux

Institut für Biochemie

EIDESSTATTLICHE ERKLÄRUNG

Ich erkläre an Eides statt, dass ich die vorliegende Arbeit selbstständig verfasst, andere als die angegebenen Quellen/Hilfsmittel nicht benutzt, und die den benutzten Quellen wörtlich und inhaltlich entnommenen Stellen als solche kenntlich gemacht habe. Das in TUGRAZonline hochgeladene Textdokument ist mit der vorliegenden Dissertation identisch.

26. 1. 2017

Datum

Peter Augustin

Unterschrift

ACKNOWLEDGMENT

I would like to thank all persons involved in the work related to this Thesis. Thank you Peter for your supervision and for having me for four years as your university assistant without complaints. Thank you my dear colleagues and friends at the universities for your support and help in happy and hard times during this thesis and thank you Robert, Michael, Altijana, Tea and Karl for your collaborating help across the university boundaries of Graz. Dear Eva, Julia and Florian, you have been wonderful students to supervise and every single one of you will have a great time if you decide to pursue biochemistry in future. I am looking forward to drinking one or two beers with all of you guys after my exam.

My great gratitude goes also to my family, Mama, Papa and Chrisi, for your emotional and financial support when needed. I would like to thank Anita, Birgit, Martina, Corinna, Meli and Roman as well as all my other friends for being and staying with me through all those years and for your advice and your support in so many different things. I cannot put in words how amazing you are. Soon, I will have a lot more time for you again, if you like it or not.

Liebe Mamama, lieber Opapa, danke für eure Unterstützung in all meinen Jahren als Student und ich freue mich schon sehr, wenn wir meinen Abschluss gebührend gemeinsam feiern können!

Dear Flo, the greatest thing I ever learned is just to love and be loved in return. Thank you for being part of my life.

TABLE OF CONTENTS

Acknowledgment.....	3
Abstract	6
Kurzfassung.....	7
Preface and Thesis Structure	8
CHAPTER I – Flavoproteins and their Role in Mitochondrial Electron Transport	9
Cofactor Binding, Oxidation States and Reactivity of Flavins with Molecular Oxygen	10
Naturally Occurring Riboflavin Analogs	13
Flavoproteins Associated with the Human Mitochondrial Electron Transport.....	14
Flavoproteins Involved in Metabolic Errors of the Human Mitochondria.....	17
References	19
CHAPTER II - Structure and Biochemical Properties of Recombinant Human Dimethylglycine Dehydrogenase and Comparison to the Disease-Related H109R Variant	23
Abstract	24
Introduction	25
Results	27
Discussion	36
Experimental Procedures.....	44
Acknowledgments	49
Author Contributions.....	49
References	50
CHAPTER III - The Human electron transferring flavoprotein catalyzes the oxidation of its FAD cofactor to the 8-formyl derivative	54
Abstract	55
Introduction	56
Results	58
Discussion	68
Conclusion.....	75
Experimental Procedures.....	76
Author Contributions.....	80
Acknowledgments	80
Additional Observations.....	81
Missing Experiments.....	85
References	91

CHAPTER IV - Insights into the Protein-Protein Interaction of Human Dimethylglycine Dehydrogenase and Human Electron Transferring Flavoprotein.....	95
Abstract	96
Introduction	97
Results	99
Discussion	103
Conclusion.....	108
Experimental Procedures.....	109
Author Contributions.....	112
Acknowledgment.....	112
References	113
CHAPTER V - Characterization of the function of dimethylglycine dehydrogenase in the sarcosine-metabolism of human prostate cancer cells	115
Preface	116
Introduction	117
Results and Discussion.....	121
References	124
Curriculum vitae	126

ABSTRACT

The characterization of the two human flavoproteins dimethylglycine dehydrogenase (hDMGDH) and electron transferring flavoprotein (hETF) symbolizes exemplary the versatility of flavoproteins and their important roles in mitochondrial electron transport. hDMGDH is able to perform one- and two-electron transfer reactions and combines the three metabolic pathways folate one-carbon metabolism, choline catabolism and electron transfer in the mitochondrial matrix. We performed a detailed characterization of hDMGDH, identified the biochemical background that triggers the metabolic disorder dimethylglycine dehydrogenase deficiency and for the first time solved the crystal structure of the human enzyme. hETF on the other hand stabilizes a semiquinone flavin redox state and lies at a key metabolic branch point of the mitochondrial respiratory chain. Our work with the already well characterized protein brought new insights in the protein mechanism and above all the surprise finding that the enzyme catalyzes the formation of 8-formyl FAD. This unusual FAD analog changes key functions of the enzyme, however, a detailed characterization of the potential physiological relevance must await further studies. Furthermore, we investigated the interaction mechanism of hETF with hDMGDH which is so far only the second interaction study of hETF with one of its thirteen partner proteins. Last, we evaluated the physiological role of hDMGDH in the sarcosine metabolism of human cells, especially in connection with prostate cancer.

KURZFASSUNG

Die Charakterisierung der Dimethylglycinderhydrogenase (hDMGDH) und des elektronentransferierenden Flavoproteins (hETF) zeigt vorbildhaft die außerordentliche biochemische Vielfalt von humanen Flavoproteinen und ihre Rolle im mitochondrialen Elektronentransport. hDMGDH kann sowohl einen Ein- als auch den Zweielektronentransport katalysieren und verbindet Folsäuremetabolismus, Cholinabbau und Elektronentransport in der mitochondrialen Matrix miteinander. Unsere umfangreiche Charakterisierung von hDMGDH identifizierte die biochemischen und strukturellen Auslöser von der seltenen, metabolischen Störung DMGDH-Defizienz. Zum ersten Mal ist es uns auch gelungen, die Kristallstruktur des humanen Enzyms zu lösen. Auf der anderen Seite zeigen wir mit hETF ein Protein, das eine gewichtige Rolle in der Atmungskette spielt, ein Flavosemiquinon stabilisiert und ausschließlich Einelektronentransportreaktionen katalysiert. Obwohl das Protein bereits umfangreich charakterisiert wurde haben wir neue Aspekte des Reaktionsmechanismus entdeckt, insbesondere die Bildung von 8-Formyl FAD, was noch nicht beschrieben wurde. Dieses ungewöhnliche FAD Analogon veränderte einige Schlüsselfunktionen des Proteins *in vitro*, jedoch ist eine mögliche Bedeutung *in vivo* noch nicht erforscht. Weiters untersuchten wir mit der Protein-Protein-Interaktion von hDMGDH und hETF, erst die zweite Interaktion eines der dreizehn Partnerproteine von hETF. Zum Abschluss zeigen wir noch die Zusammenfassung unserer Untersuchungen über die Bedeutung von hDMGDH im Sarkonsinmetabolismus in humanen Zellen, insbesondere in Zusammenhang mit Prostatakrebs.

PREFACE AND THESIS STRUCTURE

This Thesis is organized in five chapters, which are by themselves self-sufficient with separated abbreviations section and References.

Chapter I gives a general background on flavoproteins and their characteristics. Special emphasis was put on natural occurring flavoprotein analogs and the role of flavoproteins in the mitochondrial respiratory chain. All features are discussed in connection with the two flavoproteins this work is about, the human dimethylglycine dehydrogenase (hDMGDH) and the human electron transferring flavoprotein (hETF). Both enzymes can cause mitochondrial disorders, which are discussed in the last part of this introduction.

In Chapter II, the detailed biochemical characterization of hDMGDH and its pathogenic variant H109R, as well as the crystal structure of the wild-type enzyme, are shown. This part was published as “Structure and Biochemical Properties of Recombinant Human Dimethylglycine Dehydrogenase and Comparison to the Disease-related H109R Variant” in 2016, in FEBS journal, volume 283(19), pages 3587-3603.

The formation of 8-formyl FAD and the effects of this unusual flavin analog on hETF are in the focus of Chapter III. This chapter provides a paper draft that is planned to be published in 2017 under the title “The Human Electron Transferring Flavoprotein Catalyzes the Oxidation of its FAD Cofactor to the 8-Formyl Derivative”. Following the paper draft, additional experiments and observations in connection with the project, as well as the description of important missing experiments are included to help to finalize the publication.

Chapter IV deals with the protein-protein interaction of hETF and hDMGDH. This chapter also is organized as a paper draft, nevertheless, in contrast to Chapter III, the quantity and quality of the presented data are not sufficient yet to be published. A future publication of these data is not planned at the moment.

Finally, Chapter V summarizes the results obtained by Michael Haider during his Master’s Thesis, supervised by Univ.-Ass. Mag. Dr.scient.med Robert Fuchs and me in a collaboration with the Medical University of Graz. The aim was to evaluate a possible role of hDMGDH in prostate cancer progression and sarcosine metabolism.

CHAPTER I - INTRODUCTION

FLAVOPROTEINS AND THEIR ROLE IN MITOCHONDRIAL ELECTRON TRANSPORT

Abbreviations

8fFAD, 8-formyl FAD; CoQ, coenzyme Q or ubiquinone; FMN, flavin mononucleotide; FAD, flavin adenine dinucleotide; hDMGDH, human dimethylglycine dehydrogenase; hETF, human electron transferring flavoprotein; hETF-QO, human electron transferring flavoprotein ubiquinone oxidoreductase; MRC, mitochondrial respiratory chain; OMIM, Online Mendelian Inheritance in Man (www.omim.org).

Flavoproteins have the potential to brighten up a mediocre laboratory day just by presenting their most obvious feature: a bright, shiny, happy, yellow color. Since the discovery of the flavin structure in the 1930s [1,2], the yellow color of the flavin cofactor has been a welcoming distraction on a dark and strenuous laboratory day, but also has facilitated daily enzymatic and biophysical lab work in many different ways. Not only protein purification can be followed more easily, but also the determination of protein purity, protein concentrations, steady-state and pre-steady state kinetics, the investigation of light sensitive reactions, protein crystallography and many more techniques are a lot easier to perform thanks to the visible light absorption. The story of this thesis features two flavoproteins, the human dimethylglycine dehydrogenase (hDMGDH, EC 1.5.8.4.) and the human electron transferring flavoprotein (hETF) as the main characters. In the following chapters both proteins will be introduced and characterized with all their abilities, flaws, peculiarities, weaknesses and unexpected features.

While many bacteria, yeasts and plants are able to synthesize riboflavin (vitamin B₂), the precursor of the active flavin cofactors [3], it has to be ingested by animals and humans through the nutrition and incorporated into the cells. Afterwards, riboflavin is enzymatically converted in all kingdoms of life to the biological active coenzymes flavin mononucleotide (FMN) and flavin adenine dinucleotide (FAD), [4]. First, the ribityl side chain of riboflavin, which is attached to N10 of the isoalloxazine ring of riboflavin is phosphorylated by riboflavin kinase (EC 2.7.1.26) to FMN and if necessary further converted to FAD by FAD synthetase, also called FAD-adenylyl transferase (EC 2.7.7.2.), (Figure 1).

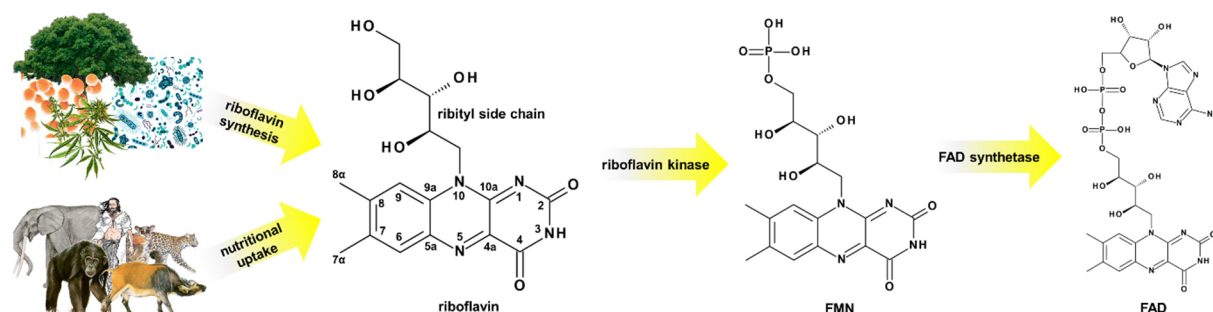


Figure 1 – Biosynthesis of the redox active flavin cofactors. Many plants, bacteria and yeasts can synthesize riboflavin while animals and humans have to take up riboflavin through their nutrition. Riboflavin is converted to FMN by the riboflavin kinase (EC 2.7.1.26) and further to FAD by the FAD synthetase (EC 2.7.7.2.). The riboflavin structure in this figure shows the atom-numbering within the isoalloxazine ring.

Cofactor Binding, Oxidation States and Reactivity of Flavins with Molecular Oxygen

The tricyclic, heteroaromatic isoalloxazine ring of FAD and FMN is the place where flavin catalyzed enzymatic magic happens. It is not only responsible for the yellow color, but also confers the unique features to accept and donate one or two electrons in redox reactions and to activate molecular dioxygen [5]. hDMGDH exemplary shows this versatility by coupling the two-electron reduction of bound FAD during the oxidative demethylation of dimethylglycine with the subsequent one-electron transfer to the

electron transferring flavoprotein [6]. hETF on the other hand only accepts one electron at a time from one of its flavin-dehydrogenase partners or donates one electron to the electron transferring flavoprotein ubiquinone dehydrogenase (hETF-QO), respectively. Apart from dehydrogenase and electron transferring activity, flavoenzymes are furthermore involved in enzyme catalyzed oxidations, monooxygenations, halogenations, reductions and also react with light to induce photomodifications [7]. Due to the redox-active cofactor, the majority of flavoenzymes are oxidoreductases (91%), [8].

In general, 25% of all flavoproteins use FMN as cofactor making FAD by far the more abundant species [8]. The detailed analysis of the human flavoproteome showed an even greater bias towards FAD, which is bound to a total of 84% of the known human flavoproteins [9]. Furthermore, a non-covalent attachment of FAD or FMN is more common and only approximately 11% of the flavoproteins bind the cofactor covalently. Here again, covalent binding is much more common with FAD than FMN [8]. For instance, in the human flavoproteome, 5 out of 77 proteins have a covalent attached FAD, but none a covalent bound FMN [9]. Binding of the cofactor can be achieved by various mechanisms linking the isoalloxazine ring to the active site of the protein via its 8 α or C6 position (see numbering of riboflavin in Figure 1). The most common binding is to the N1 or N3 of a histidine but also cysteine thiols, tyrosine hydroxyls or the attachment with an aspartate carboxyl group have been described [10]. In non-covalent cofactor binding, the N10 attached ribityl side chain is mainly responsible for protein interaction to ensure a tight connection [5]. In the human flavoproteome, only covalent bound 8 α attachment of FAD was observed and hDMGDH is one of three human flavoproteins that binds FAD via an 8 α -(N3)-histidine bond [9]. On the other side, hETF utilizes a non-covalently bound FAD cofactor. Additionally, also bi-covalent attachment, first described in 2005, was seen in several bacterial, fungal and plant flavoenzymes but is absent in the human flavoproteome [11,12]. The binding mode of the flavin cofactor to the active site of the protein and especially a covalent attachment are important to adapt the necessary redox potential, which was shown to be mainly influenced by amino acids near the binding site [10]. For example, we show in Chapter II that the covalent attachment of hDMGDH significantly increased the redox potential of the enzyme as was already shown for other enzymes [6,13]. Furthermore, mutational studies of hETF showed that the variations of amino acids adjacent to the N5 of FAD have a great influence on the redox potential of proteins (Chapter III and IV), [14,15].

The ability of the flavin isoalloxazine ring to take part in one- and two-electron transfer reactions implicates that several different redox states have to be involved during reduction and oxidation (Figure 2). The yellow, oxidized flavin is reduced by one electron to a radical semiquinone state, which can be stabilized, depending on the pH and the geometry of the cofactor binding pocket, as the anionic (red) or the neutral (blue) form. Also mixtures of both forms have been observed (Chapter III), [16,17]. The reduction significantly alters the flavin absorption spectrum and the semiquinones can easily be distinguished by their different absorption spectra [18]. The blue semiquinone features unique peaks around 500-600 nm (not shown), whereas a maximum around 350-400 nm emerges upon reduction to

the anionic, red form (Figure 2, spectrum B). The further reduction by another electron leads to the fully reduced, colorless hydroquinone state (Figure 2, spectrum C). Covalent or tight non-covalent binding of the flavin cofactor to the protein, substituted flavin species (see below), or bending of the cofactor in the binding pocket all influence the flavin spectrum, which helps to characterize the protein (Figure 2, spectrum A). hDMGDH gets easily reduced to its hydroquinone form during its reaction and the semiquinone state is not stabilized [6]. In comparison to free FAD, the flavin absorption spectrum of hDMGDH features additional peaks and shifts of the maxima due to its covalent attachment (Figure 2, spectrum A). On the other hand, hETF is only reduced to the red semiquinone upon electron transfer *in vivo* and is readily re-oxidized by hETF-QO back to its oxidized form (Chapter III and IV), [19]. A full reduction only can be achieved *in vitro* with high concentrations of dithionite and is thought to be unimportant *in vivo* (Chapter III).

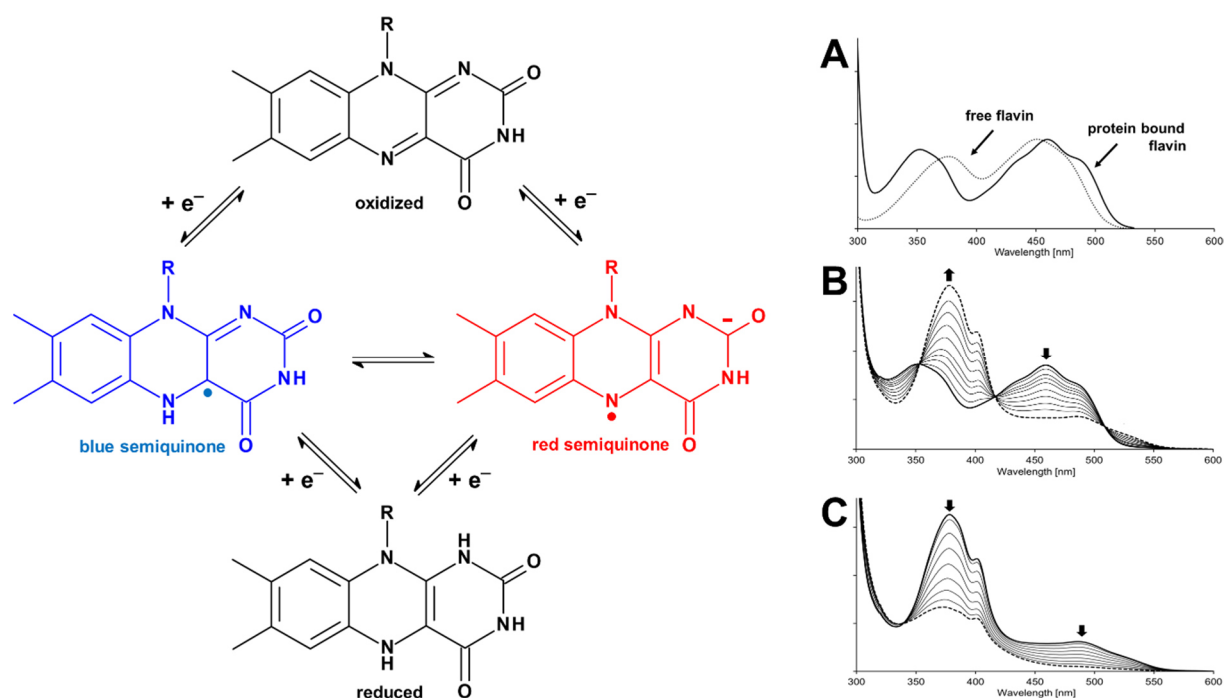


Figure 2 – Oxidation states of isoalloxazine. The isoalloxazine ring can exist in four different oxidation states, fully oxidized, as two radical semiquinones and fully reduced. The absorption spectrum of a protein significantly changes upon reduction from the oxidized state (spectrum A) to the red semiquinone (spectrum B) and finally to the fully reduced form (spectrum C). The spectrum of a blue semiquinone is not shown but can be found for instance in [18]. All spectra are derived from the photoreduction of hDMGDH which is described in detail in Chapter II. In spectrum A, the dashed line corresponds to free FAD in contrast to the $\delta\alpha$ -(N3)-His bound FAD in hDMGDH, showing that covalent binding significantly alters the flavin absorption spectrum of FAD. For spectra B and C, the dashed line represents the final and the bold line the starting spectrum of the reduction experiment.

The stabilization of the semiquinone state and the reactivity of reduced states with oxygen is crucial for the reaction mechanism of the enzyme [20]. Flavoproteins remarkably differ in their oxygen reactivity and depending on the velocity of re-oxidation of the reduced flavin are roughly divided into three groups:

dehydrogenases react slowly with molecular oxygen, electron transferases usually form stable semiquinone radicals and oxidases are rapidly re-oxidized by oxygen to the oxidized state [21]. Furthermore, it has to be noted that the reaction of reduced flavins with oxygen very often form reactive oxygen species which are a major source of oxidative stress and also can form lipid hydroperoxides that can damage our tissue [5]. hDMGDH is a dehydrogenase and only slowly reacts with molecular oxygen, which is by far slower than re-oxidation by its natural partner protein hETF (Chapter II and IV), [6]. The electron transferase hETF stabilizes the anionic semiquinone that enables further electron transfer to mitochondrial membrane bound hETF-QO. Here again, the semiquinone is sufficiently stable against oxygen and the re-oxidation by oxygen is too slow to play a physiological importance (Chapter III).

Naturally Occurring Riboflavin Analogs

Modifications of FMN or FAD in flavoproteins mainly occur through mono- or bi-covalent attachment (see above), [10]. Although the exact mechanisms are, very often, still poorly understood, in most cases the 8 α methylgroup of the isoalloxazine gets activated in the flavin binding site and subsequently auto-catalytically binds to the enzyme [10,13]. Apart from covalent bound flavins only very few additional, natural occurring, active riboflavin derivatives have been described [22,23]. They mainly occur in micro-organisms and therefore are good targets for anti-infective drugs. For example, the riboflavin derivative F₄₂₀, which is absent in animals, plays a central role in archaeal methanogenesis or is used by *Streptomyces* species in antibiotics biosynthesis [24,25]. *Mycobacterium tuberculosis* uses F₄₂₀ in its vital glucose-6-phosphate dehydrogenase and could therefore be a reasonable target-compound for anti-tuberculosis drugs [26]. *Streptomyces davawensis* synthesizes an 8 α -dimethylated-aminoriboflavin derivative called roseoflavin (3,8-dimethylaminoriboflavin), which is the only known flavin with an antibiotic activity against gram-positive bacteria [27–29]. During the bioluminescent reaction catalyzed by luciferase in bioluminescent bacteria, myristylated FMN (myr FMN) is built, which is thought to have an auto-regulatory effect on the bioluminescent reaction [30]. Also chemically synthesized riboflavin analogs can be used as regulators and are investigated as drugs to directly target and inhibit vital flavoenzymes in pathogens [31]. All structures of the mentioned flavin derivatives can be found in Figure 3.

However, there are also a handful of flavin derivatives that actively take part in enzymatic redox reactions. Enzymes employing molybdopterin, for instance, catalyze the transfer of oxygen to or from substrates in connection with a molybdenum ion and are found in bacteria, plants and animals [32]. During the isolation of the electron transferring flavoprotein and the NADH dehydrogenase from *Peptostreptococcus elsdenii* the riboflavin derivatives 6-hydroxy-7,8-dimethyl-isoalloxazine and 8-hydroxy-7-methyl-isoalloxazine, respectively, were identified in the purified protein preparations [33]. The latter compound was also found during purification of the pig liver glycolate oxidase. Yet, it is still unsure, if these cofactors truly take part in enzyme catalysis *in vivo* or were generated during the isolation procedure [34]. At least for pig liver glycolate oxidase a catalytical importance is doubtful

because the very similar analog human enzyme, the (*S*)-2-hydroxy-acid oxidase (HOX1) employs a non-covalently bound FMN as cofactor [35,36]. Without any doubt, Marshall *et al.* identified a non-covalently bound 6-hydroxy-FAD in the human apoptosis inducing protein AMID, which is converted from FAD during the aerobic turnover with NADPH [37]. Structurally very similar to 7-methyl-8-hydroxy-isoalloxazine, we identified the redox active 8-formyl-7-methyl FAD (8fFAD) in hETF-WT and some of its variants (Chapter III). This unusual flavin derivative was slowly built at elevated pH values (> 7.5) and changed the chemical properties of the protein. For instance, steady-state kinetics revealed an increased hETF-hDMGDH protein-protein affinity. Also, 8fFAD was stabilized in the oxidized form of the enzyme as a mixture of red and blue 8-formyl-semiquinone radical which was completely unreactive with molecular oxygen. Recently, 8 α -formylated cofactors also were identified in formate oxidase from *Aspergillus oryzae* and in old enzyme preparations of a lactate oxidase variant from *Aerococcus viridans* [17,38].

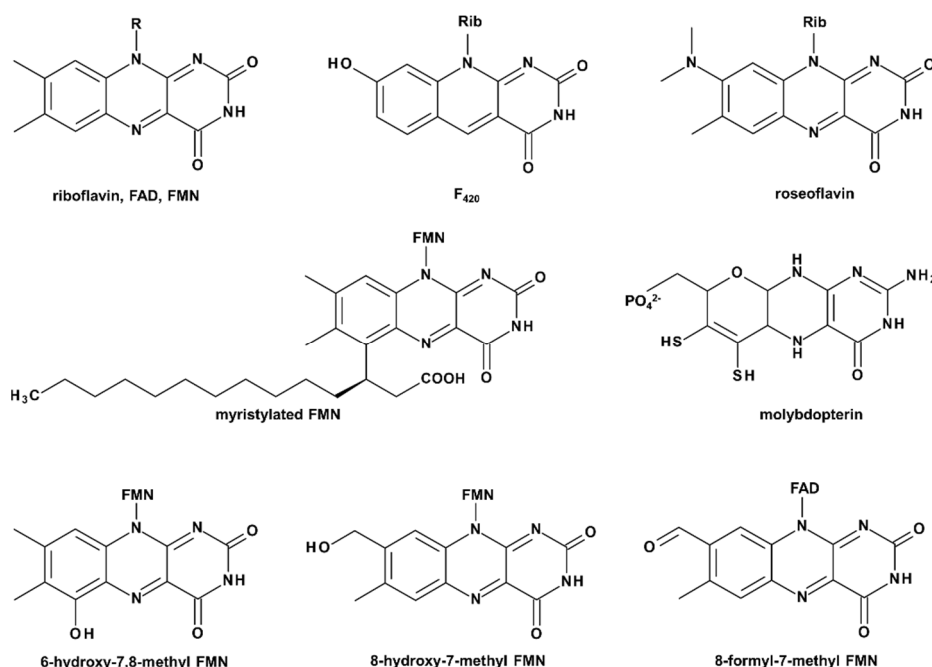


Figure 3 – Natural occurring riboflavin derivatives. The natural occurring riboflavin analogs mainly differ in their isoalloxazine ring composition. The side chains are indicated by Rib, for the riboflavin, FMN and FAD for the cofactor specific side chains.

Flavoproteins Associated with the Human Mitochondrial Electron Transport

The mitochondrial respiratory chain oxidative phosphorylation provides mammalian cells under normal conditions with at least 80% of the energy a cell needs to survive [39]. Mitochondrial respiration is accomplished by an amazing variety of enzymes, proteins and protein complexes in the mitochondrial matrix, the inner mitochondrial membrane and the intermembrane space. They accomplish the complete oxidation of nutrition derived substrates to H₂O, CO₂ and NH₃, regulate the electron transport and build up the proton gradient across the mitochondrial membrane, which drives ATP production [39].

Electron transfer through proteins mainly depends on the reaction thermodynamics of the protein, which is defined by the redox potentials of the donor and acceptor cofactors [40]. It is a sequence of reactions between pairs of cofactors and charge transfer can be described as quantum mechanical tunneling [41]. The redox-active sites of proteins where electron transfer (i.e. oxidation/reduction of cofactors) occurs can contain metal groups like heme, iron-sulfur clusters or copper-centers, but can also be flavins, disulfides or quinones [42]. Many electron transfer proteins are organized as protein complexes and contain multiple electron transfer cofactors, such as protein complex I, II or III of the mitochondrial respiratory chain (MRC), [39,43,44].

Flavoproteins play a vital, essential role in various processes of the MRC - oxidative phosphorylation. Already in reactions occurring before the actual respiratory chain, a large set of at least thirteen dehydrogenases with FAD as cofactor, including hDMGDH (see Chapter III and IV), involved in β -oxidation, amino acid metabolism and choline degradation catalyze a two-electron dehydrogenation of numerous organic compounds and transfer the substrate derived electrons to the FAD cofactor of hETF) (Figure 4). hETF further transfers these electrons to the $[4\text{Fe-4S}]^{2+, 1+}$ iron-sulfur cluster of the mitochondrial membrane bound, FAD dependent, electron transferring flavoprotein ubiquinone oxidoreductase (hETF-QO), which directly reduces ubiquinone (CoQ) to ubiquinol in the mitochondrial membrane [45,46]. This short pathway represents one alternative entry point for electrons into MRC, apart from the membrane bound protein complexes I and II [43,44].

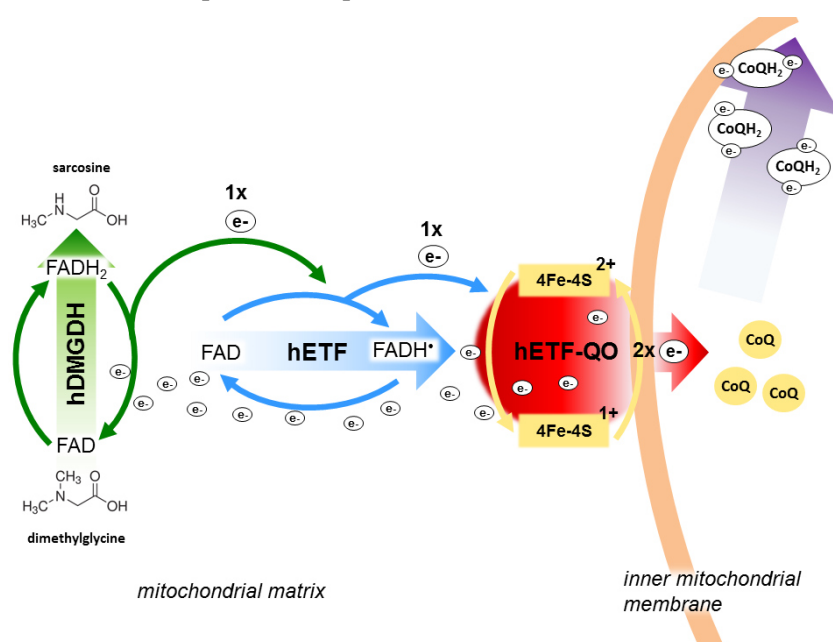


Figure 4 – Electron transfer pathway from hDMGDH to Coenzyme Q (CoQ). Exemplary for all hETF interacting enzymes, the electron transfer from hDMGDH is sketched. hDMGDH derives two electrons from dimethylglycine demethylation and donates one electron to hETF which further donates one electron to the iron-sulfur cluster of hETF-QO. hETF-QO is bound to the inner mitochondrial membrane and reduces CoQ. CoQH₂ is then transported in the mitochondrial membrane to complex III.

A further alternative way to feed electrons into the MRC of mammalian tissue is through mitochondrial glycerol 3-phosphate dehydrogenase (GPD2, EC 1.1.5.3.). GPD2 catalyzes the oxidation of glycerol-3-phosphate to dihydroxyacetone phosphate, which simultaneously transfers two electrons from FADH₂ to CoQ in the inner mitochondrial membrane [47].

Nevertheless, the main routes for electrons to enter the mitochondrial respiratory chain is via protein complex I and II, which also includes flavoenzymes at key positions. In the first reaction step of complex I, the NADH-CoenzymeQ oxidoreductase, the binding and oxidation of NADH, is achieved by the FMN dependent reaction of the NDUFV1 subunit (EC 1.6.5.3.) [43]. Generated FMNH₂ further passes the electrons to iron-sulfur clusters, which finally leads to the reduction of CoQ. This process also translocates four protons per molecule NADH across the inner membrane to build up the electrochemical potential difference that drives ATP generation. The human complex I consists of 14 central and 30 accessory subunits and also requires several chaperones for correct assembly [43]. Upon them, also two FAD-dependent enzymes, acyl-CoA dehydrogenase family member 9 (ACAD9) and the FAD-dependent oxidoreductase (FOXRED1), play an important role in complex I biogenesis [48,49]. On the one hand, ACAD9 has unambiguously been shown to be necessary for complex I formation, on the other hand it is also able to take over the activity of very long chain acyl-CoA dehydrogenase (VLCAD) *in vivo* in VLCAD deficient fibroblasts and interacts with hETF as part of β -oxidation [50,51]. Interestingly, Nouws *et al.* demonstrated that the function in complex I assembly does not depend on acyl-CoA dehydrogenase activity [50]. A mutation of FOXRED1 was associated with complex I deficiency (OMIM: 252010), the most commonly reported mitochondrial disorder presented in childhood, which causes reduced complex I steady-state levels and activity [48]. This confirms the importance of the enzyme for complex I assembly.

Important for the functionality of protein complex II, the flavoprotein subunit of the succinate dehydrogenase (EC 1.3.5.1.) not only catalyzes the conversion of succinate to fumarate in the citric acid cycle, but also initiates the electron transfer through the tetrameric, membrane bound complex II [44]. During succinate conversion, the covalent bound FAD is reduced to FADH₂ and the electrons are then further transferred through three iron-sulfur clusters to cytochrome *b*₅₆₀, which eventually reduces CoQ.

The FMN-dependent dihydroorotate dehydrogenase (DHODH, EC 1.3.3.1.), located on the inner membrane of mitochondria catalyzes the oxidation of dihydroorotate to orotate and transfers the substrate derived electrons to the respiratory molecule ubiquinone [52]. It has been shown that DHODH is functionally dependent on an intact protein complex III and thereby establishes a functional link between the *de novo* pyrimidine synthesis pathway with the MRC. Complex III of the MRC passes the electrons from ubiquinol, generated amongst others in complex I and II and by hETF-QO, GPD2 and DHODH to cytochrome *c*, which transfers the electrons to complex IV, the cytochrome *c* oxidase for use in the reduction of dioxygen [39]. Protein complex III and IV also channel the translocation of

further two or four protons through the mitochondrial membrane increasing the electrostatic potential difference of the membrane for ATP production in complex V.

All preceding paragraphs of this chapter showed that flavoproteins engage key roles in the mitochondrial respiratory chain. Right in the middle are again the main characters of this story, hDMGDH and hETF. The covalently bound FAD in hDMGDH acquires two electrons by the oxidative demethylation of dimethylglycine and transfers them to hETF [6] as do twelve other flavin-dehydrogenases. Therefore, both enzymes play a small but interesting and important role in the huge respiratory system of our cells which can already be severely disturbed by single mutations as seen in the next chapter.

Flavoproteins Involved in Metabolic Errors of the Human Mitochondria

Without exception, naturally occurring mutations of all flavoproteins discussed in the previous chapter exist and are also related to metabolic errors of the mitochondria resulting in a variety of awful diseases [9]. For example, mutations of succinate dehydrogenase are connected to complex II deficiency (OMIM: 252011) and Leigh-syndrome (OMIM: 256000), [53], or, mutations in the gene of the dihydroorotate dehydrogenase lead to the Miller syndrome (OMIM: 263750), [54]. These mitochondrial disorders lead to epileptic attacks or severe facial deformations, respectively and affected patients usually do not survive their first years of living. In general, diseases caused by non-functional flavoproteins are very often caused by mutations that affect the binding affinity of the flavin cofactor and subsequently influence protein activity and stability [9].

The two diseases related to the dimethylglycine dehydrogenase and the electron transferring flavoprotein are DMGDH-deficiency (OMIM: 605850) and glutaric aciduria type II (GAI), also called multiple acyl-CoA dehydrogenase deficiency (MADD, OMIM: 231680), respectively. DMGDH-deficiency is caused by a point mutation in the hDMGDH gene leading to a histidine to arginine variation of the enzyme near its active site and for the most part is a relatively harmless metabolic disorder (Chapter II) [55]. Affected persons have significantly elevated levels of dimethylglycine in serum and urine which causes muscle fatigue and an abnormal fish like body odor. The responsible gene mutation occurs in approximately one out of 2000 investigated alleles and notably affects predominantly individuals from African descent (Exome Aggregation Consortium online browser; <http://exac.broadinstitute.org/variant/5-78351682-T-C>). On the other hand, a deficient or disturbed electron transport by mutations in the genes of hETF or hETF-QO causes the severe metabolic disorder glutaric aciduria type II (GAI), [56]. Three clinical phenotypes for GAI have been described: type I and II are the severe forms with and without congenital abnormalities with a neonatal onset and the patients usually do not survive more than a few months after birth. Patients suffer from hypotonia, hepatomegaly, hypoketotic hypoglycaemia and metabolic acidosis and eventually die of severe cardiomyopathies [57,58]. Clinical type III shows a later onset with a great heterogeneity of symptoms like lethargy, vomiting, hypoglycemia and severe muscle weakness. It also comes along a large excretion of glutaric, butyric or isovaleric acid, following an impaired protein

breakdown of the diet because of the inability of the involved proteins isovaleryl-CoA-dehydrogenase (IVD, EC 1.3.99.10), isobutyryl-CoA dehydrogenase and glutaryl-CoA dehydrogenase (EC 1.3.99.7.) to interact with hETF or hETF-QO [59]. For instance, a deficient IVD, involved in the breakdown of the amino acid leucine, causes that isovaleric acid is accumulated in the body up to toxic levels [60,61]. This deficiency is caused by mutations of IVD or by an impaired electron transfer to hETF and subsequently to hETF-QO and the MRC. The severity of GAI is depending on the immediate effect of the gene mutation on the activity or stability of the protein. Several different mutations of hETF subunit α , subunit β or hETF-QO have been reported [57,62–65]. In Chapter IV, we investigated two mutations of hETF causing GAI, R249C and T266M of the α -subunit, responsible for clinical types I and II of GAI, respectively and R191C of subunit β , which causes GAI clinical type III [57].

REFERENCES

- 1 Kuhn R, Reinemund K & Weygand F (1934) Synthese des Lumi-lactoflavins. *Berichte der Dtsch. Chem. Gesellschaft (A B Ser.)* **67**, 1460–1462.
- 2 Karrer P, Schöpp K & Benz F (1935) Synthesen von Flavinen IV. *Helv. Chim. Acta* **18**, 426–429.
- 3 Fischer M & Bacher A (2008) Biosynthesis of vitamin B2: Structure and mechanism of riboflavin synthase. *Arch. Biochem. Biophys.* **474**, 252–265.
- 4 McCormick DB, Oka M, Bowers-Komro DM, Yamada Y & Hartman HA (1997) Purification and properties of FAD synthetase from liver. *Methods Enzymol.* **280**, 407–13.
- 5 Massey V (2000) The chemical and biological versatility of riboflavin. *Biochem. Soc. Trans.* **28**, 283–96.
- 6 Augustin P, Hromic A, Pavkov-Keller T, Gruber K & Macheroux P (2016) Structure and biochemical properties of recombinant human dimethylglycine dehydrogenase and comparison to the disease-related H109R variant. *FEBS J.* **283**, 3587–3603.
- 7 Fagan RL & Palfey BA (2010) Flavin-Dependent Enzymes. *Compr. Nat. Prod. II*, 37–113.
- 8 Macheroux P, Kappes B & Ealick SE (2011) Flavogenomics - a genomic and structural view of flavin-dependent proteins. *FEBS J.* **278**, 2625–2634.
- 9 Lienhart WD, Gudipati V & Macheroux P (2013) The human flavoproteome. *Arch. Biochem. Biophys.* **535**, 150–162.
- 10 Mewies M, McIntire WS & Scrutton NS (1998) Covalent attachment of flavin adenine dinucleotide (FAD) and flavin mononucleotide (FMN) to enzymes: The current state of affairs. *Protein Sci.* **7**, 7–21.
- 11 Leferink NGH, Heuts DPHM, Fraaije MW & van Berkel WJH (2008) The growing VAO flavoprotein family. *Arch. Biochem. Biophys.* **474**, 292–301.
- 12 Huang C-H, Lai W-L, Lee M-H, Chen C-J, Vasella A, Tsai Y-C & Liaw S-H (2005) Crystal Structure of Glucosyltransferase Oxidase from *Acremonium strictum*: A Novel Flavinylation of 6-S-Cysteinylyl, 8-N1-Histidyl FAD. *J. Biol. Chem.* **280**, 38831–38838.
- 13 Fraaije MW, van den Heuvel RH, van Berkel WJ & Mattevi A (1999) Covalent flavinylation is essential for efficient redox catalysis in vanillyl-alcohol oxidase. *J. Biol. Chem.* **274**, 35514–20.
- 14 Salazar D, Zhang L, DeGala GD & Frerman FE (1997) Expression and Characterization of Two Pathogenic Mutations in Human Electron Transfer Flavoprotein. *J. Biol. Chem.* **272**, 26425–26433.
- 15 Dwyer TM, Zhang L, Muller M, Marrugo F & Frerman F (1999) The functions of the flavin contact residues, α Arg249 and β Tyr16, in human electron transfer flavoprotein. *Biochim. Biophys. Acta - Protein Struct. Mol. Enzymol.* **1433**, 139–152.
- 16 Lehman TC & Thorpe C (1992) A new form of mammalian electron-transferring flavoprotein. *Arch. Biochem. Biophys.* **292**, 594–599.
- 17 Yorita K, Matsuoka T, Misaki H & Massey V (2000) Interaction of two arginine residues in lactate oxidase with the enzyme flavin: Conversion of FMN to 8-formyl-FMN. *Proc. Natl. Acad. Sci.* **97**, 13039–13044.
- 18 Massey V & Palmer G (1966) On the Existence of Spectrally Distinct Classes of Flavoprotein Semiquinones. A New Method for the Quantitative Production of Flavoprotein Semiquinones *. *Biochemistry* **5**, 3181–3189.

- 19 Herrick KR, Salazar D, Goodman SI, Finocchiaro G, Bedzyk LA & Frerman FE (1994) Expression and characterization of human and chimeric human-*Paracoccus denitrificans* electron transfer flavoproteins. *J. Biol. Chem.* **269**, 32239–45.
- 20 Massey V (1994) Activation of molecular oxygen by flavins and flavoproteins. *J. Biol. Chem.* **269**, 22459–22462.
- 21 Massey V (1995) Introduction: flavoprotein structure and mechanism. *FASEB J.*, 473–475.
- 22 Mack M & Grill S (2006) Riboflavin analogs and inhibitors of riboflavin biosynthesis. *Appl. Microbiol. Biotechnol.* **71**, 265–275.
- 23 Pedrolli DB, Jankowitsch F, Schwarz J, Langer S, Nakanishi S & Mack M (2014) Natural Riboflavin Analogs. In *Flavins and Flavoproteins: Methods and Protocols* (Weber S & Schleicher E, eds), pp. 41–63. Springer New York, New York, NY.
- 24 DiMarco AA, Bobik TA & Wolfe RS (1990) Unusual Coenzymes of Methanogenesis. *Annu. Rev. Biochem.* **59**, 355–394.
- 25 Mao Y, Varoglu M & Sherman DH (1999) Molecular characterization and analysis of the biosynthetic gene cluster for the antitumor antibiotic mitomycin C from *Streptomyces lavendulae* NRRL 2564. *Chem. Biol.* **6**, 251–63.
- 26 Stover CK, Warrenner P, VanDevanter DR, Sherman DR, Arain TM, Langhorne MH, Anderson SW, Towell JA, Yuan Y, McMurray DN, Kreiswirth BN, Barry CE & Baker WR (2000) A small-molecule nitroimidazopyran drug candidate for the treatment of tuberculosis. *Nature* **405**, 962–6.
- 27 Otani S, Takatsu M, Nakano M, Kasai S & Miura R (1974) Letter: Roseoflavin, a new antimicrobial pigment from *Streptomyces*. *J. Antibiot. (Tokyo)*. **27**, 86–7.
- 28 Jhulki I, Chanani PK, Abdelwahed SH & Begley TP (2016) A Remarkable Oxidative Cascade That Replaces the Riboflavin C8 Methyl with an Amino Group during Roseoflavin Biosynthesis. *J. Am. Chem. Soc.* **138**, 8324–8327.
- 29 Tongsook C, Uhl MK, Jankowitsch F, Mack M, Gruber K & Macheroux P (2016) Structural and kinetic studies on RosA, the enzyme catalysing the methylation of 8-demethyl-8-amino- d - riboflavin to the antibiotic roseoflavin. *FEBS J.* **283**, 1531–1549.
- 30 Bergner T, Tabib CR, Winkler A, Stipsits S, Kayser H, Lee J, Malthouse JP, Mayhew S, Müller F, Gruber K & Macheroux P (2015) Structural and biochemical properties of LuxF from *Photobacterium leiognathi*. *Biochim. Biophys. Acta - Proteins Proteomics* **1854**, 1466–1475.
- 31 Cowden WB, Butcher GA, Hunt NH, Clark IA & Yoneda F (1987) Antimalarial activity of a riboflavin analog against *Plasmodium vinckei* in vivo and *Plasmodium falciparum* in vitro. *Am. J. Trop. Med. Hyg.* **37**, 495–500.
- 32 Kisker C, Schindelin H & Rees DC (1997) Molybdenum-cofactor-containing enzymes: structure and mechanism. *Annu. Rev. Biochem.* **66**, 233–67.
- 33 Mayhew SG, Whitfield CD, Ghisla S & Schuman-jorns M (1974) Identification and Properties of New Flavins in Electron-Transferring Flavoprotein from *Peptostreptococcus elsdenii* and Pig-Liver Glycolate Oxidase. *Eur. J. Biochem.* **44**, 579–591.
- 34 Ghisla S & Mayhew SG (1976) Identification and Properties of 8-Hydroxyflavin -Adenine Dinucleotide in Electron-Transferring Flavoprotein from *Peptostreptococcus elsdenii*. *Eur. J. Biochem.* **63**, 373–390.
- 35 Jones JM, Morrell JC & Gould SJ (2000) Identification and characterization of HAOX1, HAOX2, and HAOX3, three human peroxisomal 2-hydroxy acid oxidases. *J. Biol. Chem.* **275**, 12590–7.

- 36 Vignaud C, Pietrancosta N, Williams EL, Rumsby G & Lederer F (2007) Purification and characterization of recombinant human liver glycolate oxidase. *Arch. Biochem. Biophys.* **465**, 410–6.
- 37 Marshall KR, Gong M, Wodke L, Lamb JH, Jones DJL, Farmer PB, Scrutton NS & Munro AW (2005) The Human Apoptosis-inducing Protein AMID Is an Oxidoreductase with a Modified Flavin Cofactor and DNA Binding Activity. *J. Biol. Chem.* **280**, 30735–30740.
- 38 Doubayashi D, Ootake T, Maeda Y, Oki M, Tokunaga Y, Sakurai A, Nagaosa Y, Mikami B & Uchida H (2011) Formate oxidase, an enzyme of the glucose-methanol-choline oxidoreductase family, has a His-Arg pair and 8-formyl-FAD at the catalytic site. *Biosci. Biotechnol. Biochem.* **75**, 1662–7.
- 39 Papa S, Martino PL, Capitanio G, Gaballo A, De Rasmio D, Signorri A & Petruzzella V (2012) The Oxidative Phosphorylation System in Mammalian Mitochondria. In *Advances in Experimental Medicine and Biology* pp. 311–327.
- 40 Beratan DN & Skourtis SS (2013) Electron Transfer Through Proteins. In *Encyclopedia of Biophysics* (Roberts GCK, ed), pp. 625–630. Springer Berlin Heidelberg, Berlin, Heidelberg.
- 41 Page CC, Moser CC & Dutton PL (2003) Mechanism for electron transfer within and between proteins. *Curr. Opin. Chem. Biol.* **7**, 551–556.
- 42 Ichiye T (2013) Electron Transfer Proteins: Overview. In *Encyclopedia of Biophysics* (Roberts GCK, ed), pp. 614–621. Springer Berlin Heidelberg, Berlin, Heidelberg.
- 43 Wirth C, Brandt U, Hunte C, Zickermann V & Zick V (2016) Structure and function of mitochondrial complex I. *BBA - Bioenerg.* **1857**, 902–914.
- 44 Rutter J, Winge DR & Schiffman JD (2010) Succinate dehydrogenase - Assembly, regulation and role in human disease. *Mitochondrion* **10**, 393–401.
- 45 Swanson MA, Usselman RJ, Frerman FE, Eaton GR & Eaton SS (2008) The Iron - Sulfur Cluster of Electron Transfer Flavoprotein - Ubiquinone Oxidoreductase Is the Electron Acceptor for Electron Transfer Flavoprotein. , 8894–8901.
- 46 Watmough NJ & Frerman FE (2010) The electron transfer flavoprotein: Ubiquinone oxidoreductases. *Biochim. Biophys. Acta - Bioenerg.* **1797**, 1910–1916.
- 47 Mráček T, Drahoř Z & Houšťek J (2013) The function and the role of the mitochondrial glycerol-3-phosphate dehydrogenase in mammalian tissues. *Biochim. Biophys. Acta - Bioenerg.* **1827**, 401–410.
- 48 Fassone E, Duncan AJ, Taanman JW, Pagnamenta AT, Sadowski MI, Holand T, Qasim W, Rutland P, Calvo SE, Mootha VK, Bitner-Glindzicz M & Rahman S (2010) FOXRED1, encoding an FAD-dependent oxidoreductase complex-I-specific molecular chaperone, is mutated in infantile-onset mitochondrial encephalopathy. *Hum. Mol. Genet.* **19**, 4837–4847.
- 49 Nouws J, Nijtmans L, Houten SM, Van Den Brand M, Huynen M, Venselaar H, Hoefs S, Gloerich J, Kronick J, Hutchin T, Willems P, Rodenburg R, Wanders R, Van Den Heuvel L, Smeitink J & Vogel RO (2010) Acyl-CoA dehydrogenase 9 is required for the biogenesis of oxidative phosphorylation complex I. *Cell Metab.* **12**, 283–294.
- 50 Nouws J, Te brinke H, Nijtmans LG & Houten SM (2014) ACAD9, a complex I assembly factor with a moonlighting function in fatty acid oxidation deficiencies. *Hum. Mol. Genet.* **23**, 1311–1319.
- 51 Ensenaer R, He M, Willard JM, Goetzman ES, Corydon TJ, Vandahl BB, Mohsen AW, Isaya G & Vockley J (2005) Human Acyl-CoA dehydrogenase-9 plays a novel role in the mitochondrial beta-oxidation of unsaturated fatty acids. *J. Biol. Chem.* **280**, 32309–32316.

- 52 Fang J, Uchiumi T, Yagi M, Matsumoto S, Amamoto R, Takazaki S, Yamaza H, Nonaka K & Kang D (2013) Dihydro-orotate dehydrogenase is physically associated with the respiratory complex and its loss leads to mitochondrial dysfunction. *Biosci. Rep.* **33**.
- 53 Horvath R (2006) Leigh syndrome caused by mutations in the flavoprotein (Fp) subunit of succinate dehydrogenase (SDHA). *J. Neurol. Neurosurg. Psychiatry* **77**, 74–76.
- 54 Ng SB, Buckingham KJ, Lee C, Bigham AW, Tabor HK, Dent KM, Huff CD, Shannon PT, Jabs EW, Nickerson DA, Shendure J & Bamshad MJ (2010) Exome sequencing identifies the cause of a mendelian disorder. *Nat. Genet.* **42**, 30–35.
- 55 Moolenaar SH, Poggi-Bach J, Engelke UFH, Corstiaensen JMB, Heerschap A, De Jong JGN, Binzak BA, Vockley J & Wevers RA (1999) Defect in dimethylglycine dehydrogenase, a new inborn error of metabolism: NMR spectroscopy study. *Clin. Chem.* **45**, 459–464.
- 56 Loehr JP, Goodman SI & Frerman FE (1990) Glutaric Acidemia Type II: Heterogeneity of Clinical and Biochemical Phenotypes. *Pediatr. Res.* **27**, 311–315.
- 57 Schiff M, Froissart R, Olsen RKJ, Acquaviva C & Vianey-Saban C (2006) Electron transfer flavoprotein deficiency: Functional and molecular aspects. *Mol. Genet. Metab.* **88**, 153–158.
- 58 Angelini C (2014) Multiple Acyl-CoA Dehydrogenase Deficiency. In *Genetic Neuromuscular Disorders: A Case-Based Approach* pp. 279–284. Springer International Publishing, Cham.
- 59 Cornelius N, Frerman FE, Corydon TJ, Palmfeldt J, Bross P, Gregersen N & Olsen RKJ (2012) Molecular mechanisms of riboflavin responsiveness in patients with ETF-QO variations and multiple acyl-CoA dehydrogenation deficiency. *Hum. Mol. Genet.* **21**, 3435–3448.
- 60 Vockley J & Ensenauer R (2006) Isovaleric acidemia: New aspects of genetic and phenotypic heterogeneity. *Am. J. Med. Genet. - Semin. Med. Genet.* **142 C**, 95–103.
- 61 Tanaka K, Budd MA, Efron ML & Isselbacher KJ (1966) Isovaleric acidemia: a new genetic defect of leucine metabolism. *Proc. Natl. Acad. Sci. U. S. A.* **56**, 236–42.
- 62 Henriques BJ, Bross P & Gomes CM (2010) Mutational hotspots in electron transfer flavoprotein underlie defective folding and function in multiple acyl-CoA dehydrogenase deficiency. *Biochim. Biophys. Acta - Mol. Basis Dis.* **1802**, 1070–1077.
- 63 Purevjav E, Kimura M, Takusa Y, Ohura T, Tsuchiya M, Hara N, Fukao T & Yamaguchi S (2002) Molecular study of electron transfer flavoprotein alpha-subunit deficiency in two Japanese children with different phenotypes of glutaric acidemia type II. *Eur. J. Clin. Invest.* **32**, 707–712.
- 64 Olsen RKJ, Andresen BS, Christensen E, Bross P, Skovby F & Gregersen N (2003) Clear relationship between ETF/ETFDH genotype and phenotype in patients with multiple acyl-CoA dehydrogenation deficiency. *Hum. Mutat.* **22**, 12–23.
- 65 Zhang J, Frerman FE & Kim J-JP (2006) Structure of electron transfer flavoprotein-ubiquinone oxidoreductase and electron transfer to the mitochondrial ubiquinone pool. *Proc. Natl. Acad. Sci. U. S. A.* **103**, 16212–16217.

CHAPTER II

STRUCTURE AND BIOCHEMICAL PROPERTIES OF RECOMBINANT HUMAN DIMETHYLGLYCINE DEHYDROGENASE AND COMPARISON TO THE DISEASE-RELATED H109R VARIANT

Peter Augustin[‡], Altijana Hromic[£], Tea Pavkov-Keller[§], Karl Gruber[£], and Peter Macheroux[‡]

[‡] Institute of Biochemistry, Graz University of Technology, Graz, Austria

[£] Institute of Molecular Biosciences, University of Graz, Graz, Austria

[§] Austrian Centre of Industrial Biotechnology, Graz, Austria

Running title

Human Dimethylglycine Dehydrogenase

Database

Structural data are available in the PDB database under the accession number 5L46.

Keywords

electron transfer; flavin adenine dinucleotide; genetic disease; recombinant protein expression; X-ray crystallography

Abbreviations

AgDMGO, *Arthrobacter globiformis* dimethylglycine oxidase; DCPIP, 2,6-dichlorophenolindophenol; DMG, dimethylglycine; (h)DMGDH, (human) dimethylglycine dehydrogenase; (h)ETF, (human) electron transferring flavoprotein; (h)ETF-QO, (human) ETF-ubiquinone oxidoreductase; (h)MCAD, (human) medium-chain acyl-CoA dehydrogenase; MRE, mean residue ellipticity; PMS, phenazine methosulfate; THF, tetrahydrofolate; WT, wild-type.

This chapter was published as “Structure and Biochemical Properties of Recombinant Human Dimethylglycine Dehydrogenase and Comparison to the Disease-related H109R Variant” in 2016, in FEBS journal, volume 283(19), pages 3587-3603.

ABSTRACT

The human dimethylglycine dehydrogenase (hDMGDH) is a flavin adenine dinucleotide (FAD) and tetrahydrofolate (THF) dependent, mitochondrial matrix enzyme taking part in choline degradation, one-carbon metabolism and electron transfer to the respiratory chain. The rare natural variant H109R causes dimethylglycine dehydrogenase deficiency leading to increased blood and urinary dimethylglycine concentrations. A detailed biochemical and structural characterization of hDMGDH was thus far hampered by insufficient heterologous expression of the protein. In the present study we report the development of an intracellular, heterologous expression system in *Komagataella phaffii* (formerly known as *Pichia pastoris*) providing the opportunity to determine kinetic parameters, spectroscopic properties, thermostability and the redox potential of hDMGDH. Moreover, we have successfully crystallized the wild-type enzyme and determined the structure to 3.1-Å resolution. The structure-based analysis of our biochemical data provided new insights into the kinetic properties of the enzyme in particular with respect to oxygen reactivity. A comparative study with the H109R variant demonstrated that the variant suffers from decreased protein stability, cofactor saturation and substrate affinity.

INTRODUCTION

The human flavoproteome comprises 90 enzymes with versatile functions, structures and protein characteristics. Sixty percent of the known flavoproteins are involved in human diseases and disorders emphasizing their importance in human metabolism [1]. The human mitochondrial matrix flavoprotein dimethylglycine dehydrogenase (hDMGDH, EC: 1.5.8.4) catalyzes the oxidative demethylation of dimethylglycine (DMG) to sarcosine, and also to a lesser extent the conversion of sarcosine to glycine as part of choline degradation (Figure 1) [2,3]. Choline is an essential nutrient and building block in a variety of vital biomolecules such as the membrane phospholipid phosphatidylcholine and the neurotransmitter acetylcholine [4]. Degradation of choline proceeds by consecutive oxidations via betaine aldehyde, betaine, dimethylglycine and sarcosine to the amino acid glycine (Figure 1) [5]. hDMGDH, a key-enzyme of this pathway, requires two cofactors: FAD and tetrahydrofolate (THF). The FAD is covalently attached via its $\delta\alpha$ -position to the N3 of a histidyl residue and serves as the electron acceptor in the oxidation of DMG. On the other hand, THF is used as the acceptor of the incipient methyl group and thus prevents the release of cell-toxic formaldehyde during catalysis [3,6]. In the course of this reaction *N*-5,10-methylene tetrahydrofolate is formed, which plays an important role in one-carbon metabolism. Regeneration of oxidized FAD is achieved by electron transfer to the human electron transferring flavoprotein (hETF), which in turn transfers the electrons to the membrane-anchored ETF-ubiquinone oxidoreductase (ETF-QO) for further utilization in the mitochondrial respiratory chain [7,8].

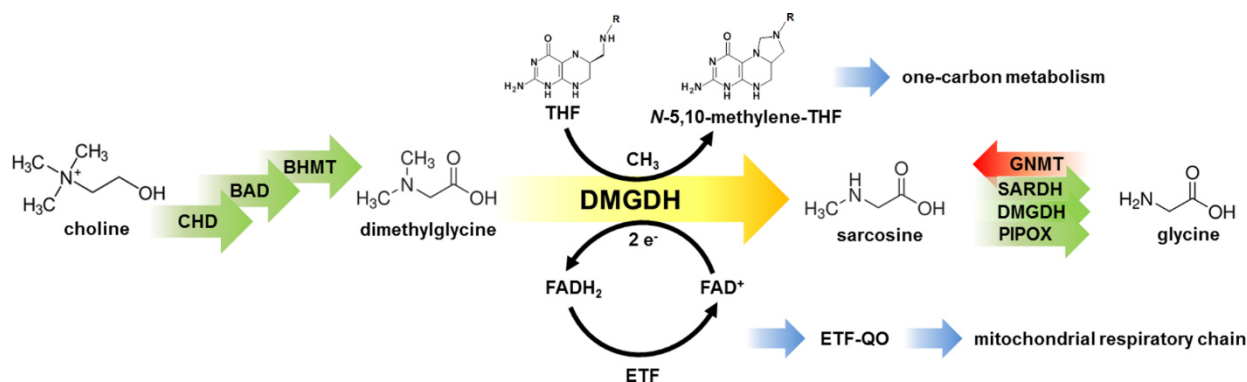


Figure 1. Mammalian choline degradation pathway with hDMGDH as metabolic branch point. Choline degradation to dimethylglycine is catalyzed by three enzymes, choline dehydrogenase (CHD), betaine aldehyde dehydrogenase (BAD) and betaine homocysteine *S*-methyltransferase (BHMT). Conversion of dimethylglycine (DMG) to sarcosine by DMGDH reduces the FAD cofactor and a methyl group is donated to THF resulting in FADH₂ and *N*-5,10-methylene-THF. The enzyme is reoxidized by the interaction with hETF and the derived electrons are further channeled by ETF-QO to the mitochondrial respiratory chain. *N*-5,10-methylene-THF is consumed in further reactions catalyzed by methylene-THF reductase (MTHFR) and serine hydroxymethyltransferase (SHMT). hDMGDH is the only enzyme converting dimethylglycine to sarcosine and the only other known route to sarcosine is via glycine *N*-methyl transferase (GNMT). Sarcosine is further converted to glycine, mostly by sarcosine dehydrogenase (SARDH), but is also a substrate for dimethylglycine dehydrogenase and peroxisomal sarcosine oxidase (PIPOX).

A rare naturally occurring point mutation found in 58 out of 118 656 (0.049%) analyzed human gene sequences (Exome Aggregation Consortium online browser; <http://exac.broadinstitute.org/variant/5-78351682-T-C>) results in the exchange of histidine 109 to arginine (H109R). This variant reportedly suffers from lower stability and enzymatic activity [9,10]. The observed phenotype was described as dimethylglycine dehydrogenase deficiency with significantly higher levels of dimethylglycine in human body fluids causing muscle fatigue and a fish like odor (OMIM: 605850). Interestingly, the mutation is predominantly found in individuals of African descent. In recent years, also the product of the reaction catalyzed by hDMGDH, sarcosine, attracted attention as a biomarker for aggressive prostate cancer [11,12]. Therefore, investigations on the regulation of sarcosine levels and the enzymes involved are in the focus of research. Furthermore, a recent epidemiological study revealed a possible connection of dimethylglycine dehydrogenase deficiency to the development of diabetes, further emphasizing the importance of the enzyme [13]. DMGDH was first identified and purified from rat liver in the 1950s and early 60s [14,15]. Since then several publications have dealt with the characterization of mammalian dimethylglycine dehydrogenases from rat [2,3,16] and pig liver [8] as well as the recombinant rat [17,18] and human enzyme [19] using *Escherichia coli* as expression host. Furthermore, dimethylglycine oxidase from *Arthrobacter globiformis* (AgDMGO) was characterized in biochemical and structural detail [6,20–23]. However, the available information on the hDMGDH appears insufficient and partly contradictory. In order to overcome these deficiencies, we present a profound analysis of the recombinant hDMGDH and the H109R variant concerning kinetics, redox behavior and spectral properties. Furthermore, we have elucidated the crystal structure of the human wild-type enzyme.

In order to characterize hDMGDH we have established a recombinant expression system for wild-type and the H109R variant in *Komagataella phaffii* (formerly known as *Pichia pastoris* or *Komagataella pastoris* [24]) and a subsequent purification protocol. This approach enabled us to determine key kinetic parameters as well as physical and spectroscopic properties of wild-type DMGDH. Consequently, we have also employed our expression system to generate the H109R variant to address the putative loss of function that leads to DMGDH-deficiency in humans. Moreover, successful crystallization of the WT and subsequent crystallographic analysis provided us with the opportunity to analyze the structure with regard to substrate binding and oxygen reactivity. The latter issue is especially interesting as the control of oxygen reactivity in flavoenzymes is still a controversial topic. The direct comparison of a dehydrogenase (hDMGDH) and an oxidase (AgDMGO) allowed new insights into the structural elements involved in oxygen reactivity and supports concepts that are based on gatekeeper residues in the vicinity of the isoalloxazine ring system. In this vein, we show that a previously proposed model to rationalize oxygen reactivity in the vanillyl oxidase family is applicable to the family of sarcosine and dimethylglycine dehydrogenases and oxidases, respectively [25,26].

RESULTS

Enzyme Expression and Purification

Initial attempts to express the gene encoding human dimethylglycine dehydrogenase (hDMGDH) in *Escherichia coli* (BL21 DE3) yielded largely insoluble protein. On the other hand, heterologous expression in the methanotrophic yeast *Komagataella phaffii* (formerly known as *Pichia pastoris* [24]) was successful. As shown in Figure 2A, Western blot analysis of *K. phaffii* cell lysates at different time points indicates a stable expression of the protein after induction with methanol. Typically, fermentations were stopped after 96 h after methanol induction resulting in 1.6 to 1.9 kg of wet cell pellet. A comparison of signal intensities showed that the WT was expressed in higher amounts than the variant under identical fermentation conditions thus leading to a higher yield of WT (Figure 2A). After cell disruption and Ni-NTA affinity chromatography, the yield of proteins (Figure 2B, lanes 3) was approximately 70 and 25 mg of the WT and H109R variant, respectively (40 or 15 μg enzyme/g wet cell weight). In order to achieve higher purity for crystallization trials, the proteins were further purified using anion exchange chromatography (Figure 2B, lanes 4) resulting in lower protein yields of 30 and 2 mg (17 or 1 μg enzyme/g wet cell weight) of WT and H109R variant, respectively. The protein loss mainly occurred during the necessary buffer change to lower salt concentrations after Ni-NTA affinity chromatography required for the subsequent anion exchange chromatography. Although we experienced that hDMGDH tends to precipitate at low salt concentrations, other chromatographic methods, like size-exclusion chromatography or hydrophobic interaction chromatography, were explored but did not give a similar purity.

The A_{280}/A_{450} ratios of the highly pure protein fractions were usually between 14-16 and 20-25 for the WT and variant protein, respectively. The UV-Vis absorption spectra show a clear difference between enzyme bound FAD and free FAD (Figure 2C) whereas hDMGDH-WT and the variant featured similar spectral properties with identical absorption maxima. In comparison with free FAD in solution, the UV-Vis absorption maxima of FAD bound to either WT or the H109R variant exhibits a hypsochromic shift from 370 to 350 nm and a bathochromic shift from 445 to 460 nm (Figure 2C).

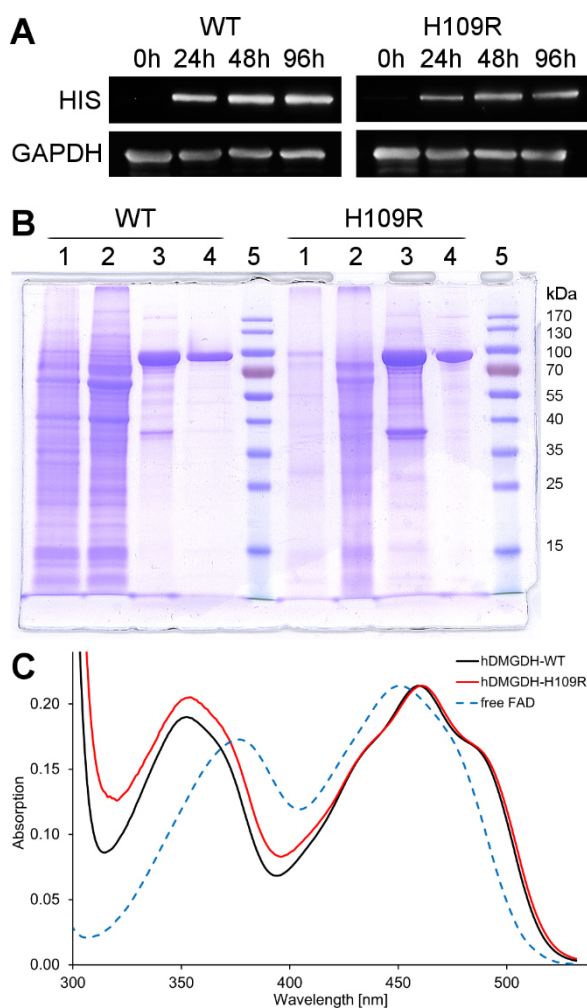


Figure 2. Heterologous expression and purification of hDMGDH-WT and hDMGDH-H109R variant. (A) Western blot of *K. phaffii* cell lysates taken at different time points after methanol induction. Antibodies are directed against a C-terminal nona-histidine tag fused to the recombinant enzymes and, as loading control, against *K. phaffii* GAPDH. (B) SDS-PAGE of the different purification steps of WT and variant shows efficient enzyme purification with Ni-NTA affinity and MonoQ anion exchange chromatography. Lane 1, fermentation pellet fraction; 2, *K. phaffii* lysate; 3, enzyme fraction after Ni-NTA affinity chromatography; 4, enzyme fraction after Mono Q; 5, protein standard. (C) UV-Vis absorption spectra of DMGDH wild-type (black line) and the H109R variant (red line) after anion exchange chromatography. The spectra were normalized to the long-wavelength absorption maxima (445 and 450 nm, respectively). Free FAD in solution is shown as a dotted blue line.

Determination of Kinetic Parameters for hDMGDH-WT and H109R Variant

The evaluation of the steady-state kinetic parameters for hDMGDH-WT and H109R variant was conducted using either ferrocene or 2,6-dichlorophenolindophenol (DCPIP) as electron acceptor to oxidize the reduced FAD cofactor. The obtained parameters show significant differences between the two assay systems both in terms of the k_{cat} as well as the K_M for DMG (Figure 3, Table 1). When ferrocene was used as the artificial electron acceptor the k_{cat} was 5-fold greater than with DCPIP (213 ± 4 versus $44 \pm 1 \text{ min}^{-1}$, Table 1) and the K_M was significantly higher (1.4 ± 0.1 versus $0.3 \pm 0.002 \text{ mM}$, Table 1). Interestingly, the H109R variant exhibited a two-fold higher activity than the WT in both assays. At the same time, the K_M of DMG was strongly increased by a factor of 23 and 16 in the ferrocene

and DCPIP assay, respectively, resulting in an approximately 10-fold lower catalytic efficiency of the H109R variant (Table 1). Notably, when DCPIP was used as electron acceptor data linearization using the method of Eadie and Hofstee revealed a second, much higher K_M value of ≈ 30 mM for DMG (inset Figure 3A). Since the rate at which FAD is oxidized by ferrocene is closer to the rate of flavin reduction, it appears that ferrocene is superior to DCPIP as electron acceptor.

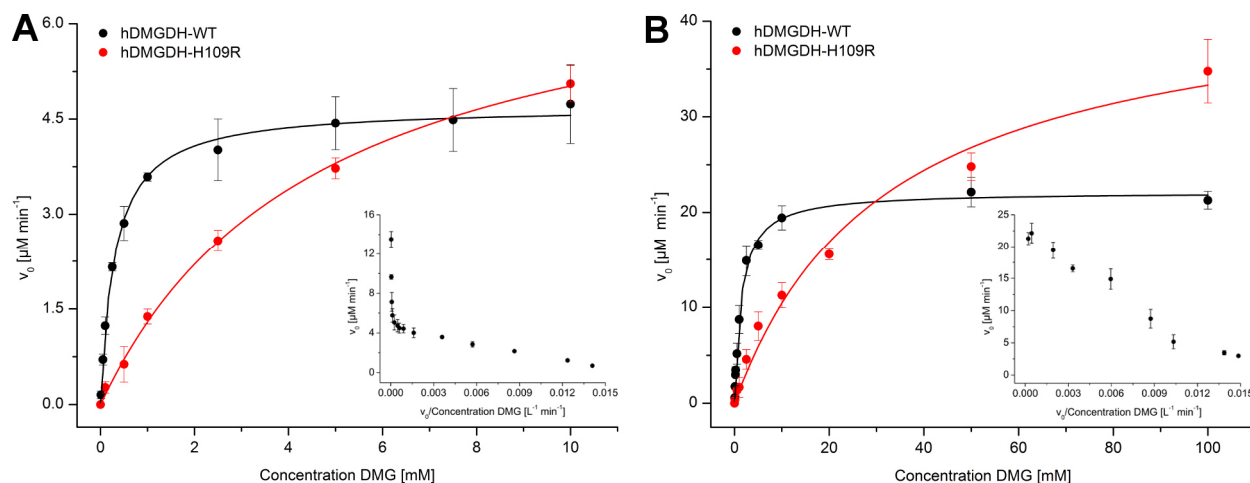


Figure 3. Steady-state kinetics of hDMGDH-WT and H109R variant. Steady-state kinetic experiments were performed with DCPIP (A) and ferrocene activity assays (B) by plotting initial reaction velocities (v_0) against the substrate concentration. Data obtained for WT and H109R variant are represented in black and red, respectively. Kinetic parameters are summarized in Table 1. Linearization of the data in Eadie-Hofstee diagrams reveal two K_M values for the DCPIP assay, one at low (0-10 mM DMG) and one at very high substrate concentrations (> 50 mM DMG, inset panel A). In contrast, the ferrocene assay produced a single K_M value when measured in the same concentration range (inset panel B). Error bars are shown as standard deviations; $n=3$.

Table 1. Summary of kinetic parameters obtained with steady-state kinetics for hDMGDH-WT and hDMGDH-H109R variant with two different activity assays (DCPIP and ferrocene).

	K_M	v_{\max}	k_{cat}	A_{spec}	k_{cat}/K_M
	<i>mM</i>	$\mu\text{M min}^{-1}$	min^{-1}	$\mu\text{mol mg}^{-1} \text{min}^{-1}$	$\text{mM}^{-1} \text{min}^{-1}$
WT DCPIP	0.3 ± 0.002 $\sim 30^a$	4.7 ± 0.1 $\sim 11^a$	44 ± 1	0.5 ± 0.01	146 ± 12
WT ferrocene	1.4 ± 0.1	22.1 ± 0.3	213 ± 4	2.0 ± 0.04	137 ± 16
H109R DCPIP	4.7 ± 0.4 $\sim 90^a$	7.4 ± 0.3 $\sim 22^a$	91 ± 4	1 ± 0.04	20 ± 2
H109R ferrocene	32.2 ± 5.6	44.1 ± 3.2	544 ± 40	6 ± 0.4	11 ± 1

^aTwo K_M and v_{\max} values were obtained with the DCPIP assay, the higher was roughly estimated from Eadie-Hofstee plots (Figure 3).

Due to much lower enzyme amounts available of the H109R variant pre-steady-state kinetics were solely measured with the wild-type enzyme. As shown in Figure 4A, the rate of reduction as a function of DMG concentration fitted to a hyperbolic equation yielding a limiting reductive rate of $17 \pm 0.3 \text{ s}^{-1}$ and a dissociation constant of $4.9 \pm 0.3 \text{ mM}$ for DMG. Thus, the reductive rate is 5 to 20 times faster than

k_{cat} determined in the ferrocene and DCPIP assay (Table 1) indicating that the electron transfer from the reduced FAD to the artificial electron acceptor is rate limiting in the assays used to evaluate steady-state kinetics. Reoxidation of hDMGDH with air-saturated buffer proceeds very slowly with an observed rate of reoxidation of $0.006 \pm 0.001 \text{ s}^{-1}$ at an oxygen concentration of $135 \mu\text{M}$ (inset Figure 4A). Rapid reaction measurements with sarcosine yielded a limiting rate of reduction of $0.7 \pm 0.1 \text{ s}^{-1}$ and a dissociation constant of $280 \pm 10 \text{ mM}$ clearly indicating that sarcosine is a much poorer substrate than DMG (Figure 4A).

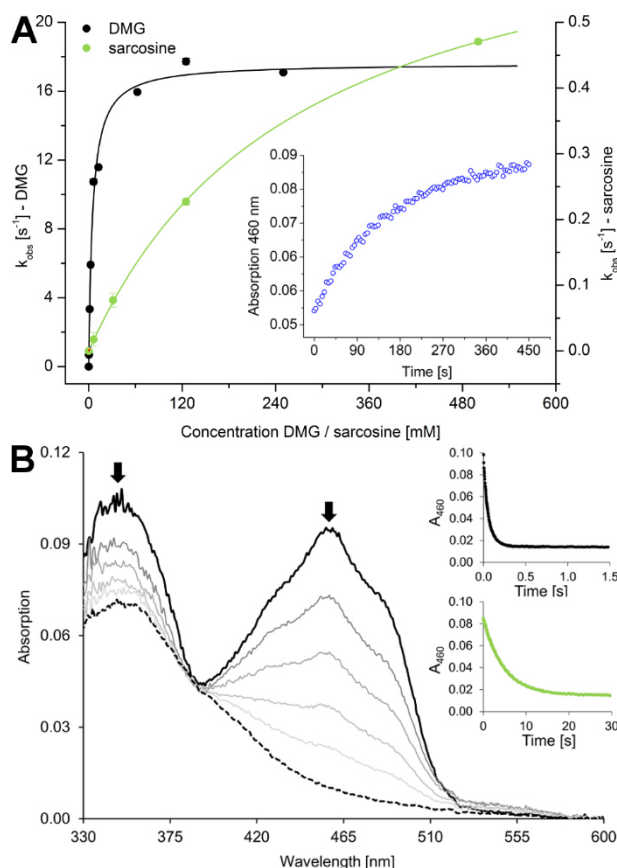


Figure 4. Pre-steady-state kinetics of hDMGDH-WT. Reductive and oxidative rates were measured under anoxic conditions with the stopped flow device. (A) Reductive rates were determined for DMG (black, left axis) and sarcosine (red, right axis). The inset shows the re-oxidation of reduced FAD as a function of time at an oxygen concentration of 10.5% ($135 \mu\text{M O}_2$) at 460 nm. At least three independent measurements were performed, error bars are shown as standard deviations. (B) Selected absorption spectra of the anoxic reduction of $10 \mu\text{M}$ hDMGDH-WT with 125 mM DMG. The direction of the change in absorption is depicted by arrows. The top inset shows the absorption change at 460 nm observed by mixing WT with 125 mM DMG, the bottom inset the change at 460 nm mixing WT with 125 mM sarcosine.

Finally, we also studied the effect of tetrahydrofolate (THF) on the activity of hDMGDH using the ferrocene assay (Figure 5). The activity measurements were done similarly to the ferrocene activity assay as described above at $25 \text{ }^\circ\text{C}$ and pH 7.8 in 50 mM HEPES/NaOH with 150 mM NaCl, 100 nM DMGDH, 1 mM DMG, 0.1 mM EDTA and 0.2 mM freshly prepared ferrocene in a concentration range

of 0-75 μM THF. As shown in Figure 5, the activity of WT decreases as a function of the THF concentration.

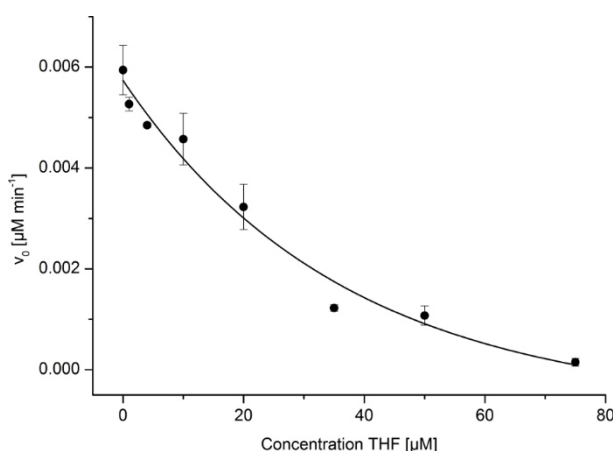


Figure 5. hDMGDH-WT activity as a function of the THF concentration. The activity was measured using the ferrocene activity assay. The error bars show the standard deviation of at least three measurements for each THF concentration.

Photoreduction and Determination of the Redox Potential of hDMGDH

Reduction of hDMGDH by DMG shows a monophasic conversion of the oxidized FAD to the two-electron reduced dihydroquinone state (Figure 4B) without any transient appearance of a semiquinone radical. In contrast to substrate reduction, photoreduction of hDMGDH leads to the anionic (red) flavin semiquinone with a typical absorption maximum at 372 nm (Figure 6A). Further photoreduction eventually leads to the fully reduced dihydroquinone (Figure 6B), which is directly converted to the oxidized state without the occurrence of a semiquinone upon reaction with molecular dioxygen (Figure 6C). This was also seen when reduced hDMGDH was reacted with air-saturated buffer in the stopped flow device (data not shown).

In order to determine the redox potential of hDMGDH we employed the xanthine oxidase/xanthine method described by Massey [27] using indigotrisulfonic acid potassium salt as reference dye. The slope of the double logarithmic plot was close to unity indicating that the dye and the flavin receive an equal number of electrons (*i.e.* two) although the anionic semiquinone radical is clearly observable during the redox titration (Figure 6D). The redox potential for the reduction of FAD bound to hDMGDH was calculated from six independent measurements to -93 ± 1 mV.

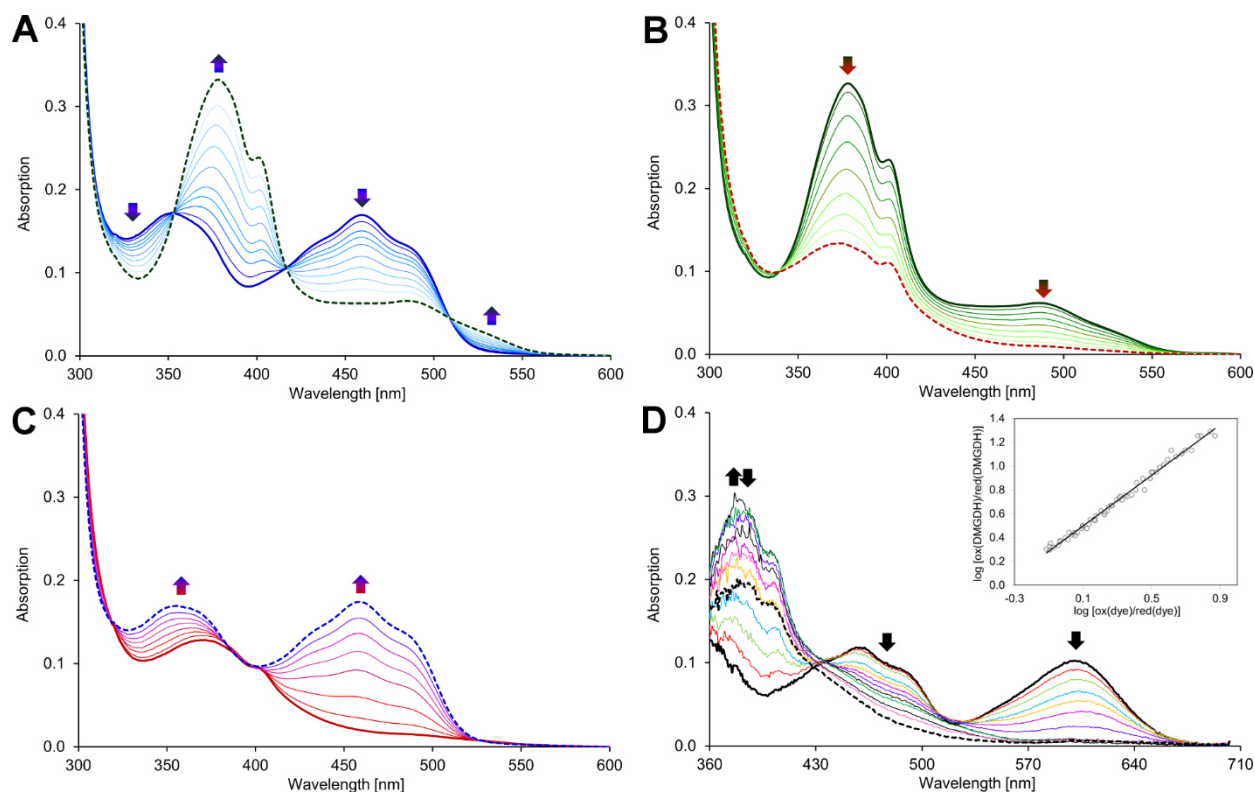


Figure 6. Photoreduction and redox potential of hDMGDH-WT. (A) and (B) show selected absorption spectra of the anoxic photoreduction of the wild-type enzyme. 20 μM of hDMGDH were photoreduced in the presence of 1 mM EDTA, 2 μM 5-deaza FMN and 2 μM methylviologen. First, the enzyme is reduced to the red semiquinone radical state (A) before proceeding to the typical spectrum of a fully reduced hydroquinone species (B). The admission of oxygen to the enzyme shows that re-oxidation does not proceed through a semiquinone redox state and directly yields the oxidized state (C). (D) The redox potential for the WT was determined with the xanthine/xanthine oxidase system described by Massey [27]. The plot shows the simultaneous reduction of the enzyme and the dye with the double logarithmic evaluation of the data according to Minnaert [28] in the inset. 20 μM hDMGDH were reduced at 25 $^{\circ}\text{C}$ over 120 min with indigotrisulfonic acid potassium salt and the evaluation for the enzyme was done at 480 nm where the dye does not show a contribution to the absorption. Values for the dye were measured at 600 nm. Initial absorption spectra in all panels are depicted in bold lines, whereas final absorption spectra are shown as dashed lines. Only selected absorption spectra are shown. The direction of the change in absorption is depicted by arrows.

Thermal Stability of hDMGDH-WT and hDMGDH-H109R

The thermal stability of both enzymes was determined using Thermofluor[®] and CD-spectroscopy. Thermofluor[®] temperature scans from 25-95 $^{\circ}\text{C}$ showed that the WT and the H109R variant have melting points (T_m) of 52 $^{\circ}\text{C}$ and 47 $^{\circ}\text{C}$, respectively (Figure 7A). A similar result was obtained by means of CD-spectroscopy yielding a T_m of 53 $^{\circ}\text{C}$ and 47 $^{\circ}\text{C}$, for WT and the variant, respectively (Figure 7B). Thus, both independent methods confirm that the variant exhibits reduced thermal stability.

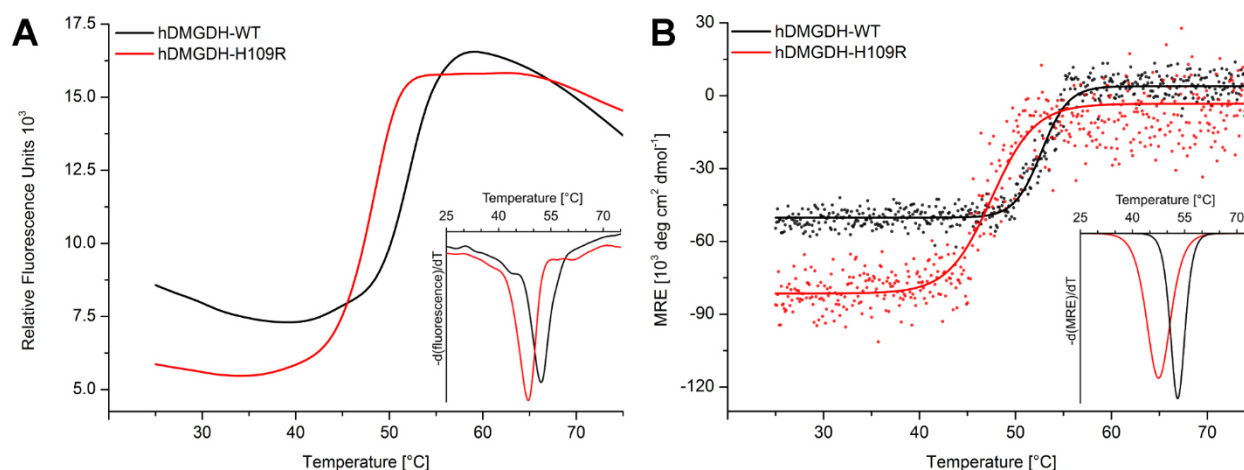


Figure 7. Thermal stability of hDMGDH-WT and the H109R variant. The melting temperatures of wild-type and the variant enzyme differ significantly when measured with ThermoFluor[®] (A) or CD-spectroscopy (B). ThermoFluor[®] was done with 2 μM enzyme and the addition of SYPRO Orange. The change in fluorescence during heating is shown for WT and H109R variant in black and red lines, respectively. The inset in panel A shows the $-\text{d}(\text{fluorescence})/\text{dT}$ derivative curves of the raw data. CD-spectroscopy was done with approximately 6 μM enzyme. Mean residue ellipticity (MRE) was measured every 0.1 $^{\circ}\text{C}$ at 208 nm which is shown by black and red filled circles for WT and variant, respectively. The data were fitted with a sigmoidal curve in Origin. The inset in panel B shows the $-\text{d}(\text{MRE})/\text{dT}$ derivative curves of the sigmoidal fits. The variant (red line) exhibits an inflection point at a lower temperature as the wild-type (black line) in both measurements.

Protein Structure Analysis

The X-ray crystal structure of hDMGDH was determined at 3.1 \AA resolution (Table 2). The crystal belongs to the monoclinic space group ($P2_1$) and contains two dehydrogenase molecules in the asymmetric unit. The two molecules in the asymmetric unit are very similar to each other with an rmsd of 0.22 \AA calculated after the superposition of 810 out of 828 $\text{C}\alpha$ -atoms using the program PyMOL (DeLano Scientific). As previously observed in rDMGDH and also after superposition with the rat enzyme (rmsd of 0.37 \AA calculated for 739 out of 809 $\text{C}\alpha$ -atoms), the human enzyme consists of two domains: the FAD binding domain (N-terminal domain with residues 46-466) and the folate binding domain (C-terminal domain with residues 467-855, Figure 8A). The FAD cofactor is covalently attached to the protein through a linkage between N3 of His91 and the 8α -methyl-group of the isoalloxazine moiety as confirmed by the crystal structure. The folate binding domain can be divided into three subdomains positioned in a “cloverleaf”-like arrangement as previously described for the rat enzyme [18]. Subdomain 1 (residues 467-537 and 626-728) contains a Greek-key motif surrounded by α -helices. Subdomain 2 (residues 538-625 and 729-770) is defined by a five-stranded antiparallel β -sheet with flanking α -helices. Subdomain 3 (residues 771-850) adopts a jellyroll fold. The structure of the rDMGDH was determined in complex with tetrahydrofolate [18]. We also observed some difference electron density in the same area in the folate binding domain. Due to the lower resolution of the diffraction data and/or an incomplete occupancy of the ligand, however, this density was not clear enough to unequivocally position a folate molecule. Based on the structural similarity of the two enzymes, it is still very likely that folate binds in the same position (Figure 8B).

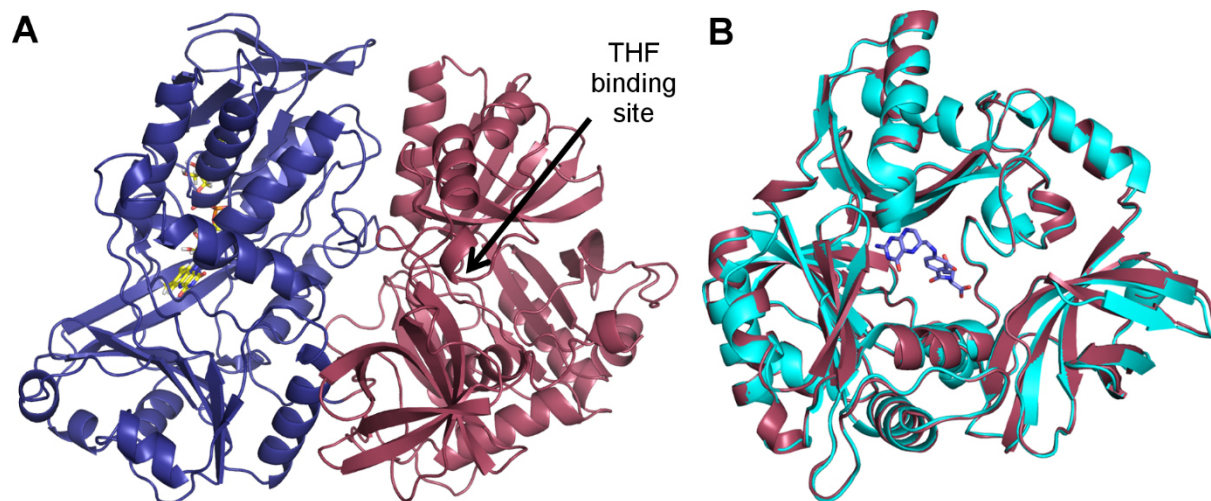


Figure 8. Crystal structure of hDMGDH. (A) The overall structure of hDMGDH with the FAD binding domain is shown in deep blue and the folate binding domain in raspberry. The THF binding site is depicted with an arrow and the FAD-cofactor shown in yellow sticks. (B) Superposition of the folate binding domains of DMGDH from human (raspberry) and rat (cyan). The THF cofactor is shown in blue sticks representation.

Table 2. Data collection and refinement statistics.

X-ray source	ID29, ESRF, Grenoble, France
Wavelength (Å)	0.972
Temperature (K)	100
Space group	<i>P</i> 2 ₁
Cell dimensions	
<i>a, b, c</i> (Å)	83.38, 119.87, 86.47
β (°)	92.59
Resolution (Å)	
High resolution shell	58.65-3.09 (3.2-3.09)
Total no. reflections	86727 (7935)
Unique no. reflections	30495 (2897)
Multiplicity	2.8 (2.7)
Completeness (%)	97.7 (93.81)
$\langle I/\sigma I \rangle$	4.81 (1.53)
Wilson B-factor	47.09
<i>R</i> _{merge}	0.2058 (0.6573)
<i>R</i> _{meas}	0.2531
CC _{1/2}	0.958 (0.604)
CC*	0.989 (0.868)
<i>R</i> _{work} / <i>R</i> _{free}	17.90/26.93
Number of non-hydrogen atoms	
Macromolecules	12782
Ligands	106
Water	6
Protein residues	1617
Average B-factor	38.1
Macromolecules	38.2
Ligands	30.1
Solvent	15.2
R.m.s. deviations	
Bond lengths (Å)	0.010
Bond angles (°)	1.37
Ramachandran outliers (%)	0.31
Ramachandran favored (%)	94
Clashscore	9.40
PDB	5L46

DISCUSSION

Heterologous Enzyme Expression and Purification

In this study we demonstrated that intracellular expression of hDMGDH in *K. phaffii* is feasible and provides enough hDMGDH to perform a detailed biochemical and structural characterization. The expression of the full-length protein and a $\Delta 50$ truncated version as well as secretory expression were unsuccessful. However, an N-terminal $\Delta 28$ truncation of the enzyme was expressed successfully representing the mature form of the enzyme lacking its mitochondrial targeting sequence [29]. The intracellular co-expression of the *Saccharomyces cerevisiae* protein disulfide isomerase enzyme resulted in improved protein yields. The expression of hDMGDH in *E. coli* as reported before [19] was unsuccessful and failed to yield detectable amounts of protein as judged by Western blotting. A C-terminal nona-histidine-tag was added to the gene in order to facilitate purification by means of affinity chromatography. According to the previously published structure of the rat enzyme [18], this C-terminal tag should not interfere with the native fold of the protein or catalytic activity. Western blot analysis showed that the H109R variant is expressed in lower amounts compared to the WT (Figure 2A).

A theoretical A_{280}/A_{450} ratio for hDMGDH fully saturated with FAD cofactor can be roughly calculated to 14. The observed A_{280}/A_{450} ratios of the highly pure proteins, 14-16 and 20-24 for WT and H109R variant respectively, revealed that the WT is almost fully loaded with the covalently attached FAD. In the case of the variant, the ratio was much higher indicating a much lower saturation compared to the WT (ca. 40-50% apo-protein), similar to previously reported observations [19]. The higher fraction of apo-protein may be responsible for the recurring protein precipitation during purification of the variant. Overall, this led to substantially reduced yields of the variant protein and limited the scope of experiments that could be conducted.

Spectral Characteristics and Steady-state Kinetics of hDMGDH

Recombinant hDMGDH features characteristic UV-Vis absorption properties that clearly distinguish the bound FAD from FAD free in solution (Figure 2C). These spectral characteristics are very similar to those reported earlier for DMGDH isolated from rat and pig liver as well as for recombinant *AgDMGO* [8,16,20]. In contrast, the UV-Vis absorption spectra for heterologously expressed rat DMGDH [17] and human DMGDH [19] are either of very poor quality or apparently lack the spectral features that are typically found in these enzymes. In fact, the only published spectrum of hDMGDH expressed in *E. coli* is very similar to free FAD in solution (compare spectra shown in Figure 9).

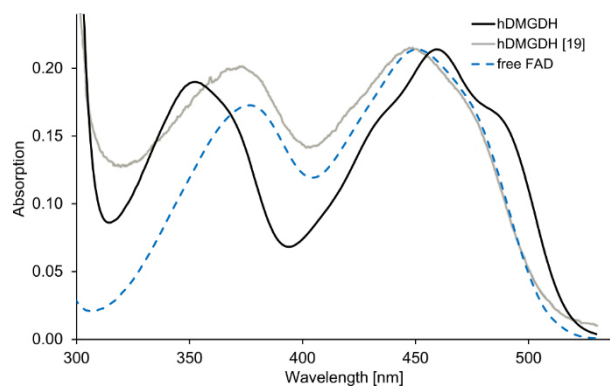


Figure 9. Protein spectrum of this study (black line) compared with the published hDMGDH spectrum (grey line, [19]) and free FAD in solution (dotted blue line). The published spectrum resembles free FAD in solution and not our spectral findings.

Table 3. Comparison of steady-state kinetic parameters of published results for the DMGDH from *Homo sapiens* (human), *Rattus norvegicus* (rat), *Sus scrofa* (pig) as well as the dimethylglycine oxidase from *A. globiformis* (*Ag*).

Enzyme	e-Acceptor	Conditions	K_M <i>mM</i>	k_{cat} <i>min⁻¹</i>	A_{spec} <i>$\mu\text{mol mg}^{-1} \text{min}^{-1}$</i>	k_{cat}/K_M <i>$\text{mM}^{-1} \text{min}^{-1}$</i>
human - this study	DCPIP	pH 7.8, 25 °C	0.3 ± 0.002^b	44 ± 1	0.5 ± 0.01	146 ± 12
human - this study	ferrocene	pH 7.8, 25 °C	1.4 ± 0.1	213 ± 4	2.0 ± 0.04	137 ± 16
human - [19]	ferrocene	pH 7.5, 25 °C	0.04 ± 0.01^b	18 ± 2	0.165^a	450 ± 110
rat - [18] ^a	ferrocene	pH 7.5, 25 °C	0.6	160	nd	270
rat - [17] ^a	DCPIP	pH 7.0, 30 °C	0.05^b	12.1	0.24	nd
rat - [16] ^a	DCPIP	pH 7.0, 25 °C	0.05^b	8.4	0.14	nd
pig - [8] ^a	DCPIP	pH 7.0, 25 °C	nd	nd	0.157	nd
<i>Ag</i> - [22]	O ₂	pH 8.5, 25 °C	2.4 ± 0.2	640 ± 20	nd	270 ± 32

nd... Not determined or stated in the publication. ^a No standard deviations available. ^b Two K_M values were observed but only the physiologically relevant is displayed.

A summary of our data and the previously published kinetic steady-state data is given in Table 3. These values were obtained using two different enzymatic activity assays, on the one hand with ferrocenium hexafluorophosphate as electron acceptor and on the other hand the combination of phenazine methosulfate (PMS) as electron mediator and 2,6-dichlorophenolindophenol (DCPIP) as terminal electron acceptor. Both assays are physiologically irrelevant as all mammalian DMGDHs interact with the electron transferring flavoprotein (hETF) for reoxidation of the reduced cofactor. With the ferrocene assay, we have obtained comparable results as reported for the rat enzyme [18] and also for the bacterial DMGO [22]. However, analysis of the data obtained with the PMS/DCPIP assay yielded two Michaelis-Menten constants similar to previously published data for the rat enzyme [16,17]. Interestingly, apart from the results reported by McAndrew *et al.* [19] two K_M values were only observed for the two component DCPIP activity assay, with PMS as electron mediator, but not in the one component ferrocene or H₂O₂ assay suggesting that it is an experimental artifact. In view of this apparent inconsistency, speculations that the presence of two K_M values reflect the presence of activating or regulatory sites in the enzyme are unwarranted [16,17]. Moreover, we have shown that the rate of

enzyme reduction is faster than k_{cat} indicating that reoxidation is rate-limiting for turnover in both assays. Thus, the affinity of DMG to hDMGDH is more reliably expressed as the dissociation constant determined in pre-steady-state experiments.

Effects of a Naturally Occurring H109R Enzyme Variation

The rare naturally occurring enzyme variant H109R causes a non-fatal disease called dimethylglycine dehydrogenase deficiency (OMIM: 605850). The defect results in an accumulation of DMG in blood serum and urine and patients suffer from a mild phenotype including muscle fatigue and fish like odor [9,10]. During heterologous expression in *K. phaffii* we noticed decreased expression levels resulting in much lower yields of the variant protein. Further characterization of the variant protein demonstrated lower cofactor saturation and thermal stability. Interestingly, the variant showed elevated turnover rates in both of our assay systems although K_M values were 15-25 times higher and the catalytic efficiency 10-fold lower than for the WT (Table 1). Hence, our results are clearly in contradiction with previously published data [19] that claimed significantly decreased catalytic activity of the H109R variant. Since the spectral properties of DMGDH preparations obtained from the *E. coli* expression system lacks the characteristic features typically observed for DMGDH isolated from natural sources (*e.g.* rat and pig liver) it is conceivable that recombinant DMGDH generated in bacterial host cells suffers from an altered FAD binding mode, such as non-covalent binding. In fact, the absorption spectrum reported for wild-type DMGDH and its H109R variant is clearly more similar to that of free FAD (Figure 9). In our hands, the bacterial expression system produced solely insoluble protein and therefore analysis of FAD binding to the protein could not be inspected further.

Previous reports on the structure of bacterial DMGO and rat DMGDH identified a large internal cavity in the protein [6,18]. This cavity serves as “reaction chamber” responsible for substrate delivery to the active site, substrate conversion, as well as intermediate channeling to THF and product formation. The binding site of THF is the only entry-exit point of the protein, which was revealed by MD simulations for the structurally related DMGO [6] and also confirmed by cavity analysis of our structure (Figure 10A). In accordance with this interpretation, increasing THF concentrations exhibited a negative effect on the turnover rate (Figure 5) as the substrate DMG competes with THF for entrance into the cavity at the THF binding site.

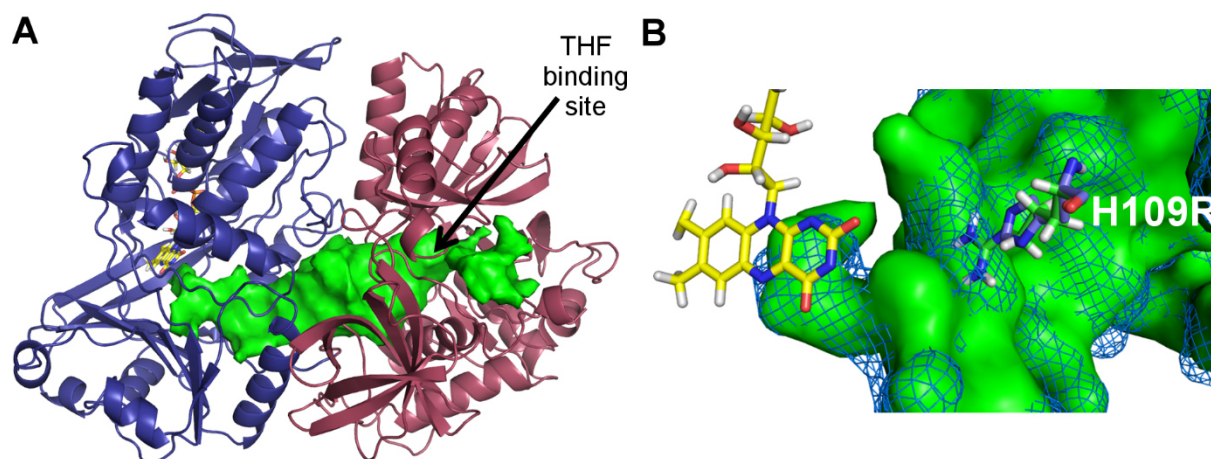


Figure 10. hDMGDH internal cavity analysis and effect of H109R variation. (A) Cavity analysis of hDMGDH done with CASoX in PyMOL without a bound THF cofactor. The protein cavity is shown in green surface view and the THF binding site indicated by an arrow. (B) Close-up view of the site of amino acid replacement (*i.e.* H109R) near the active site of the protein. A cavity analysis at this site was done in the wild-type enzyme (His-109, blue mesh) and the H109R variant (Arg-109, green surface). The bulky, charged arginine extends into the cavity calculated for the wild-type protein and potentially reduces the size of the substrate tunnel, thus substrate delivery to the FAD binding site. FAD cofactor is shown in yellow, the residues at position 109 in green and blue sticks, respectively.

The consistently (16 to 23-fold) higher K_M observed in both steady-state assays with the variant suggests that replacement of histidine by the bulkier arginine impedes access of DMG to the binding site (Figure 10B). On the other hand, the H109R variant possessed higher k_{cat} values indicating that the variant is more permissible in transferring electrons from the reduced FAD to the artificial electron acceptors.

In conclusion, our analysis of the disease related H109R variant has revealed a lower thermal stability and an approximately 10-fold lower catalytic efficiency (Table 1) as major effects of the single amino acid exchange. The diminished protein expression and cofactor saturation found in our expression system may also be relevant for homologous expression of the variant in human cells and thus contribute to the overall reduced DMGDH activity manifested in affected human subjects.

Substrate Specificity, Redox Behavior and Active Site Composition

The overall protein structure and the active site of hDMGDH with the covalently bound FAD as well as the THF binding site are very similar to the rat enzyme (PDB ID: 4PAA; [18]), and the structure of *AgDMGO* [21]. In 2003, *AgDMGO* could be crystallized with a bound folic acid (PDB ID: 1PJ6) but additionally also with a bound acetate ion that mimics the negatively charged carboxylate group of DMG (PDB ID: 1PJ5). Most residues in the active site of *AgDMGO* described to play a role in catalysis and substrate binding are also present in hDMGDH (Figure 11). Docking of DMG and sarcosine to the active site of the hDMGDH structure results in a similar positioning of both substrates (Figure 11A, B) and thus do not rationalize the differences observed in affinity and catalytic activity. This binding mode is

similar to the acetate moiety in the crystal structure of DMGO (Figure 11C). Pre-steady-state measurements comparing DMG and sarcosine as substrate for hDMGDH-WT show a 25-fold decrease of the reductive rate for sarcosine as the substrate and a more than 50-fold higher K_D . These results are in very good agreement with data obtained for the bacterial DMGO (Table 4) [22]. Therefore, sarcosine is a poor but possibly physiologically relevant substrate for the enzyme as already shown previously for the pig enzyme [3] and *AgDMGO* [22]. On the other hand, sarcosine is apparently oxidized by a homologous sarcosine dehydrogenase (SARDH) [16] and also by peroxisomal sarcosine oxidase (PIPOX) [30]. Therefore, the relative turnover of sarcosine by these three FAD-dependent enzymes must await further studies.

Table 4. Summary and comparison of transient kinetic data of hDMGDH (this study) with published results from *A. globiformis* DMGO [22,23]. Measurements were done in a stopped flow at pH 7.8 and 25 °C for hDMGDH and 25 °C and pH 8.5 for the bacterial enzyme.

	K_D , DMG	k_{red} , DMG	K_D , SAR	k_{red} , SAR	K_{ox}	$k_{obs,ox}$
	<i>mM</i>	<i>s⁻¹</i>	<i>mM</i>	<i>s⁻¹</i>	<i>mM⁻¹ s⁻¹</i>	<i>s⁻¹</i>
hDMGDH	4.9 ± 0.3	17 ± 0.3	280 ± 10	0.7 ± 0.1	0.04 ± 0.01	0.006 ± 0.001 ^b
<i>AgDMGO</i>	~ 10 ^a	15 ± 0.2	850 ± 100	0.16 ± 0.1	201	26 ^c

^a Retrieved from Table 2 in [23] ^b Measured at an oxygen concentration of 135 μM with $p_{O_2} = 0.105$ bar, $K_{H,pc} = 791$ bar M⁻¹ [31] for the substrate reduced enzyme. ^c Estimation from Figure 8 in [22].

In the bacterial enzyme, a catalytic dyad, consisting of a histidine and a tyrosine, is responsible for deprotonation of the substrate amine [21]. This catalytic dyad is also present in the human enzyme (Figure 11). Furthermore, residues interacting with DMG (and sarcosine) were identified in the structure of hDMGDH (Figure 11A). After binding and conversion of the substrate at the active site, an intermediate, most likely a cyclic lactone is channeled through the protein cavity to the THF binding site [6]. The THF binding sites of mammalian and bacterial enzymes are again very similar and were already extensively discussed by Luka *et al.* [18].

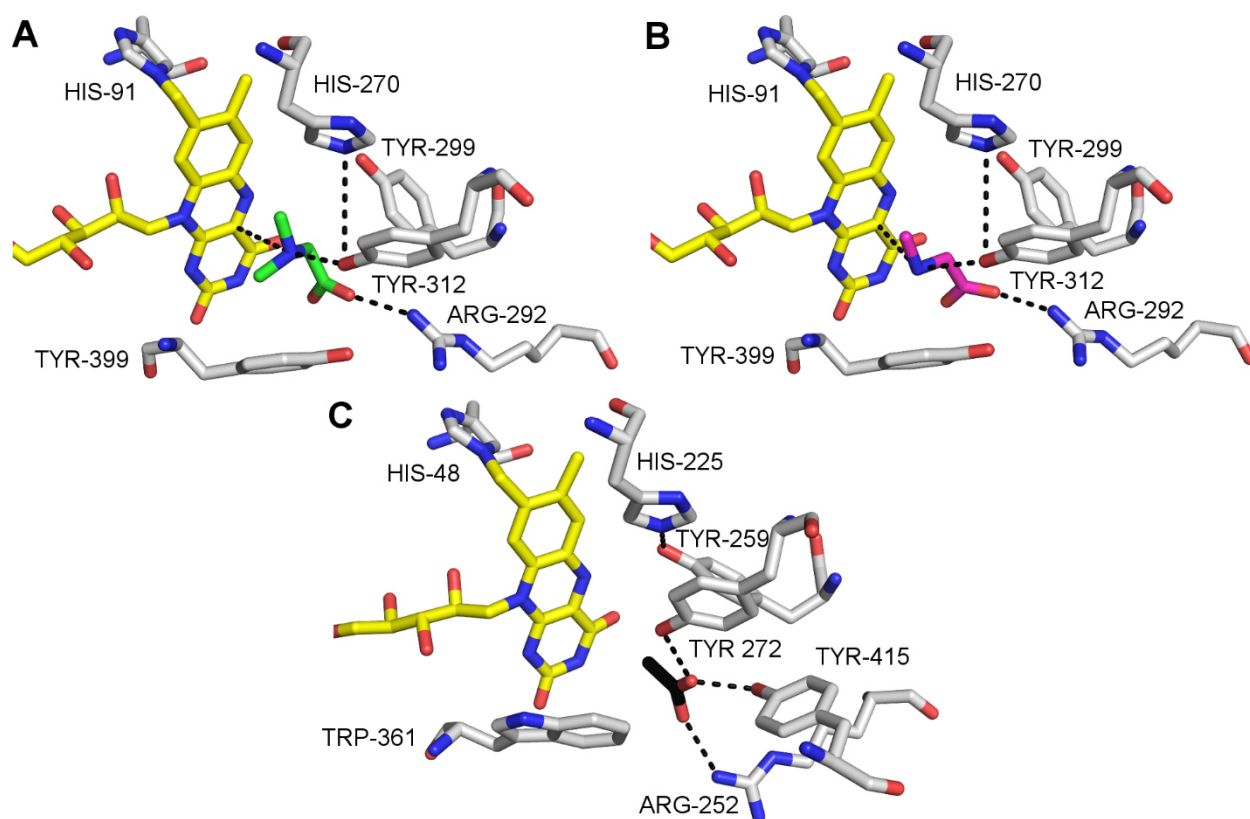


Figure 11. Docking and active site composition of hDMGDH in comparison with bound acetate in DMGO structure. DMG (A) and sarcosine (B) were docked into the active site of hDMGDH with Autodock/VINA [32]. The active site of DMGO with bound acetate was retrieved from **PDB ID: 1PJ5**. The docked substrates and the bound acetate are shown in green, magenta and black. FAD is shown in yellow and all residues are depicted in stick representation colored according the atom type. Key hydrogen bonds are shown with black dotted lines.

Basran *et al.* reported a multistep kinetic model for the reduction of DMGO by DMG. In contrast, the reduction of hDMGDH by DMG was adequately fit by a single exponential equation. The actual measurement of the intermediate cyclic lactone could not be observed, most likely due to its short lifetime as described in detail elsewhere [6].

The two dehydrogenases in choline degradation belong to a family of enzymes that delivers electrons to the electron transferring flavoprotein (ETF). Among these clients only the redox potential for the two-electron reduction of human medium-chain acyl-CoA dehydrogenases (hMCAD) was previously determined [33,34]. This prompted us to determine the redox potential for the covalently bound FAD in hDMGDH. The obtained value of -93 ± 1 mV is 40 mV more positive than that of hMCAD (-135 mV [33,34]) in agreement with the fact that covalent linkages to the 8-methyl group increase the redox potential [35]. In any case, the much higher redox potential of hETF (+37 mV for the oxidized/semiquinone couple, [36]) ensures that electrons from hDMGDH are readily transferred to the ETF-bound FAD.

The rates of reduction determined for hDMGDH are in good agreement with those observed for bacterial DMGO (Table 4). In contrast to that, the oxygen reactivity of reduced hDMGDH is more than 300 times lower and apparently physiologically irrelevant as re-oxidation by its cognate partner protein hETF proceeds over 30 times faster (unpublished results).

Recently, a study concerning steric control of dioxygen reduction in enzymes of the vanillyl-alcohol oxidase (VAO) family, discovered a new “gate keeper” residue in berberine bridge enzyme and the pollen allergen Phl p 4 [25]. This gate keeper appears to control access to an oxyanion hole essential to stabilize reaction intermediates during oxidation of the reduced isoalloxazine ring by dioxygen. In this family, valine was found to grant access to the oxyanion hole whereas isoleucine denies access [25]. Similarly, Leferink *et al.* discovered that a large number of oxidases in the VAO family contain either a glycine or a proline at a structurally conserved position near the isoalloxazine ring [26]. Although hDMGDH does not belong to the VAO-protein superfamily, comparison of the hDMGDH to the *AgDMGO* structure reveals that hDMGDH features residues typical for dehydrogenases suppressing oxygen reactivity, *i.e.* an alanine and isoleucine, whereas *AgDMGO* possesses residues compatible with high oxygen reactivity, *i.e.* proline and valine (Figure 12). Nevertheless, in order to further support, if the emerging concept of how oxygen reactivity is controlled in flavoproteins is applicable to DMGDH, a member of the D-amino acid oxidase (DAO) family of FAD-dependent oxidoreductases (pfam: 01266), a detailed mutagenesis study of the concerned residues has to be conducted.

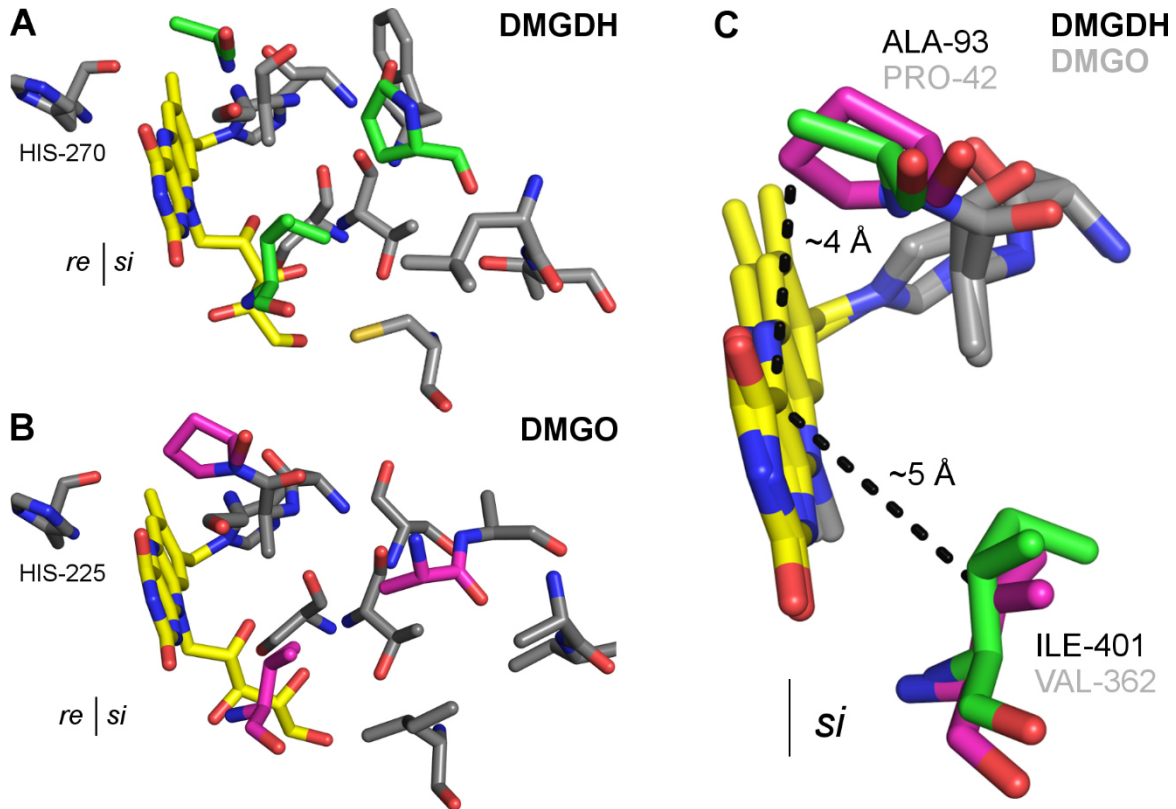


Figure 12. Active site composition of the oxygen binding site of hDMGDH and AgDMGO. The human structure is shown in panel A with the most significant alternated residues on the *si*-face of the flavin isoalloxazine ring shown in green sticks. The bacterial structure is shown in panel B; important residues are shown in magenta. For a better orientation, the catalytic active histidine on the *re*-face is also displayed. Panel C shows the alignment of the bacterial and the human enzyme with the supposed gate-keeper residues shown corresponding to the reactive C(4a) carbon of the isoalloxazine ring. All residues are depicted in stick representation, FAD in yellow and colored according to the atom type.

EXPERIMENTAL PROCEDURES

Enzymes and Reagents – Restriction enzymes and Phusion DNA polymerase were from Thermo Fisher Scientific (Waltham, MA, USA), purification columns and materials from GE Healthcare (Chalfont St Giles, UK) and salt free purified oligos for site directed mutagenesis from VBC-Biotech (Vienna, Austria). Antibodies used for Western blot were from Cell Signaling Technology (Cambridge, UK). The redox dye for the determination of the redox potential, indigotrisulfonic acid potassium salt, was from TCI Europe N.V. (Zwijndrecht, Belgium). All other chemicals and media were from Carl Roth GmbH (Karlsruhe, Germany) and Sigma-Aldrich (St. Louis, MO, USA) and were of the highest grade available.

hDMGDH Expression Strain Generation – hDMGDH and hDMGDH-H109R expression plasmids were designed for intracellular enzyme expression in *Komagataella phaffii* KM71H strain (formerly known as *Pichia pastoris* or *Komagataella pastoris* [24]). The hDMGDH sequence was codon optimized for expression in *K. phaffii* using GeneOptimizer[®] (Thermo Fisher Scientific). In accordance to Binzak *et al.*, the sequence of the mature form of hDMGDH (lacking the first 28 amino acids, [29]) was used, flanked with *XhoI* and *NotI* restriction sites. For enzyme expression and purification, a Kozak sequence in front of the start codon (AAAA) and a C-terminal nona-histidine tag were added. The designed gene was cloned into a pPICZ B expression vector (Thermo Fisher Scientific) and verified by automated sequencing. The recombinant plasmid was transformed to *K. phaffii* KM71H strain (Thermo Fisher Scientific), harboring a pPICK-PDI vector containing the gene for the protein-disulfide isomerase from *Saccharomyces cerevisiae* following the guidelines of the Invitrogen EasySelect[™] *Pichia* Expression Kit (Thermo Fisher Scientific). Positive clones were selected by Zeocin resistance and verified by Western blot. The H109R variant was constructed by a two-step site directed mutagenesis method employing Phusion DNA polymerase and 5'-AACTTGAAGAAGATCAGATATCGACTCCATCAAG-3' as forward and 5'-CTTGATGGAGTCGATTCTGATCTTCTTCAAGTT-3' as reverse primer (alternated codon underlined). For the first reaction step, two separate PCR reactions using either the forward or the reverse primer were run (98 °C (2 min) – [98 °C (50 sec) – 60 °C (20 sec) – 68 °C (16.5 min)] x 5 – 4 °C ∞). Afterwards, the two PCR reactions were combined and the same program was employed for another 20 cycles. Then, after a 2 h *DpnI* digestion step, the plasmid was transformed to *Escherichia coli* TOP10 cells for amplification before transformation to *K. phaffii* KM71H [pPICK-PDI]. Strain selection was done as described above.

Enzyme Expression – hDMGDH and hDMGDH-H109R expression was carried out in a 7 L glass fermenter BBI CT5-2 system (Sartorius, Göttingen, Germany). Preparation of inoculum, preparation of the fermenter, batch and fed-batch were carried out as described by Schrittwieser *et al.* [37]. The fermentation medium was a minimal basal salt medium (MgSO₄ · 7 H₂O – 1.2 g/L; K₂SO₄ – 14.9 g/L; KOH – 18.2 g/L; NaCl – 4.13 g/L; glycerol – 40 g/L; 85% H₃PO₄ – 27 mL/L). After the fed-batch, the methanol induction was started by injection of 5 g MeOH directly into the fermenter and afterwards by a stepwise increase of methanol feed from 0 to 6 g/h over 2 h. Glycerol feed was reduced from 15 g/h

to 6 g/h over 2 h and a mixed MeOH/glycerol feed was maintained until the end of the fermentation. In total, 400-500 g methanol were fed to the cultures before harvest after 96 h of induced growth. Samples were taken for Western blot analysis at different time points. The cell pellet was collected by centrifugation (4 000 rpm, 30 min, 4 °C) and stored at -20 °C.

Enzyme Purification – Cell lysates were prepared by Merckenschlager (Braun Biotech International, Melsungen, Germany) glass beads cell homogenization under CO₂ cooling (3 min disruption steps). For every 1 g harvested wet cell pellet, 2 mL cell lysis buffer (50 mM HEPES/NaOH, 150 mM NaCl, 35 mM imidazole, 1 mM PMSF, pH 7.8) and a spatula tip of FAD were added before cell disruption. The lysates were cleared by centrifugation (18 000 rpm, 30 min, 4 °C) and filtration through a paper filter. Nickel ion affinity chromatography was done by applying the lysates onto self-packed nickel-Sepharose 6 Fast Flow columns (GE Healthcare) at 4 °C. Afterwards, the material was washed with washing buffer (50 mM HEPES/NaOH, 150 mM NaCl, 75 mM imidazole, pH 7.8) and the enzyme stripped with elution buffer (50 mM HEPES/NaOH, 150 mM NaCl, 300 mM imidazole, pH 7.8). The purification was monitored by SDS-PAGE and fractions containing hDMGDH were concentrated and rebuffered to storage buffer (50 mM HEPES/NaOH, 150 mM NaCl, pH 7.8) using Amicon ultracentrifugal filter units (50 kDa cut-off, Merck-Milipore, Darmstadt, Germany). The obtained enzyme purity was sufficient for kinetic and photometric studies of the enzymes. If a higher enzyme purity was needed, especially for protein crystallization, the eluted fractions of the affinity chromatography were rebuffered to buffer A (25 mM HEPES/NaOH, 25 mM NaCl, pH 7.8) and anion exchange chromatography with a MonoQ 5/50 GL column (GE Healthcare) was done on an ÄKTA FPLC system (GE Healthcare) at 4 °C. The protein was eluted with a gradient from 0-50% buffer B (25 mM HEPES/NaOH, 1 M NaCl, pH 7.8). The chromatography was controlled by SDS-PAGE and fractions containing hDMGDH were concentrated and rebuffered to storage buffer as described above. Purification was done identically for the wild-type and the variant enzyme.

SDS-PAGE – Enzyme samples were separated by SDS-PAGE, with 12.5% separation gels (for Western blot 10%), under reducing conditions as described by Laemmli [38]. Gels were either used for Western blot analysis or stained with Coomassie Brilliant Blue R-250 for purification control. As protein standard a PageRuler Prestained protein ladder (Thermo Fisher Scientific) was employed.

Western Blot – *K. phaffii* cell lysates for Western blot screening and control of fermentation were prepared by glass bead disruption following the Invitrogen EasySelect™ *Pichia* Expression Kit manual (p. 42, Thermo Fisher Scientific). Western blot analysis was done on nitrocellulose membranes essentially following the General Protocol for Western blotting from Bio-Rad (Hercules, CA, USA, Bulletin 6376). As antibodies, a rabbit anti-histidine IgG antibody at 1:2000 overnight at 4 °C as primary and an HRP-linked goat anti-rabbit IgG antibody at 1:5000 for 1 h at room temperature as secondary antibody were used. As loading control, a rabbit anti-GAPDH antibody was used in a 1:1000 dilution

overnight. Immunoreactive signals were obtained using SuperSignal West Pico Chemiluminescent Substrate (Thermo Fisher Scientific) and detection in a G:BOX (Syngene, Cambridge, UK).

UV-Vis Absorption Spectroscopy – UV-Vis absorption spectra to assess protein concentration, activity, purity, quality and cofactor saturation as well as for steady-state kinetic measurements and photoreduction were recorded with a Specord 210 spectrophotometer (Analytik Jena, Jena, Germany).

Enzyme Quantification and Calculation of the Extinction Coefficient – Protein concentrations of purified hDMGDH enzymes were determined according the characteristic absorption of bound FAD at 450 nm. The molar extinction coefficient for hDMGDH was calculated using the method described by Macheroux [39] to $11\,600\text{ M}^{-1}\text{ cm}^{-1}$.

Steady-state Kinetics – Steady-state kinetic parameters were determined using 2,6-dichlorophenol-indophenol (DCPIP) according to Okamura-Ikeda *et al.* [40] or ferrocenium hexafluorophosphate (Fc^+PF_6^-) as described by Lehman *et al.* [41] as terminal electron acceptor and measurable dimension in the spectrophotometer. In short, DCPIP-assays were performed at 25 °C and pH 7.8 in 50 mM HEPES/NaOH, 150 mM NaCl, 135 μM DCPIP and 100 nM hDMGDH with freshly prepared 3 mM phenazine methosulfate (PMS) as intermediate electron mediator and 0-100 mM dimethylglycine (DMG) following the change of absorption spectrophotometrically at 600 nm over 3 min. Ferrocenium assays were performed at 25 °C at pH 7.8 in 50 mM HEPES/NaOH, 150 mM NaCl, 0.1 mM EDTA, 100 nM hDMGDH, 0-100 mM DMG and freshly prepared 0.2 mM Fc^+PF_6^- following the change of absorption at 300 nm over 3 min. For each concentration at least a triplicate measurement was performed, the initial velocities determined and K_M and k_{cat} assessed by non-linear hyperbolic fit in Origin 8.6 (OriginLab Corp., Northampton, MA, USA).

Pre-steady-state Kinetics – Pre-steady-state reaction kinetics were measured anaerobically with a Hi-Tech stopped flow instrument (SF-61DX2, TgK Scientific Limited, Bradford-on-Avon, UK) in a glove box (Belle Technology, Weymouth, UK) at 25 °C. For determination of the reductive rates of enzyme bound FAD, 20 μM purified hDMGDH in 50 mM HEPES/NaOH, pH 7.8 containing 150 mM NaCl was shot against different concentrations of DMG (0.25-250 mM) or sarcosine (0-500 mM) dissolved in 50 mM HEPES/NaOH, 150 mM NaCl pH 7.8 and monitored at 460 nm with a KinetaScanT diode array detector (MG-6560, TgK Scientific Limited). Each concentration was measured in triplicates and the observed rate constants (k_{obs}) for different substrate concentrations were calculated using an exponential fitting function in the Kinetic Studio software (TgK Scientific Limited). The dissociation constant (K_D) was determined by a hyperbolic fitting curve employing Origin 8.6 (OriginLab Corp.). The oxidative rate (k_{ox}) of the enzyme was measured three times at an oxygen concentration of 10.5% O_2 (135 μM O_2), by mixing substrate reduced hDMGDH with air equilibrated buffer (50 mM HEPES/NaOH, 150 mM NaCl, pH 7.8).

Determination of the Redox Potential – The redox potential (E_0) of the enzyme bound FAD was measured by the dye-equilibration method using the xanthine/xanthine oxidase system as described by Massey [27]. The concentrations of enzyme and redox dye were chosen in a way that their absorption maxima were in the same range. The reactions were performed with a Hi-Tech stopped-flow device (SF-61DX2, TgK Scientific Limited). The measurements took place under anaerobic conditions in a glove box (Belle Technology) at 25 °C in 50 mM HEPES/NaOH, 150 mM NaCl, pH 7.0. The simultaneous reduction of FAD and the redox dye was monitored with a KinetaScanT diode array detector (MG-6560, TgK Scientific Limited). The reaction was started by mixing a solution containing 300 μ M xanthine, 5 μ M benzyl viologen and an appropriate amount of enzyme with a solution containing catalytic amounts of xanthine oxidase (approx. 200 nM, from bovine milk, Grade III purity, Sigma-Aldrich) and the redox dye indigotrisulfonic acid dipotassium salt (E_0 , pH 7.0, 25 °C = -81 mV). The redox potential was calculated using double logarithmic plots, $\log(\text{ox/red})$ of the enzyme versus $\log(\text{ox/red})$ of the dye, according to Minnaert [28]. A linear least-squares fit was done with Excel 2010 (Microsoft, Redmond, WA, USA).

Anaerobic Photoreduction and Reoxidation – Photoreduction of hDMGDH was done according to the procedure reported by Massey and Hemmerich [42]. 20 μ M purified enzyme sample in 50 mM HEPES/NaOH, pH 7.8 containing 150 mM NaCl, 1 mM EDTA, 1 μ M 5-diaza-FMN and 2 μ M methyl viologen were rendered anaerobic by 2 h incubation in sealable quartz cuvettes in a glove box (Belle Technology). Photoirradiation was carried out with a 10 W LED flood light (Luminea, Buggingen, Germany) and cooling of the cuvette to 15 °C. Spectra were recorded until no further changes were observed. For reoxidation of the enzyme, the cuvettes were exposed to air oxygen and absorption spectra were recorded until no further changes were observed.

Temperature Stability – 1) *Thermofluor*[®] – The temperature stability of the enzymes was assessed by monitoring the change in fluorescence using the solvatochromic dye SYPRO Orange (Sigma-Aldrich) in a Thermofluor[®] assay. Thermofluor[®] measurements were carried out as reviewed elsewhere [43] in an FX Connect real time PCR system (Bio-Rad) in 25 μ L of 50 mM HEPES/NaOH, pH 7.8, containing 150 mM NaCl, 10 μ M of enzyme and 2.5 μ L of a 500 x dilution of a SYPRO Orange Enzyme Gel stain. The samples were pre-heated to 25 °C and then the temperature was increased in 0.5 °C/min steps to 95 °C. Fluorescence data were collected using the FRET channel. Melting temperatures (T_m) were determined using CFX Manager 3.0 software (Bio-Rad). 2) *Circular Dichroism (CD) Spectroscopy* – CD spectra were recorded on a PS-150J spectropolarimeter (Jasco, Groß-Umstadt, Germany) using a 0.02 cm water-jacketed cylindrical cell thermostatically controlled by an external computer-controlled water bath (Julabo F25, Seelbach, Germany). Thermal denaturation data were recorded in a temperature range from 25–95 °C with a heating rate of 1 °C/min, a response of 1 sec and a resolution of 0.1 °C. The protein concentration used was approximately 6 μ M in 50 mM HEPES/NaOH, 50 mM NaCl, pH 7.8.

The melting temperature was estimated as the point of inflection of the temperature dependent mean residue ellipticity at 208 nm.

Crystallization of hDMGDH – Crystallization experiments were performed with the microbatch method using different commercial crystallization screens (Index and Morpheus Screen from Hampton Research (Aliso Viejo, CA, USA) and Molecular Dimensions (Newmarket, UK), respectively). Drops were prepared by mixing 0.5 μ L of the protein solution (at a concentration of 4 mg/ml in 25 mM HEPES, 25 mM NaCl and 2 mM DTT, pH 7.5) with an equal volume of mother liquor using an ORYX 8 pipetting robot (Douglas Instruments, Hungerford, UK). The drops were sealed with a 3:1 mixture of paraffin and silicon oil and the trays incubated at 20 °C. First crystal clusters were observed after approximately one month in various conditions. Further optimization involved dilutions of the original condition using 25 mM HEPES, 25 mM NaCl, 2 mM DTT, pH 7.5. Diffracting hDMGDH crystals were obtained with a 1:3 dilution of the original condition H5 of the Morpheus Screen consisting of 10% w/v PEG 20000, 20% v/v PEG MME 550, 0.02 M of each amino acid and 0.1 M MOPS/HEPES-Na pH 7.5.

Data Collection and Processing – X-ray diffraction data were collected to a maximum resolution of 3.1 Å on beam line ID29 ($\lambda=0.972$ Å) at the ESRF Grenoble, France. The crystals were monoclinic (space group $P2_1$) with unit-cell parameters $a=83.38$ Å, $b=119.87$ Å, $c=86.47$ Å and $\beta=92.6^\circ$. The data were processed using the XDS package [44] and the structure was solved by molecular replacement using the structure of the rat dimethylglycine dehydrogenase (**PDB ID: 4PAA**, 90% sequence identity) [18]. Structure rebuilding and refinement were performed using the programs Coot [45] and PHENIX [46]. The model contained one B-factor per amino acid residue. Non-crystallographic-symmetry (NCS) restraints were applied. A small number of water molecules were added manually only into the most significant electron difference electron density peaks before the last cycle of refinement. Clear electron density was observed for the majority of the amino acids except of the first 18 N-terminal residues and the 13 C-terminal residues in both chains present in the asymmetric unit. Residual density was interpreted as flavin adenine dinucleotide (FAD) in both chains. The final structure was validated using MolProbity [47]. Detailed statistics pertaining to data processing and structure refinement are summarized in Table 2. The atomic coordinates and structure factors have been deposited in the Protein Data Bank under the accession number 5L46.

In Silico Procedures – Figures for structural analyses were prepared using PyMOL (DeLano Scientific [48]). *In silico* mutagenesis of hDMGDH residue H109 to R109 in the crystal structure was performed with the mutagenesis wizard of PyMOL (DeLano Scientific, San Carlos, CA, USA) and subsequent energy minimization using YASARA (Yasara Biosciences, Vienna, Austria). Docking experiments of DMG and sarcosine into the hDMGDH structure was done using Autodock/VINA [32] as implemented in YASARA. Cavity analyses after and before mutagenesis was performed with the LIGSITE algorithm (CASoX plugin of PyMOL, [49]).

ACKNOWLEDGMENTS

This work was supported by a grant from the Austrian Science Foundation (FWF) to KG and PM (Doctoral program “Molecular Enzymology” W901). The authors would like to thank the *Exome Aggregation Consortium* and the groups that provided exome variant data for comparison. A full list of contributing groups can be found at <http://exac.broadinstitute.org/about>.

AUTHOR CONTRIBUTIONS

PA has expressed, purified and characterized the wild-type enzyme and the variant; AH, TPK and KG crystallized proteins and determined the crystal structure of WT hDMGDH; PA and PM designed biochemical experiments and interpreted the data; PA, AH, TPK, KG and PM wrote the manuscript.

REFERENCES

- 1 Lienhart WD, Gudipati V & Macheroux P (2013) The human flavoproteome. *Arch. Biochem. Biophys.* **535**, 150–162.
- 2 Wittwer AJ & Wagner C (1981) Identification of the folate-binding proteins of rat liver mitochondria as dimethylglycine dehydrogenase and sarcosine dehydrogenase. Purification and folate-binding characteristics. *J. Biol. Chem.* **256**, 4102–4108.
- 3 Wittwer AJ & Wagner C (1981) Identification of the folate-binding proteins of rat liver mitochondria as dimethylglycine dehydrogenase and sarcosine dehydrogenase. Flavoprotein nature and enzymatic properties of the purified proteins. *J. Biol. Chem.* **256**, 4109–4115.
- 4 Ueland PM (2011) Choline and betaine in health and disease. *J. Inherit. Metab. Dis.* **34**, 3–15.
- 5 Wittwer AJ (1980) Identification of Folate Binding Protein of Mitochondria as Dimethylglycine Dehydrogenase. *Proc. Natl. Acad. Sci.* **77**, 4484–4488.
- 6 Tralau T, Lafite P, Levy C, Combe JP, Scrutton NS & Leys D (2009) An internal reaction chamber in dimethylglycine oxidase provides efficient protection from exposure to toxic formaldehyde. *J. Biol. Chem.* **284**, 17826–17834.
- 7 Ruzicka FJ & Beinert H (1977) A new iron-sulfur flavoprotein of the respiratory chain. *J. Biol. Chem.* **252**, 8440–8445.
- 8 Steenkamp DJ & Husain M (1982) The effect of tetrahydrofolate on the reduction of electron transfer flavoprotein by sarcosine and dimethylglycine dehydrogenases. *Biochem. J.* **203**, 707–715.
- 9 Moolenaar SH, Poggi-Bach J, Engelke UFH, Corstiaensen JMB, Heerschap A, De Jong JGN, Binzak BA, Vockley J & Wevers RA (1999) Defect in dimethylglycine dehydrogenase, a new inborn error of metabolism: NMR spectroscopy study. *Clin. Chem.* **45**, 459–464.
- 10 Binzak B a, Vockley JG, Jenkins RB & Vockley J (2000) Structure and analysis of the human dimethylglycine dehydrogenase gene. *Mol. Genet. Metab.* **69**, 181–7.
- 11 Sreekumar A, Poisson LM, Rajendiran TM, Khan AP, Cao Q, Yu J, Laxman B, Mehra R, Lonigro RJ, Li Y, Nyati MK, Byun J, Omenn GS, Ghosh D, Pennathur S, Alexander DC, Berger A, Shuster JR, Wei JT, Varambally S, Beecher C & Chinnaiyan AM (2009) Metabolomic profiles delineate potential role for sarcosine in prostate cancer progression. *Nature* **457**, 910–914.
- 12 Ferro M, Buonerba C, Terracciano D, Lucarelli G, Cosimato V, Bottero D, Deliu VM, Ditunno P, Perdonà S, Autorino R, Coman I, De Placido S, Di Lorenzo G & De Cobelli O (2016) Biomarkers in localized prostate cancer. *Futur. Oncol.* **12**, 399–411.
- 13 Magnusson M, Wang TJ, Clish C, Engström G, Nilsson P, Gerszten RE & Melander O (2015) Dimethylglycine Deficiency and the Development of Diabetes. *Diabetes* **64**, 3010–6.
- 14 Hoskins DD & Mackenzie CG (1961) Solubilization and electron transfer flavoprotein requirement of mitochondrial sarcosine dehydrogenase and dimethylglycine dehydrogenase. *J. Biol. Chem.* **236**, 177–83.

- 15 Frisell WR & Mackenzie CG (1962) Separation and purification of sarcosine dehydrogenase and dimethylglycine dehydrogenase. *J. Biol. Chem.* **237**, 94–98.
- 16 Porter DH, Cook RJ & Wagner C (1985) Enzymatic properties of dimethylglycine dehydrogenase and sarcosine dehydrogenase from rat liver. *Arch. Biochem. Biophys.* **243**, 396–407.
- 17 Brizio C, Brandsch R, Bufano D, Pochini L, Indiveri C & Barile M (2004) Over-expression in *Escherichia coli*, functional characterization and refolding of rat dimethylglycine dehydrogenase. *Protein Expr. Purif.* **37**, 434–42.
- 18 Luka Z, Pakhomova S, Loukachevitch L V, Newcomer ME & Wagner C (2014) Folate in demethylation: the crystal structure of the rat dimethylglycine dehydrogenase complexed with tetrahydrofolate. *Biochem. Biophys. Res. Commun.* **449**, 392–8.
- 19 McAndrew RP, Vockley J & Kim J-JP (2008) Molecular basis of dimethylglycine dehydrogenase deficiency associated with pathogenic variant H109R. *J. Inherit. Metab. Dis.* **31**, 761–8.
- 20 Meskys R, Harris RJ, Casaitė V, Basran J & Scrutton NS (2001) Organization of the genes involved in dimethylglycine and sarcosine degradation in *Arthrobacter* spp.: implications for glycine betaine catabolism. *Eur. J. Biochem.* **268**, 3390–8.
- 21 Leys D, Basran J & Scrutton NS (2003) Channelling and formation of “active” formaldehyde in dimethylglycine oxidase. *EMBO J.* **22**, 4038–48.
- 22 Basran J, Bhanji N, Basran A, Nietlispach D, Mistry S, Meskys R & Scrutton NS (2002) Mechanistic aspects of the covalent flavoprotein dimethylglycine oxidase of *Arthrobacter globiformis* studied by stopped-flow spectrophotometry. *Biochemistry* **41**, 4733–43.
- 23 Basran J, Fullerton S, Leys D & Scrutton NS (2006) Mechanism of FAD reduction and role of active site residues His-225 and Tyr-259 in *Arthrobacter globiformis* dimethylglycine oxidase: Analysis of mutant structure and catalytic function. *Biochemistry* **45**, 11151–11161.
- 24 Kurtzman CP (2009) Biotechnological strains of *Komagataella (Pichia) pastoris* are *Komagataella phaffii* as determined from multigene sequence analysis. *J. Ind. Microbiol. Biotechnol.* **36**, 1435–1438.
- 25 Zafred D, Steiner B, Teufelberger AR, Hromic A, Karplus PA, Schofield CJ, Wallner S & Macheroux P (2015) Rationally engineered flavin-dependent oxidase reveals steric control of dioxygen reduction. *FEBS J.* **282**, 3060–3074.
- 26 Leferink NGH, Fraaije MW, Joosten HJ, Schaap PJ, Mattevi A & van Berkel WJH (2009) Identification of a gatekeeper residue that prevents dehydrogenases from acting as oxidases. *J. Biol. Chem.* **284**, 4392–4397.
- 27 Massey V (1991) A simple method for the determination of redox potentials. In *Flavins and Flavoproteins* (Curti B, Zanetti G, & Ronchi S, eds), pp. 59–66. Walter de Gruyter, Como, Italy.
- 28 Minnaert K (1965) Measurement of the equilibrium constant of the reaction between cytochrome c and cytochrome a. *Biochim. Biophys. Acta - Enzymol. Biol. Oxid.* **110**, 42–56.

- 29 Binzak B a, Wevers R a, Moolenaar SH, Lee YM, Hwu WL, Poggi-Bach J, Engelke UF, Hoard HM, Vockley JG & Vockley J (2001) Cloning of dimethylglycine dehydrogenase and a new human inborn error of metabolism, dimethylglycine dehydrogenase deficiency. *Am. J. Hum. Genet.* **68**, 839–47.
- 30 Dodt G, Kim DG, Reimann SA, Reuber BE, McCabe K, Gould SJ & Mihalik SJ (2000) L-Pipecolic acid oxidase, a human enzyme essential for the degradation of L-pipecolic acid, is most similar to the monomeric sarcosine oxidases. *Biochem. J.* **345 Pt 3**, 487–94.
- 31 Sander R (2015) Compilation of Henry's law constants (version 4.0) for water as solvent. *Atmos. Chem. Phys.* **15**, 4399–4981.
- 32 Trott O & Olson AJ (2010) AutoDock Vina: improving the speed and accuracy of docking with a new scoring function, efficient optimization, and multithreading. *J. Comput. Chem.* **31**, 455–61.
- 33 Gustafson W, Feinberg B & McFarland, JT (1986) Energetics of beta-oxidation. Reduction potentials of general fatty acyl-CoA dehydrogenase, electron transfer flavoprotein, and fatty acyl-CoA substrates. *J. Biol. Chem.* **261**, 7733–7741.
- 34 Lenn ND, Stankovich MT & Liu HW (1990) Regulation of the redox potential of general acyl-CoA dehydrogenase by substrate binding. *Biochemistry* **29**, 3709–3715.
- 35 Fraaije MW, van den Heuvel RH, van Berkel WJ & Mattevi A (1999) Covalent flavinylation is essential for efficient redox catalysis in vanillyl-alcohol oxidase. *J. Biol. Chem.* **274**, 35514–20.
- 36 Salazar D, Zhang L, deGala GD & Frerman FE (1997) Expression and Characterization of Two Pathogenic Mutations in Human Electron Transfer Flavoprotein. *J. Biol. Chem.* **272**, 26425–26433.
- 37 Schrittwieser JH, Resch V, Wallner S, Lienhart W-D, Sattler JH, Resch J, Macheroux P & Kroutil W (2011) Biocatalytic organic synthesis of optically pure (S)-scoulerine and berbine and benzyloquinoline alkaloids. *J. Org. Chem.* **76**, 6703–14.
- 38 Laemmli UK (1970) Cleavage of Structural Proteins during the Assembly of the Head of Bacteriophage T4. *Nature* **227**, 680–685.
- 39 Macheroux P (1999) UV-visible spectroscopy as a tool to study flavoproteins. *Methods Mol. Biol.* **131**, 1–7.
- 40 Okamura-Ikeda K, Ikeda Y & Tanaka K (1985) An essential cysteine residue located in the vicinity of the FAD-binding site in short-chain, medium-chain, and long-chain acyl-CoA dehydrogenases from rat liver mitochondria. *J. Biol. Chem.* **260**, 1338–45.
- 41 Lehman TC & Thorpe C (1990) Alternate electron acceptors for medium-chain acyl-CoA dehydrogenase: Use of ferricenium salts. *Biochemistry* **29**, 10594–10602.
- 42 Massey V, Hemmerich P, Knappe WR, Duchstein HJ & Fenner H (1978) Photoreduction of flavoproteins and other biological compounds catalyzed by deazaflavins. Appendix: photochemical formation of deazaflavin dimers. *Biochemistry* **17**, 9–17.

- 43 Boivin S, Kozak S & Meijers R (2013) Optimization of protein purification and characterization using Thermofluor screens. *Protein Expr. Purif.* **91**, 192–206.
- 44 Kabsch W (2010) XDS. *Acta Crystallogr. Sect. D Biol. Crystallogr.* **66**, 125–132.
- 45 Emsley P, Lohkamp B, Scott WG & Cowtan K (2010) Features and development of Coot. *Acta Crystallogr. Sect. D Biol. Crystallogr.* **66**, 486–501.
- 46 Adams PD, Afonine P V., Bunkóczi G, Chen VB, Davis IW, Echols N, Headd JJ, Hung L-W, Kapral GJ, Grosse-Kunstleve RW, McCoy AJ, Moriarty NW, Oeffner R, Read RJ, Richardson DC, Richardson JS, Terwilliger TC & Zwart PH (2010) PHENIX : a comprehensive Python-based system for macromolecular structure solution. *Acta Crystallogr. Sect. D Biol. Crystallogr.* **66**, 213–221.
- 47 Chen VB, Arendall WB, Headd JJ, Keedy DA, Immormino RM, Kapral GJ, Murray LW, Richardson JS & Richardson DC (2010) MolProbity : all-atom structure validation for macromolecular crystallography. *Acta Crystallogr. Sect. D Biol. Crystallogr.* **66**, 12–21.
- 48 DeLano WL (2002) The PyMOL Molecular Graphics System, Version 1.5.0.4 Schrödinger, LLC. .
- 49 Hendlich M, Rippmann F & Barnickel G (1997) LIGSITE: automatic and efficient detection of potential small molecule-binding sites in proteins. *J. Mol. Graph. Model.* **15**, 359–363.

CHAPTER III

THE HUMAN ELECTRON TRANSFERRING FLAVOPROTEIN CATALYZES THE OXIDATION OF ITS FAD COFACTOR TO THE 8- FORMYL DERIVATIVE

Peter Augustin[§], Eva Christine Gerstmann[§], Ruth Prassl[§] and Peter Macheroux[§]

[§]Institute of Biochemistry, Graz University of Technology, Graz, Austria

[§]Institute of Molecular Biosciences, University of Graz, Graz, Austria

Running title

8-Formyl-FAD Formation in hETF

Keywords

8-formyl FAD, inter-protein electron transfer, flavin semiquinone, flavin adenine dinucleotide (FAD), pH dependent enzyme catalysis, stable protein radical.

Abbreviations

8f-FAD, 8-formyl FAD; (h)DMGDH, (human) dimethylglycine dehydrogenase; (h)ETF, (human) electron-transferring flavoprotein; ETF-QO, ETF-ubiquinone oxidoreductase; (h)MCAD, (human) medium chain acyl-CoA dehydrogenase;

ABSTRACT

The human electron transferring flavoprotein (hETF) catalyzes the transfer of one electron from up to thirteen different flavin dehydrogenases to the mitochondrial respiratory chain through a non-covalently bound FAD cofactor. During our studies, we observed the modification of the cofactor at elevated pH and identified a significant fraction of 8-formyl-FAD (8f-FAD) present in the protein. So far, in 50 years of research concerning the electron transferring flavoprotein, 8f-FAD formation has never been described, in fact, an 8 α formylated cofactor has only been observed *in vivo* in the formate oxidase from *Aspergillus oryzae*. We created and characterized several hETF variants and were able to identify important amino acids for the conversion of FAD to 8f-FAD and propose a possible reaction mechanism. Furthermore, we show that protein bound 8f-FAD is stabilized as radical semiquinone and that formylated FAD enhances protein affinity of hETF to its interaction partner the human dimethylglycine dehydrogenase. Although further studies are necessary to estimate the true physiological importance of 8f-FAD formation in hETF, this study presents completely new aspects, which can be important for hETF protein-protein interaction, activation, regulation and stabilization.

INTRODUCTION

In 1956, Crane and coworkers identified the electron transferring ability of an unknown flavoprotein from the pig liver which they named electron transferring flavoprotein (ETF) [1]. Now, 50 years later, numerous publications on ETF have been produced and analog enzymes have been described in all kingdoms of life [2]. The heterodimeric human electron-transferring flavoprotein (hETF) lies at a key metabolic branch point in the mitochondrial matrix and serves as electron carrier from at least thirteen different flavin dehydrogenases to the human ETF-ubiquinone oxidoreductase (hETF-QO), an inner mitochondrial membrane bound flavoprotein that feeds these electrons into the mitochondrial respiratory chain [2–4]. The primary flavin dehydrogenases are involved in such different tasks as β -oxidation, amino acid and one-carbon metabolism (Figure 1) and are structurally and functionally utterly distinct.

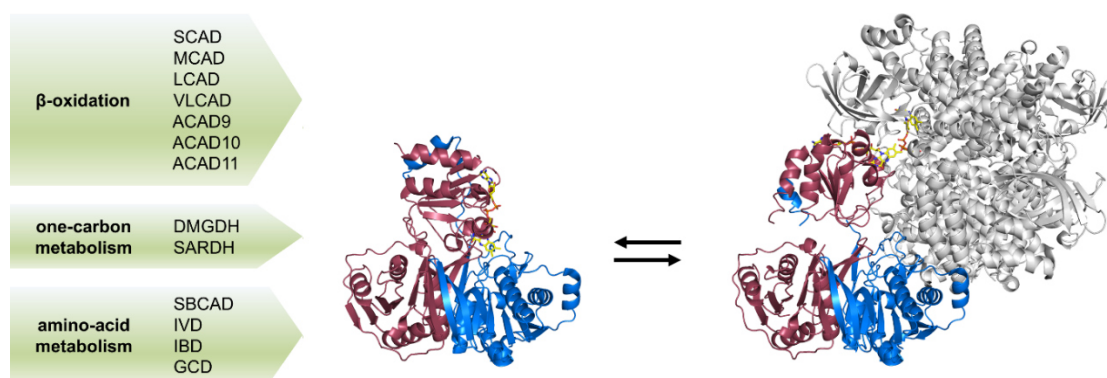


Figure 1 – Interaction of human flavin dehydrogenases with hETF. So far thirteen flavin dehydrogenases, involved in β -oxidation, one-carbon metabolism and amino acid metabolism were identified to interact with hETF. hETF exhibits a flexible interaction mechanism and co-exists in solution in a closed, non-productive form (**pdb:1EFV**) and in an open, productive conformation, here shown bound to hMCAD (**pdb:2A1T**). The α -subunit of hETF is shown in raspberry and the β -subunit in marine cartoon view. hETF bound hMCAD is displayed in grey. hETF bound FAD is presented in yellow sticks, hMCAD bound FAD in pink stick representation. SCAD, short chain acyl-CoA dehydrogenase; MCAD, medium chain acyl-CoA dehydrogenase; LCAD, long chain acyl-CoA dehydrogenase; VLCAD, very long chain acyl-CoA dehydrogenase; ACAD9-11, acyl-CoA dehydrogenase family member 9-11; DMGDH, dimethylglycine dehydrogenase; SARDH, sarcosine dehydrogenase; SBCAD, short branched chain acyl-CoA dehydrogenase; IVD, iso-valeryl acyl-CoA dehydrogenase; IBD, isobutyryl acyl-CoA dehydrogenase; GCD, glutaryl-CoA dehydrogenase.

hETF developed a flexible mechanism to interact with all dehydrogenases as well as with hETF-QO [2]. The protein co-exists in solution in a closed, non-interactive, therefore unproductive and in an open, productive form with a highly flexible upper protein domain (Figure 1). In a dual interaction mechanism, a recognition peptide of the hETF β -subunit first docks to the partner dehydrogenase protein and then the mobile flavin binding domain, with its highly solvent exposed FAD, initiates electron transfer [5]. Toogood *et al.* identified the amino acid residue β E165 which stabilizes non-productive, closed hETF conformations by a salt bridge with residue α N259. If this binding is destroyed by site-directed mutagenesis to an alanine, the protein favors the flexible, productive open conformation in solution as visualized by SAXS measurements [5]. As a consequence, variant β E165A displayed a greater protein

affinity to the human medium chain acyl-CoA dehydrogenase (hMCAD) and also to the rat dimethylglycine dehydrogenase (rDMGDH).

Along with the human ETF, several mammalian and bacterial enzymes of group I of the ETF family were characterized in literature, which show a very conserved structure of the FAD binding site [5–11]. Yet, the formation of 8-formyl FAD in any ETF has never been described, mentioned or hypothesized. The only reference to a modified FAD in pig kidney and liver ETF was drawn by Lehman and Thorpe in 1992, who describe an unusual cofactor fraction after protein denaturation and subsequent HPLC purification. The spectrum of this species resembles the spectral features of free 8-formyl FAD in our observations.

In flavoprotein chemistry, 8α substituted flavins have widely been described as intermediates in the mechanism of FAD or FMN covalent protein attachment [12–15]. It is common in flavoproteins that the cofactor, FMN or FAD, is covalently linked to the protein via the 6 or the 8α position of the isoalloxazine ring [12–15]. In most cases the intermediate flavin species that interacts with an amino acid to form the covalent bound is the 8-hydroxy flavin. Nevertheless, there have been reports that also an 8-formyl flavin species can serve as adduct for covalent flavin attachment [14]. Moreover, 8-formyl riboflavin was described as possible intermediate in the formation of the natural flavin antibiotic roseoflavin [16].

The presence of a naturally occurring, non-covalently bound, functional formylated flavin was only described for the formate oxidase of *Aspergillus oryzae* so far [17,18]. Unfortunately, a physiological function or effects on protein stability or reactivity were not described. The redox potential of free 8f-FAD was shown to be approximately 160 mV more positive than that of free FAD [18], as already shown in an earlier study by Dale Edmondson with artificial riboflavin derivatives [19]. A second formylated flavin, 8-formyl FMN, was observed in the lactate oxidase from *Aerococcus viridans* which was formed after months long incubation of an arginine to lysine variant [20]. The “aged” protein variant exhibited major differences in UV/Vis absorption spectra, featured a higher redox potential and thus decreased reactivity with molecular oxygen when compared with “fresh” protein and the wild-type. In lactate oxidase wild-type protein, 8f-FMN was not built.

In the following study, we present the identification of 8f-FAD as part of the extracted cofactor fraction of hETF purified at physiological pH of the mitochondrial matrix. Furthermore, we demonstrate that 8f-FAD is stabilized in hETF as semiquinone, which gets reduced to the hydroquinone during protein-protein interaction and subsequently re-oxidized to the semiquinone, which was stable to further oxidation by molecular oxygen. Finally, we can show that the presence of 8f-FAD as cofactor increases protein affinity of hETF with the partner dehydrogenase dimethylglycine dehydrogenase (DMGDH) as determined in steady-state assays and identified amino acids involved in the reaction mechanism of 8f-FAD formation.

RESULTS

Expression and Purification of hETF Proteins at Different pH Levels Resulted in Significantly Altered Flavoprotein Spectra

hETF expression in *Escherichia coli* and purification yielded two mg pure protein per g wet cell pellet after Ni-NTA affinity chromatography for the WT and all expressed protein variants respectively. The yield was independent of the pH and buffer used for purification. After affinity chromatography, the protein fractions showed a high purity suitable for all performed spectrometric experiments (Figure 2, lane 5).

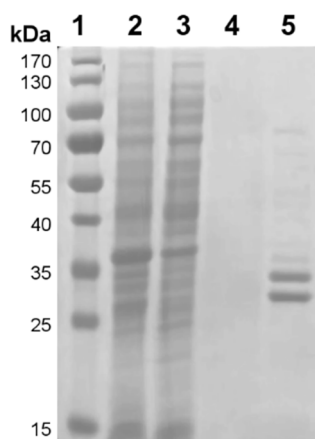


Figure 2 – Purification of hETF-WT. The SDS-PAGE of hETF Ni-NTA affinity chromatography shows in lane 1, PageRuler® prestained protein ladder (Thermo Fisher Scientific); lane 2, *E. coli* cell lysate; lane 3, column flow through; lane 4, washing fraction and lane 5, elution fraction.

The purification of hETF-WT at pH 7.0, at physiological pH of the mitochondrial matrix (pH 7.8), [21,22] and in basic conditions at pH 8.5 resulted in three different flavin absorption spectra (Figure 3A). Protein purified at pH 7.0 gave a spectrum for ETF with maxima at 375 and 436 nm and was very similar to spectra published for the human protein by Herrick *et al.* [23] and for pig liver ETF by Husain and Steenkamp [24]. Purified proteins at higher pH showed a decreased, slightly blue shifted signal of the first maximum and the rise of a significant peak around 415 nm, which is overlapping all other peaks of the second maximum. Also two small peaks between 600 and 800 nm appear (Figure 3A). Moreover, also the denatured spectra of WT protein purified at pH 7.0 and pH 8.5 showed different maxima (Figure 3B). Protein purified at pH 7.0 gave a spectrum identical to free FAD, with maxima at 370 and 450 nm, whereas the other spectrum had a blueshifted first maximum with higher intensity at 354 nm and a redshifted second maximum at 456 nm.

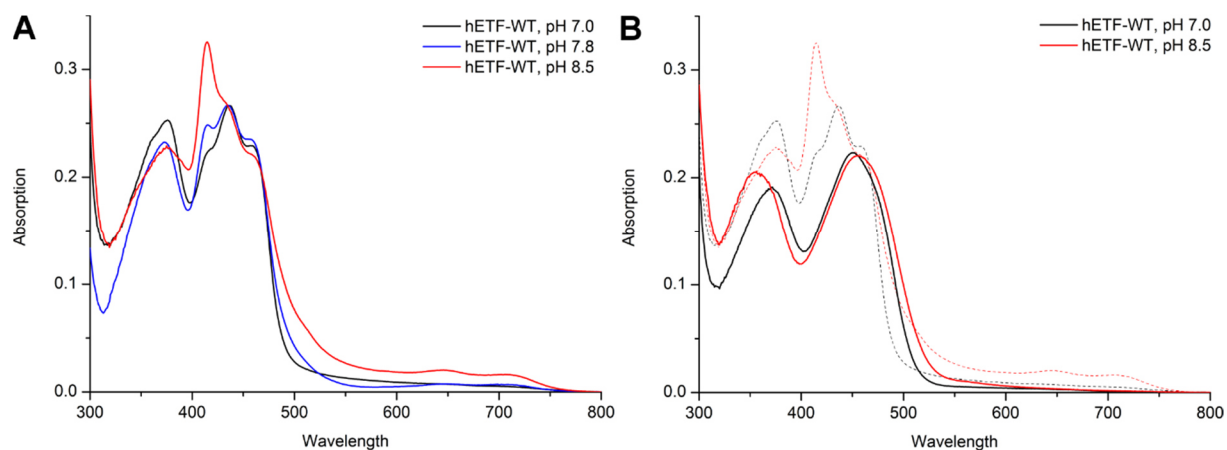


Figure 3 – UV/Vis absorption spectra of native and denatured hETF-WT purified at different pH values. The UV/Vis absorption spectra of ~20 μ M hETF-WT purified at different pH values in 50 mM HEPES/NaOH resulted in different final absorption spectra. Also after denaturation with 20% sodium dodecylsulfate the spectra of the free cofactors showed significant differences.

Cofactor Analysis of hETF-WT Revealed that 8-Formyl FAD is Accumulated at Elevated pH Levels

The altered spectra shown in Figure 3 pointed to the idea that an alternative FAD cofactor is formed in hETF-WT when purified at elevated pH values. After extraction and purification with HPLC (Figure 4A) the cofactor fraction was analyzed using HPLC/MS analysis (Figure 4C) and NMR spectroscopy (Figure 4D).

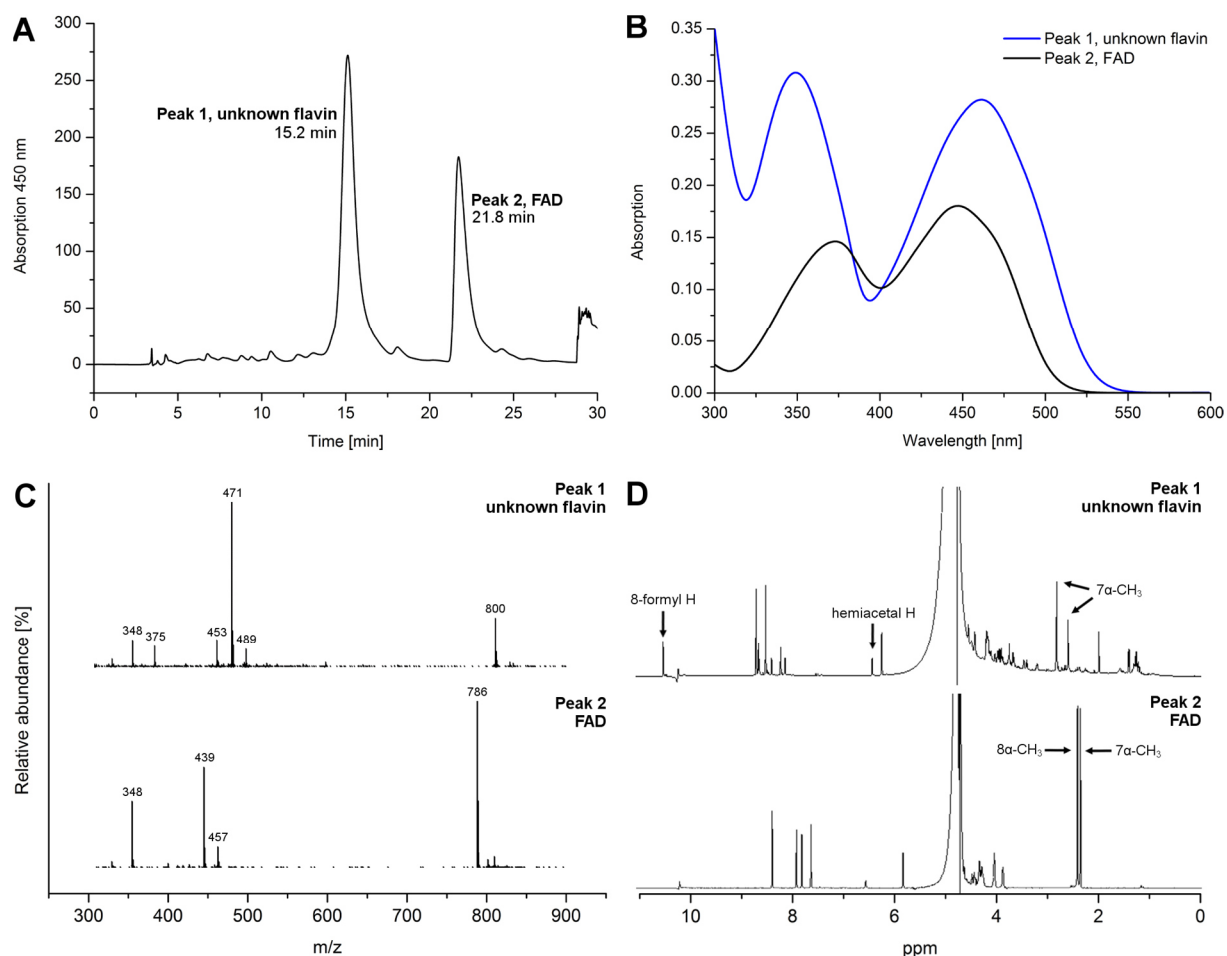


Figure 4 - Analysis and comparison of the two main flavin-containing fractions isolated from hETF. (A) HPLC reversed phase purification of the extracted cofactor(s) gave two major fractions, which were further analyzed by MS and NMR. (B) The spectra of the two peaks featured the same shifts as seen in Figure 3B. (C) Mass spectra of the two main fractions as separated by HPLC. The spectrum shown at the bottom exhibits the typical fragmentation and mass peaks of FAD. The mass spectrum at the top shows a mass shift of 14 a.u. (D) In agreement with the mass analysis, the ¹H-NMR spectrum at the bottom can be assigned to FAD, while the additional resonance at 10.4 ppm and the shifts observed for the methyl groups in position 7 α and 8 α indicate chemical changes in the dimethylbenzene ring moiety of the isoalloxazine ring. Both methods indicate that a small amount of a closed, hemiacetal form of 8f-FAD is present, as previously observed [18,19].

The program established for HPLC purification could efficiently separate two cofactor species (Figure 4A). The first peak at 15.3 min showed a UV/Vis absorption spectrum similar to the red spectrum in Figure 3B, which represents the denatured unknown flavin species. The second peak at 21.8 min showed a spectrum similar to free FAD (Figure 4B). Additionally, in some cases, two peaks turned up during the extraction and HPLC purification at 12.6 and 15.3 min respectively (Figure 5A). Both peaks had a nearly identical spectrum (Figure 5B) and therefore, it was hypothesized that both peaks represent the same unknown cofactor, which apparently exists in two different isomers when free in solution.

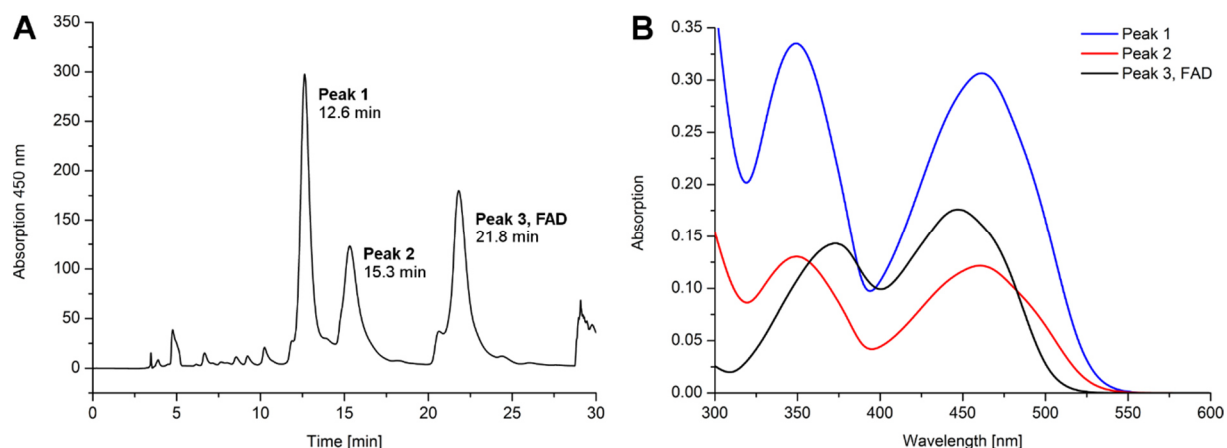


Figure 5 - HPLC purification of the extracted cofactor. (A) The cofactor extracted from hETF-WT purified at pH 8.5 was sometimes also separated into three (!) different FAD species. While the peak at 21.8 min corresponds to FAD, the other two peaks show most likely, the open and hemiacetal form of 8-formyl FAD. (B) Apparently, both forms have nearly the same spectrum and can easily be distinguished from free FAD.

The HPLC/MS analysis of the extracted and purified unknown cofactor revealed several differences when compared with pure FAD (Figure 4C): The fragmentation of FAD followed published patterns (MassBank accession number KNA00248, [25]) with major peaks at 348 for AMP, 439 and 457 for FMN and 786 for the full, unfragmented FAD. The unknown cofactor also showed the AMP peak at 348 but additional peaks at 453 and 471 which could be assigned to the mass of formylated FMN. The peak at 800 for the unfragmented molecule stands for formylated FAD. Minor peaks at 375 and 489 could be hints for the presence of the alternative, second cofactor conformation in solution (Figure 5A).

Analysis and comparison of FAD and the extracted, purified cofactor with NMR spectroscopy additionally strengthened the results of HPLC/MS (Figure 4C). Basically, we obtained the same NMR spectrum for our cofactor as Doubayashi and coworkers in their analysis of the cofactor of formate oxidase from *Aspergillus oryzae* [18]. The main differences between the NMR spectra of the unknown flavin species to FAD are marked in Figure 4D and were the presence of a singlet signal for an aldehyde hydrogen at a chemical shift of 10.4 ppm and the disintegration of the signals for the isoalloxazine methyl groups at 7α and 8α positions.

Our findings and the comparison with results in literature identified the unknown cofactor species as 8α formylated FAD. Furthermore, a small singlet signal at a shift of 6.3 ppm in NMR, two peaks at 375 and 489 in HPLC/MS, as well as a second peak in HPLC purification (Figure 5A) could point to a hemiacetal form of 8-formyl-FAD (8f-FAD) present in the purified solution. Open and hemiacetal form of 8f-FAD are thought to be in equilibrium in solution [19], which was also seen by Doubayashi *et al.* [18].

Identification of Amino Acids and Conditions Leading to 8f-FAD Formation

We constructed several hETF variants with mutated amino acid residues in close proximity to the bound cofactor and especially near the 8α position of the isoalloxazine ring. Additionally, we excluded that the formation was buffer and His-tag independent. After construction, expression and purification of several variants at pH 7.0 and pH 8.5, we identified four variants, hETF- β Y16F, hETF- α T266M, hETF- α R249C and hETF- α Q285A, which were not capable or severely disturbed in 8f-FAD formation. In contrast to hETF-WT these variants did not show any difference in their UV/Vis absorption spectra when purified at pH 7.0 or pH 8.5 respectively (Figure 6A). Additionally, we also identified two variants capable of faster formation of 8f-FAD, hETF- α N259A and hETF- β E165A.

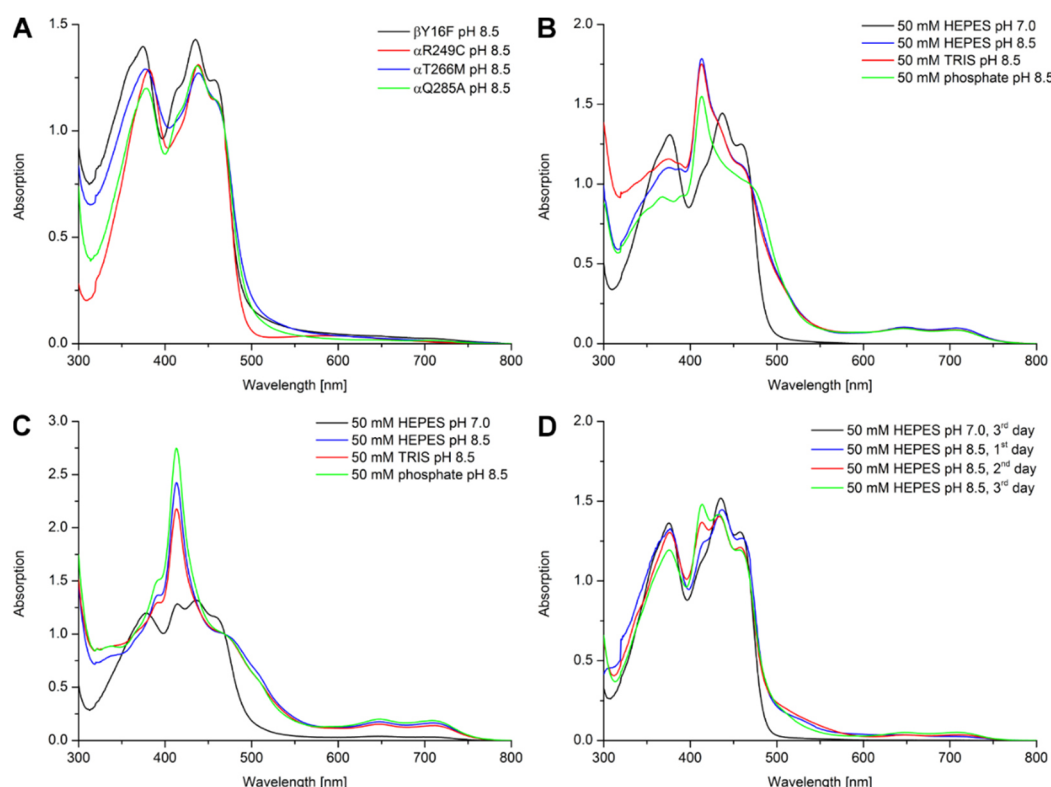


Figure 6 – 8f-FAD formation in hETF-WT and variants. hETF-variants β Y16F, α R249C, T266M were not capable of 8f-FAD formation upon purification in 50 mM HEPES/NaOH buffer with pH 8.5. Variant Q285A showed severe troubles to form 8f-FAD at these conditions. In hETF-WT (B) and hETF- α N259A (C) formation of 8f-FAD was proven to be buffer independent but pH dependent. Furthermore, WT protein purified at pH 7.0 with cleaved off His-tag still formed 8f-FAD when incubated at 4 °C in buffer pH 8.5 (D).

The expression of hETF-WT and variant α N259A in different buffers showed that 8f-FAD formation was buffer independent (Figure 6B and 6C). Variant α N259A and the WT had the same, unusual spectra when purified in phosphate, HEPES or TRIS buffer at pH 8.5. 8f-FAD formation was also His-tag independent. After the removal of the tag of the wild-type protein with a TEV protease it still formed 8f-FAD upon incubation at elevated pH values (Figure 6D).

EPR Analysis Revealed that 8-Formyl FAD is Stabilized as Radical Species in hETF

After the identification of 8f-FAD as cofactor in hETF-WT, we investigated its electronic state with EPR spectroscopy. The EPR spectra of hETF variant α N259A (fast 8f-FAD formation), hETF-variant β Y16F (no 8f-FAD formation) purified at pH 8.5 and hETF-WT purified at pH 7.0 (no 8f-FAD formation) were measured. The results revealed that variant α N259A stabilized an 8-formyl FAD radical species, whereas WT and β Y16F variant did not show an EPR signal (Figure 7). For the α N259A signal, a g-factor of 2.0048 was calculated after calibration with DPPH (g-factor of 2.0036) and a peak to peak line width of 11-13 G was measured. This linewidth is unusual narrow for flavin radicals and points to the stabilization of the red, anionic semiquinone [26].

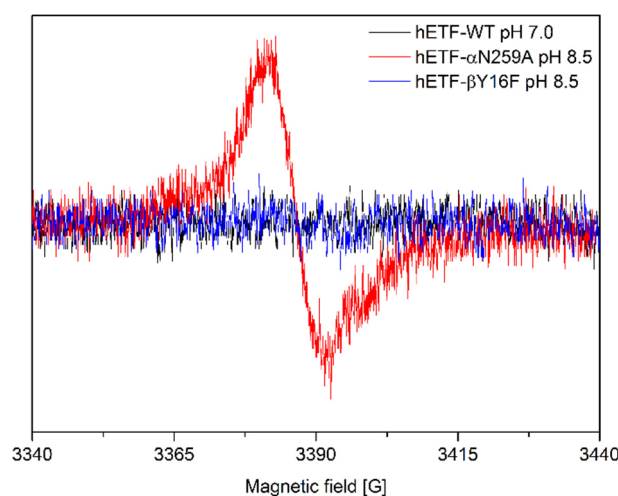


Figure 7 – EPR spectroscopy of hETF-WT, hETF- α N259A and hETF- β Y16F. The plot clearly shows that only hETF variant α N259A purified at pH 8.5 displayed a signal and therefore stabilized a radical FAD species. WT and variant β Y16F did not show a signal. The narrow peak to peak linewidth calculated for α N259A indicates that the radical is stabilized as anionic semiquinone.

Time Resolved 8f-FAD Formation and Assessment of Formylation Grade

The *in vitro* formation of 8f-FAD is a slow process with an approximate half-life of 20 hours for the wild-type and 4 hours for the hETF- α N259A variant (Figure 8D). It can be achieved by dilution and incubation of hETF proteins purified at pH 7.0 in buffers with higher pH values (Figure 8A-C). The formation of 8f-FAD changed the protein spectrum drastically and several isosbestic points could be identified. The isosbestic point at 469 nm was subsequently used to calculate protein concentrations of hETF-WT and all variants in their different formylation grades. The reverse reaction, the formation of FAD out of 8f-FAD by making the protein solution more acidic has never been observed.

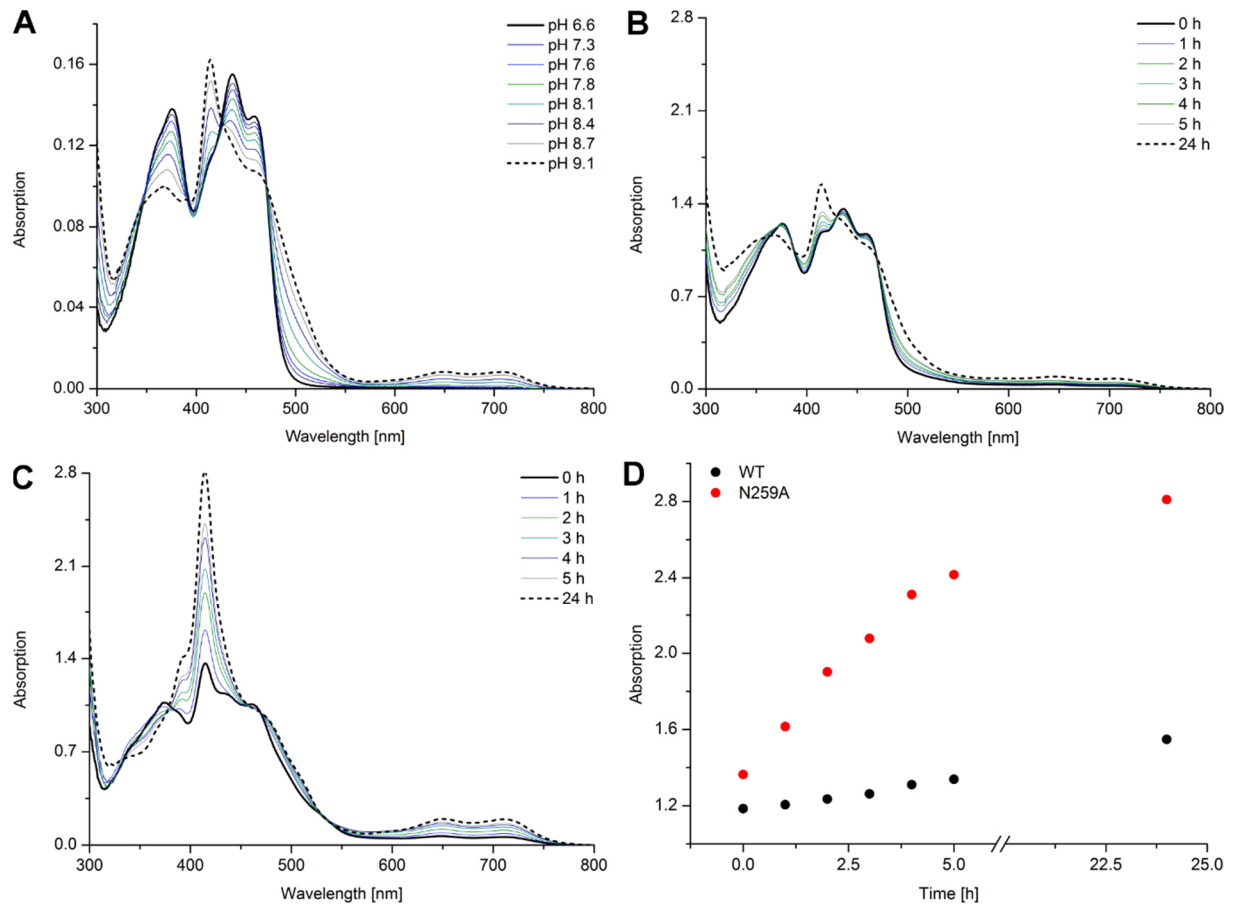


Figure 8 – Formation of 8f-FAD radical in hETF-WT and α N259A variant. (A) \sim 400 μ M hETF-WT purified at pH 6.6 was diluted 1:20 with 50 mM HEPES buffers with the indicated pH values and incubated for 48 h at 4 $^{\circ}$ C before the UV/Vis spectra were recorded. (B) \sim 400 μ M hETF-WT purified in 50 mM HEPES, pH 7.0 was diluted 1:20 with HEPES buffer pH 8.5 and incubated at 25 $^{\circ}$ C for 24 hours. (C) \sim 400 μ M hETF- α N259A purified in 50 mM HEPES, pH 7.0 was diluted 1:20 with HEPES buffer pH 8.5 and incubated at 25 $^{\circ}$ C for 24 hours. The dotted line in both panels represents the spectrum measured after 24 hours incubation. The spectra in Panels B and C were normalized to an absorption of 1 at the isosbestic point at 469 nm to simplify comparison. (D) The time-dependent absorption changes measured at the indicated time points at 415 nm for hETF-WT and hETF- α N259A variant clearly showed the different velocity 8f-FAD is built in the proteins with an approximate half-life of 4 hours for the variant and 20 hours for the wild-type.

We used the observed change of absorption during the formylation process to estimate the formylation grade of the purified proteins with the ratio of UV/Vis protein absorption at 415 and 469 nm ($A_{415/469}$). At 469 nm, the protein spectrum stayed constant upon conversion of FAD to 8f-FAD radical whereas the absorption at 415 nm showed the highest change. The $A_{415/469}$ ratio of WT purified at pH 7.0, which gave a value of 1.15, served as basis for 0% 8f-FAD and the highest measured ratio for α N259A purified at pH 8.5, with a value of 2.7, served as basis for 100% formylation grade. WT purified at pH 7.8 gave a value of 1.25, WT purified at pH 8.5 a value of 1.63 which can be theoretically calculated to 6.5% and 31% formylated cofactor in the protein fraction. Freshly prepared variant α N259A purified at pH 7.0 (!) already showed values between 1.4 and 1.6, which was converted to a theoretical formylation grade of 16-28%.

FAD Formylation Significantly Changed the Redox Behavior of hETF

Photoreduction of hETF-WT and highly formylated hETF- α N259A confirmed that 8f-FAD is stabilized as semiquinone in the protein. hETF-WT photoreduction started from the oxidized enzyme and ended up in the stable neutral semiquinone as reported previously (Figure 9A), [23,24]. The addition of a 10-fold excess of sodium dithionite to the semiquinone further reduced the protein to the fully reduced hydroquinone form (Inset Figure 9A). On the other hand, hETF- α N259A was easily photoreduced to its reduced form (Figure 9B) and was not further reduced by addition of sodium dithionite. A higher oxidized form of 8f-FAD could not be seen under standard conditions and was apparently not formed aerobically.

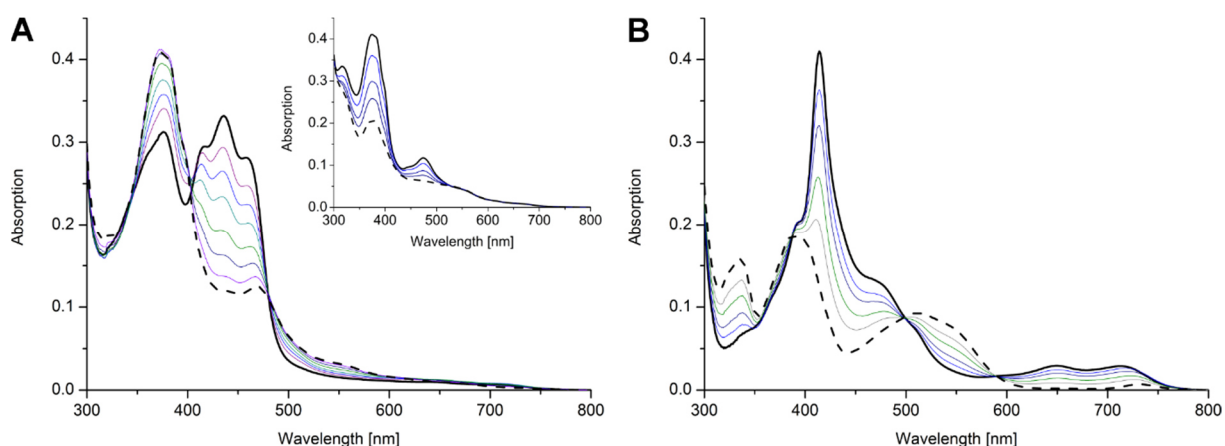


Figure 9 – Photoreduction of hETF-WT purified at pH 7.0 and hETF- α N259A purified at pH 8.5. The photoreduction of hETF-WT proceeded to a red semiquinone (A). Upon further reduction with dithionite (Inset A), a hydroquinone spectrum was formed. (B) Photoreduction of hETF- α N259A variant with 8f-FAD cofactor also was photoreduced but further reduction with dithionite was not possible. We conclude that 8f-FAD is stabilized in hETF- α N259A as anionic semiquinone which is reduced to the hydroquinone 8f-FAD during photoreduction and is also stable towards molecular oxygen.

Physiological Relevance of 8f-FAD, Effects on Stability and Protein-Protein Interaction

The effect of 8f-FAD formation on protein-protein interaction was investigated with the human dimethylglycine dehydrogenase (hDMGDH). For that purpose, WT and variant α N259A were purified in 50 mM HEPES pH 7.0 and pH 8.5, respectively and afterwards, the steady state kinetic parameters were determined at pH 7.0. The results shown in Figure 10 and listed in Table 1 conclude that reaction velocities and k_{cat} values basically remained constant upon formylation grade. K_M values, on the other hand, were significantly decreased with formylated cofactors and hence protein-protein interaction affinity was increased. It has to be noted that the purification of hETF- α N259A at pH 7.0 already resulted in slightly formylated protein (~15-30%) which could explain why the K_M value was already decreased in the first place compared to the WT (Table 1). Vice versa, hETF-WT purified at pH 8.5 is most likely not 100% but significantly lower formylated (~30-40%) and therefore, the determined K_M values were still much higher compared to highly formylated variant α N259A purified at pH 8.5. The higher k_{cat}

values measured for the unformylated proteins were most likely measuring artefacts as the measurements did not reach saturating conditions at high hETF concentrations and the hyperbolic fit had to be extrapolated (Figure 10). Additional to steady-state kinetics, also protein stability was determined for the formylated and unformylated proteins. Thermo FAD measurements showed that T_m was increased by 3.5 °C in 8f-FAD saturated α N259A variant but stayed constant in WT protein containing 8f-FAD (Table 1).

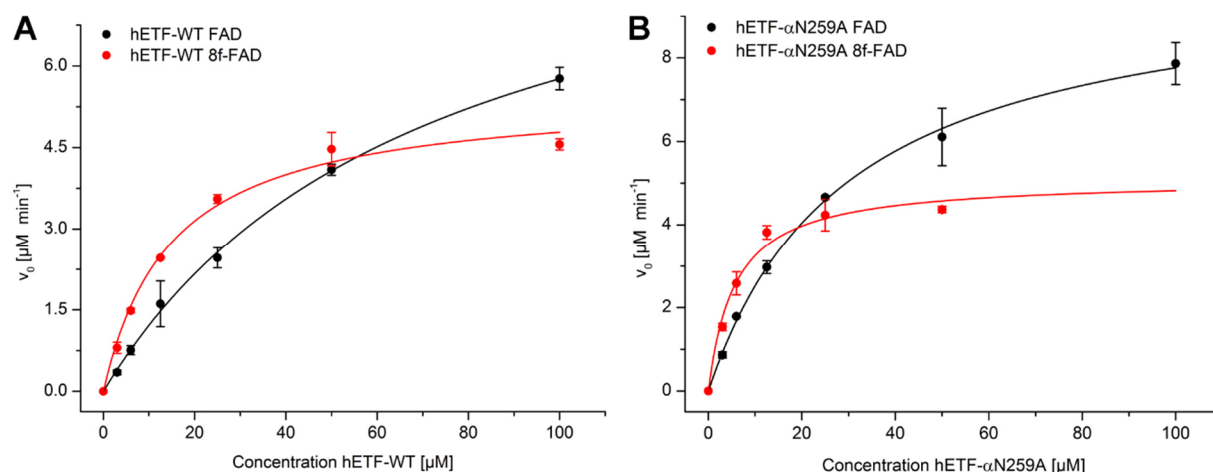


Figure 10 – Steady-state kinetics of hETF-WT and hETF- α N259A. The measurements were performed at different hETF concentrations using hDMGDH as dehydrogenase and DCPIP as final electron acceptor. The comparison of the kinetic values showed that the formylated proteins had decreased K_M values.

Table 1 – Steady-state kinetics of hETF-WT and variant α N259A.

Protein	pH	T_m	K_M	k_{cat}	k_1
		°C	μM	min^{-1}	$L mol^{-1} min^{-1}$
WT	7.0	60.5	71 ± 5	99 ± 4	1400 ± 100
WT 8fFAD	8.5	60.0	15 ± 2	56 ± 2	3700 ± 500
α N259A	7.0	60.0	30 ± 2	101 ± 2	3400 ± 200
α N259A 8fFAD	8.5	64.0	6 ± 1	51 ± 3	8000 ± 1400

Additionally to hETF-WT and variant α N259A, also the kinetic parameters of protein variants β Y16F, α Q285A, α R249A and β E165A were determined (Figure 11A-C, Table 2). Although differences in the kinetic parameters can be seen compared to hETF-WT, there is no prove that these were caused because the variants were not able to form 8f-FAD. More likely, the changes were caused because of disturbed protein-protein interaction with hDMGDH like missing hydrogen bonds, electrostatic effects or protein destabilization. The steady-state kinetics of protein variant hETF- β E165A purified at pH 7.0 resembled the values obtained for hETF-WT purified at pH 7.0 (Figure 11D, Table 2). Other to the spectrum of the analog variant hETF- α N259A at pH 7.0 (Figure 11C, black line), the spectrum of hETF- β E165A did not show any signs of FAD formylation (spectrum not shown). The kinetic behavior of formylated hETF- β E165A purified at pH 8.5 was not determined.

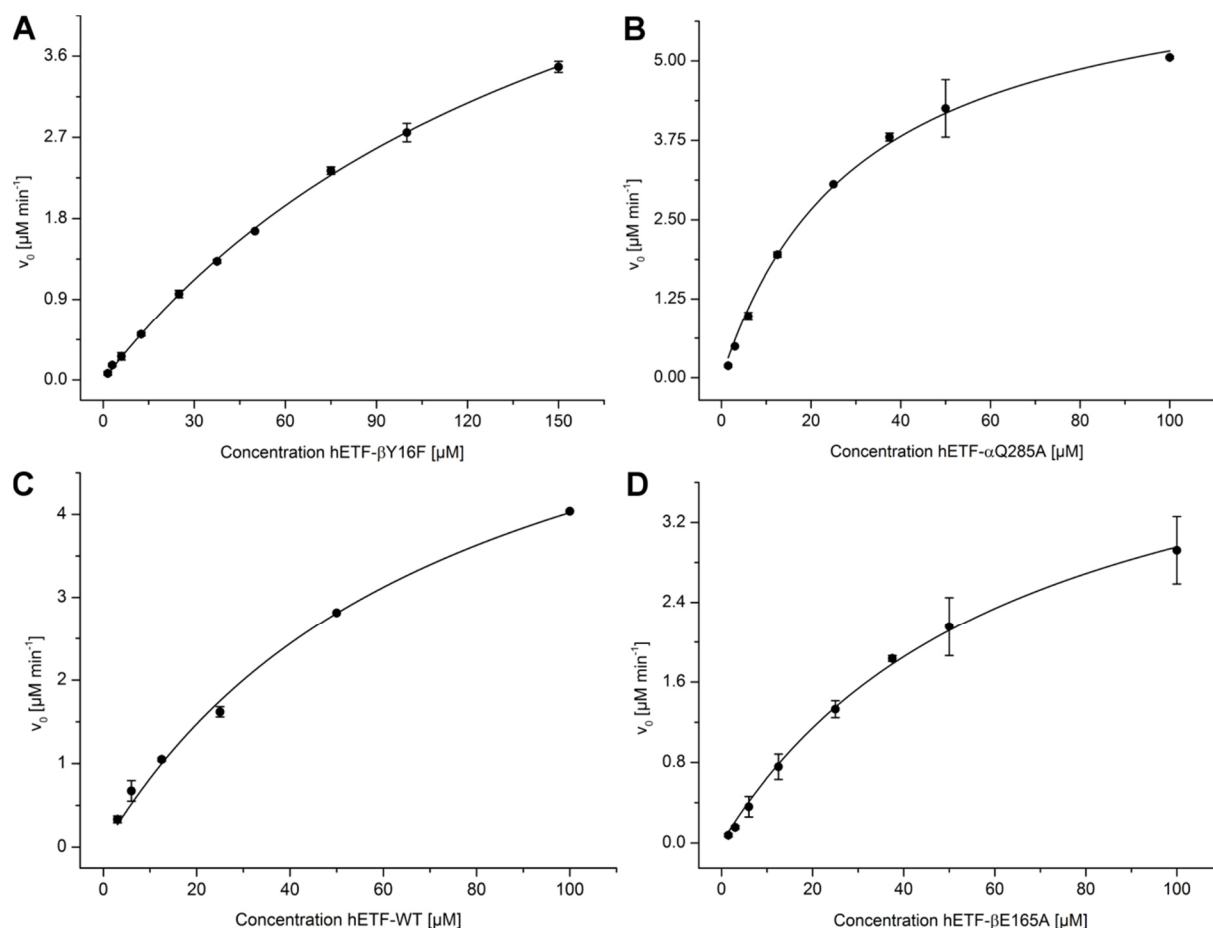


Figure 11 – Additional steady-state kinetics of variants β Y16F, α Q285A, β E165A and hETF-WT. Steady-state kinetics were measured at different hETF concentrations using hDMGDH as partner dehydrogenase and DCPIP as final electron acceptor. All variants were assayed as before in 50 mM HEPES, pH 7.0, in order to exclude an influence of the assay buffer, wild-type in panel C was measured in 50 mM sodium phosphate buffer pH 7.0 to exclude any effects of the HEPES buffer.

Table 2 – Steady-state kinetics of hETF variants β Y16F, α Q285A, α R249C and β E165A in 50 mM HEPES, pH 7.0 and hETF-WT in phosphate buffer pH 7.0 (WT (p)).

Protein	pH	K_M	k_{cat}	k_i
		μM	min^{-1}	$L mol^{-1} min^{-1}$
β Y16F	7.0	170 ± 8	74 ± 2	400 ± 20
α Q285A	7.0	31 ± 3	67 ± 2	2200 ± 200
β E165A	7.0	66 ± 5	49 ± 2	700 ± 60
α R249C	7.0	-	-	-
WT (p)	7.0	76 ± 12	71 ± 6	900 ± 100

DISCUSSION

hETF Expression and Purification

In contrast to previous studies conducted on hETF, we expressed the enzyme with a His-tag attached to the N-terminus of the β -subunit. The tag however is not expected to interfere with the behavior of the protein. According to the protein crystal structure (**pdb:1EFV**), [7] it is far away from the active site on the surface of the protein. After cleavage of the N-terminal His-tag by TEV protease protein stability and activity did not change and also formation of 8f-FAD was still observed (Figure 6D). Therefore, the His-tag was not considered to alter protein activity and stability. Also, we obtained similar values for K_M and k_{cat} with the tagged protein as published in previous reports for rat DMGDH and untagged human ETF [6]. We additionally cloned hETF with a C-terminal His-tag at the α -subunit, which was leading to significantly decreased activities, protein aggregation and bad purification behavior (data not shown).

In our purification protocol, heating of the protein to 37 °C for 30 min was an important step to obtain stable protein solutions. We assume that the heating helps to precipitate excessive purified β -subunits and aggregated, unfolded or cofactor unsaturated protein. The precipitate formed during the heating step was colorless and did not result in free cofactor in solution.

Characterization of 8f-FAD in hETF

With help of HPLC/MS, UV/Vis, NMR and EPR spectroscopy, the formation of 8 α -formylated FAD was verified in hETF at elevated pH values. Similar to the observations of Doubayashi *et al.* [18], the existence of 8f-FAD as open and hemiacetal form in solution was observed after extraction of the cofactor during HPLC purification (Figure 5) and in NMR and HPLC/MS analysis (Figure 4C and 4D). As FAD is non-covalently but still tightly bound in the active site of hETF it seems however implausibly that the hemiacetal form of the cofactor plays any physiological role or occurs *in vivo*. Formation of hemiacetal was described being enhanced by acidic catalysis [19], therefore it could be that the presence of D₂O in NMR and HCOOH and TFA in HPLC/MS measurements triggered its formation.

8f-FAD occurs in hETF as stable radical semiquinone as seen in EPR spectroscopy (Figure 7) and photoreduction (Figure 9). Most notably, the radical spectrum featured a major peak around 415 nm (Figure 9) and hETF-WT with 8f-FAD gave a protein spectrum similar to the published spectra by Yorita *et al.* for lactate oxidase, containing 8f-FMN [20] and Maeda *et al.* for formate oxidase, containing 8f-FAD [17]. Furthermore, small peaks in an area typical for the blue, neutral semiquinones [27] arise between 600 and 800 nm upon formation of 8f-FAD (Figure 8A). We suggest that 8f-FAD is stabilized as a mixture of red and blue semiquinone in hETF as also was suggested after 8f-FMN formation in lactate oxidase [20]. Yet, peak to peak linewidth measured in EPR spectroscopy suggests that the major fraction is the red, anionic semiquinone (Figure 7). Photoreduction revealed that one electron transfer

in hETF is changed from oxidized state to semiquinone state as seen in unformylated hETF-WT to semiquinone to hydroquinone state with the formylated cofactor. A further oxidation of 8f-FAD in hETF never has been observed. In vitro formation of 8f-FAD in hETF-WT was in general a rather slow process with half-lives at 25 °C of ~20 hours (Figure 8D).

Experiments on the effects of the formylation on the redox potential of hETF are still ongoing but based on observations and experiments by Dale Edmondson [19] and Yorita *et al.* [20] the redox potential of 8f-FAD should be significantly more positive than the redox potential of FAD in hETF. Therefore, we expect that the formylation of FAD in hETF would facilitate and fasten the reductive half-reaction, the interaction with its dehydrogenase partner proteins *in vivo*, but on the other hand maybe hamper interaction with hETF-QO and oxygen in the oxidative half reaction.

Interaction of Formylated and Unformylated hETF with Partner Proteins

The interaction of mammalian and bacterial ETF proteins with the human MCAD, one of its thirteen dehydrogenase partners has been studied extensively in literature and was reviewed in 2007 by Toogood *et al.* [2]. In order to test the effect of FAD formylation on the interaction properties of hETF, we assayed the interaction behavior with the human dimethylglycine dehydrogenase (hDMGDH) as partner protein. We employed a classical DCPIP based assay with the combination of dimethylglycine reduced hDMGDH to donate electrons to reduce and DCPIP as electron acceptor to re-oxidize hETF. In our hands, the assay comprised the problem that hETF alone, especially in concentrations higher than 25 μ M, already tended to reduce DCPIP significantly. Also the addition of KCN to mask unspecific redox reactions, as was described by Toogood *et al.* [6], did not inhibit the background reaction. To overcome this problem, we introduced a 10 min incubation step before starting the assay by the addition of DMG. After 10 min the unspecific DCPIP reduction always was constant and could be subtracted from the measurements. As we performed our assays at pH 7.0, *de novo* formation of 8f-FAD during the measurements should not contribute to the observed results. For future experiments using this assay we recommend to use at least 200 μ M DCPIP in the assay to avoid limiting DCPIP concentrations during the measurements.

The most striking result of our assays was the significant reduction of the K_M when hETF was formylated in contrast to unformylated or lesser formylated protein (Figure 10, Table 1). Toogood *et al.* report the similar observation that hETF variant β E165A had a greater affinity for the medium chain acyl-CoA dehydrogenase and rat dimethylglycine dehydrogenase compared to the wild-type enzyme [6]. Mutagenesis of Glu-165 or Asn-259, which form a salt bridge in the protein, results in the selective destabilization of non-productive, closed hETF conformations (Figure 1). Although the variants show a greater affinity with hDMGDH and hMCAD, complex dissociation is slowed down and subsequently also the interaction with hETF-QO. Therefore, it is doubtful if greater protein-protein affinity in this special case is favorable in nature.

On the one hand, faster formation of 8f-FAD is achieved in β E165A and α N259A variant because of the greater exposure of the cofactor to the solvent, on the other hand, the presence of 8f-FAD could shift the equilibrium to the productive open protein conformations and thus increase protein affinity. Preliminary results with hydrogen/deuterium exchange mass spectrometry (H/DX-MS) not only confirmed that variant α N259A exists in solution predominantly in its open form but also indicated that the formylation of FAD increases the tendency of hETF towards the open form in solution. Additionally, also higher temperatures, buffer type, oxygen and light exposure, as well as frequent freezing and thawing of the protein are possible factors that increase 8f-FAD formation in solution *in vitro* and/or *in vivo*.

Steady-state kinetics were also done with variants not capable of producing 8f-FAD but the observed changes in the interaction activity were assigned to loss of hydrogen bonding with the partner proteins, change of redox potential and reduction of protein stability and not to impaired 8f-FAD formation (Figure 11, Table 2). Steady-state measurements performed in phosphate buffer pH 7.0 with hETF-WT protein purified in phosphate buffer pH 7.0 and showed the same results as achieved in HEPES buffer pH 7.0 (Figure 11C, Table 2).

Possible Involvement of hETF-8f-FAD Formation in Glutaric Aciduria Type II Disease

Strikingly, two of our variants incapable of 8f-FAD formation are also involved in glutaric aciduria type II disease (GAI, OMIM: 231680), also called multiple acyl-CoA dehydrogenase deficiency (MADD). GAI is characterized by a malfunctioning hETF or hETF-QO protein caused by mutations and subsequently by a severe nonketotic hypoglycemia, metabolic acidosis and excretion of large amounts of fatty acid and amino acid-derived metabolites [28,29]. Clearly, in patients suffering from GAI, not only the metabolites of the hETF partner dehydrogenases are accumulated, but also a metabolic breakdown of the body is inevitable because the vital transfer of electrons especially from β -oxidation pathway is impeded.

hETF-variants α R249C and α T266M cause GAI, with the latter being the most abundant mutation found in affected patients [30,31]. Although a direct connection of 8f-FAD formation and GAI cannot be excluded at that point, it is more likely that other effects of these mutations, the decrease of protein stability and the loss of interacting hydrogen bonds, as mentioned above, are the cause of the disease (Chapter IV). Furthermore, there are a lot more variations causing GAI which are not in proximity to the active site but destroy protein stability and definitely are not involved in 8f-FAD formation [32].

Observations of 8 α Formylated Flavins in Literature

Apart from intermediates in the mechanism of covalent attachment of flavins to a protein, to our knowledge, thus far, non-covalently bound 8 α formylated flavins were only reported in two other proteins. 8-formyl-FAD naturally occurs as a cofactor in the formate oxidase of *Aspergillus oryzae* [17,18] and 8-formyl FMN was surprisingly formed after a lysine to arginine mutation in the active site of the lactate oxidase [20]. Similar to our results, both studies describe a significantly changed UV/Vis absorption spectrum for the formylated cofactor compared to FAD or FMN. Also, altered redox potential and therefore changed activity with substrates and oxygen were described. Other features like changed protein stability or steady-state kinetics were not investigated.

The capability of hETF to form 8f-FAD was a surprising and unexpected finding. Detailed studies on mammalian ETF date back to the middle of the 1950s and 8-formyl FAD formation in ETF still never has been reported. The only observation that might describe 8-formyl FAD formation in mammalian ETF could have been made by Lehman and Thorpe in 1992 [33]. During their studies on pig liver and kidney ETF they observed two forms of ETF; one builds the red (ETF_R), the other one the blue semiquinone (ETF_B) upon reduction. When they denatured the proteins and analyzed the cofactors of the proteins with HPLC, they observed an additional small peak that could not be assigned to FAD. The UV/Vis absorption spectrum showed a flavin like absorption but with altered maxima at 463 and 352 nm. This is very similar to the spectrum we observed for denatured hETF-WT purified at elevated pH values (Figure 3B, red line). Furthermore, the reduction of the unusual cofactor resulted in a “pink” species with a maximum at 520 nm. We also see this maximum upon photoreduction of α N259A hETF variant (Figure 9B) and also Yorita *et al.* reported the same reduction behavior of free 8-formyl FMN in their study [20]. Taken together, Lehman and Thorpe were in all likelihood the first that unknowingly described a formylated FAD cofactor in pig liver and kidney ETF but their observations have never been investigated any further.

8f-FAD Formation in ETF Analogs

Apart from the crystal structure of hETF-WT (**pdb: 1EFV**), also the crystal structures of several bacterial ETFs have been solved (Figure 12). The alignment the FAD binding site of all available structures showed that they have a very high grade of sequential and structural conservation (Figure 12), [2]. Therefore, we find it very likely that not only the human, but also all other members of the ETF family should be able to form 8f-FAD. As soon as we took a closer look into all published crystal structures of electron transferring flavoproteins with available electron densities (**pdb: 1O96, 1EFP, 4KPU, 2A1U**) the electron densities around the 8 α position always showed an unusual high intensity, and in all cases, a formyl group instead of the methyl group would also fit, in some cases even fit better the measured electron density. The determination of the crystal structure with a bound 8f-FAD in our

expressed hETF-WT or hETF- α N259A variant would significantly help to investigate the binding mode and the effects of the formylation on the surrounding.

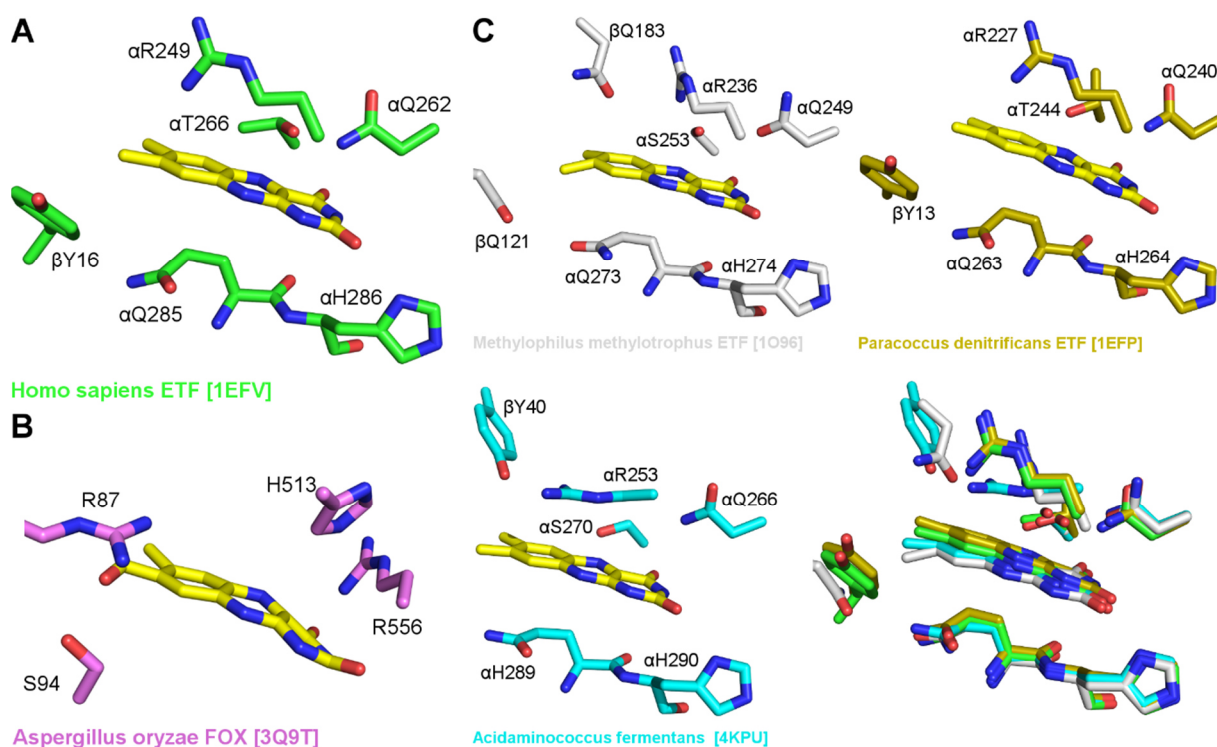


Figure 12 – Active site composition of hETF and related structures. (A) The binding site of FAD in hETF shows residues that are involved in the formation of 8f-FAD. The crystal structure of formate oxidase of *Aspergillus oryzae* shows similar amino acid functions in the active site (B) that can be aligned to human amino acids. The FAD binding site of the human electron transferring flavoprotein greatly resembles the crystal structures of *Methylophilus methylotrophus*, *Paracoccus denitrificans* and *Acidaminococcus fermentans* (C), strikingly shown in the structure alignment of hETF with these three bacterial enzymes. In square brackets, the pdb code for the respective ETF structure are shown.

Possible Reaction Mechanism of 8f-FAD Formation in ETF

In order to get an idea about the reaction mechanism of 8f-FAD formation in hETF we created several hETF variants and identified so far four variants not able or severely disturbed in forming 8f-FAD at our conditions, hETF- β Y16F, hETF- α T266M, hETF- α R249C and hETF- α Q285A (Figure 6A, Figure 12A). All affected variants have mutations in the very proximity of the FAD binding site of the protein and moreover, apart from residue β Y16, are residues highly conserved in the ETF protein family as shown in the sequence alignment of various ETF proteins [2] and in the structural alignment of the crystal structures (Figure 12C). Last but not least, also the crystal structure of formate oxidase with bound 8f-FAD comprises amino acids with similar functions as to the ones of the ETF family like stabilization of negative charges and radicals, as well as basic amino acids in the surrounding of the 8α position of the isoalloxazine ring (Figure 12B). Furthermore, in all crystal structures investigated the 8α position of the FAD is extraordinary strongly exposed to the solvent and therefore easily accessible for

conversion reactions and perfectly situated to conduct electron transfer with partner proteins, especially in its open conformation (Figure 1).

The formation of 8f-FAD begins with an oxidized FAD and ends up in a stable radical semiquinone 8-formyl FAD species (Figure 13). Amino acids in proximity to the isoalloxazine ring that might help to stabilize the final 8f-FAD radical species at positions N5, C4a and a delocalized negative charge around position C2 of the isoalloxazine ring are α T266, α R249, α Q262 as well as α H286 (Figure 12A). Variants α T266M and α R249C were constructed and tested and were not able to form 8f-FAD. Salazar *et al.* investigated the effect of the α T266M variation and came to the conclusion that it increases the stabilization of the FAD semiquinone compared to the WT 10-fold [31]. Therefore, it is more likely that the threonine hydroxyl functionality is needed for stabilization of reaction intermediates rather than the final 8f-FAD semiquinone. Dwyer *et al.* investigated the importance of hETF residue α R249 and came to the conclusion that the alteration of the arginine at position 249 negatively influences semiquinone stabilization in the protein [34]. Arg249 provides an overall positive charge distributed to the whole isoalloxazine ring able to catalyze electronic reaction throughout the ring system. The additional creation of an α Q262 and an α H286 variant could determine their importance in reaction catalysis.

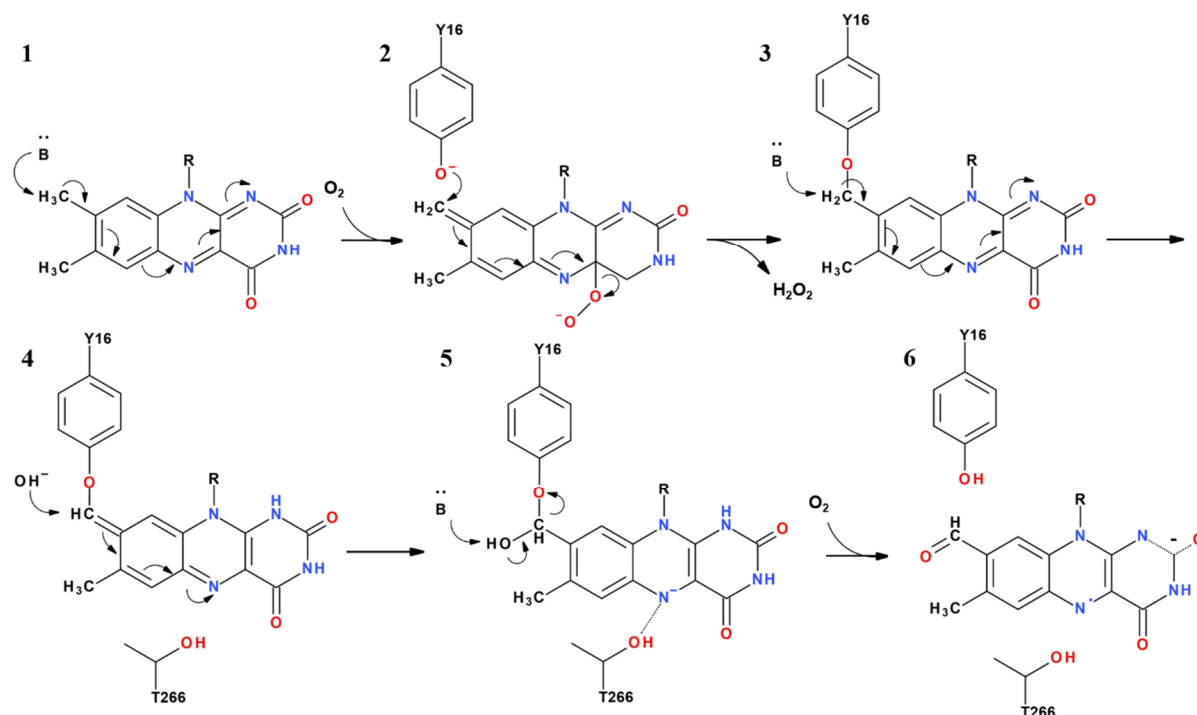


Figure 13 – Possible reaction mechanism to build 8f-FAD in hETF. In this six step mechanism the amino acid tyrosine serves as base at the 8 α position whereas the amino acids T266, H286, Q262 and R249 serve as stabilizing sidechains for negative charges throughout and at the end of the reaction.

A further conserved amino acid function in all structures are basic and glutamine amino acid residues in proximity to the 8 α position that could help to initiate and catalyze the reaction. In the human enzyme

that is β Y16 and α Q285 (Figure 12A). The loss of the hydroxyl group in variant β Y16F again eliminates the capability of the protein to form 8f-FAD and the loss of the amid function in variant α Q285A severely disturbs 8f-FAD formation. Dwyer *et al.* also investigated the importance of residue β Y16 but their variant β Y16L did not show a change in redox potential, stability or interaction behavior with MCAD and GCAD [34].

Taking our observations together, we formulated the reaction mechanism shown in Figure 13. Our mechanism is strictly base catalyzed and the abstraction of the hydrogens in step 1, 3 and 5 is most likely accomplished by hydroxide ions (OH^-) of the solvent. The reaction with oxygen and the direct interaction with residue β Y16 forms the 8f-FAD semiquinone in six steps. The great proximity of α T266 to position N5 of the isoalloxazine ring (2.7 Å) makes it very likely that it helps to stabilize negative charges throughout the reaction, especially in step 5. In a last step, the reduced flavin is re-oxidized by oxygen to the semiquinone, which is strongly stabilized by the protein environment and thus not further oxidized. In the final re-oxidation step and also in step 2, superoxide-anions are build, which could be detected by cytochrome c reduction in combination with the superoxide dismutase to strengthen our reaction mechanism.

CONCLUSION

De novo formation of 8f-FAD in hETF was investigated, observed and measured by change of pH, temperature and light exposure. However, the *in vitro* formation of 8f-FAD, also at 37 °C and pH 8.5 is a slow process in hETF-WT and it is unclear if the formation is fast enough to be physiologically relevant. Also, it is not clear yet, if the sole interaction of hETF with partner dehydrogenases forms 8f-FAD. Further *in vitro* studies with other dehydrogenase partners of hETF, especially with the hMCAD, are essential to learn more about the effects of 8f-FAD.

It still has to be determined if the protein exists *in vivo* in the cells as a mixture of unformylated and formylated form or whether it is formed spontaneously at cell stress, higher metabolic pressure due to increased β -oxidation or amino acid metabolism. Also other beneficial effects of 8f-FAD, as higher protein lifetime or the recruitment of new interaction partners cannot be excluded. A great possibility to study the effect of 8f-FAD formation *in vivo* would be experiments with the ETF of *Paracoccus denitrificans*. This gram-negative bacterium can be easily manipulated and the effects of ETF variants and 8f-FAD formation tested. Most importantly, *P. denitrificans* significantly resembles mammalian mitochondria and holds all features and enzymes present in the human mitochondrial respiratory chain [35].

In conclusion, our discovery of 8-formyl-FAD formation in human electron transferring flavoprotein was a surprising and unexpected finding that opens several new possibilities in research with this important flavoprotein.

EXPERIMENTAL PROCEDURES

Enzymes and Reagents – Restriction enzymes and Phusion DNA polymerase were obtained from Thermo Fisher Scientific (Waltham, MA, USA), purification columns from GE Healthcare (Chalfont St. Giles, UK). Salt free purified oligonucleotides for site directed mutagenesis were synthesized by VBC-Biotech (Vienna, Austria). All other chemicals and media were from Carl Roth GmbH (Karlsruhe, Germany) or Sigma-Aldrich (St. Louis, MO, USA) and were of the highest grade available.

hETF-WT Gene Expression Design – The hETF sequence for expression of the mature hETF consisting of α - and β -subunit was designed following a similar strategy as described by Bross *et al.* [36] and was optimized for expression in *Escherichia coli* using GeneOptimizer[®] (Thermo Fisher Scientific). The operon starts with a ribosomal binding site (AAGGAG), followed by a TATA box in front of the ATG start codon of the gene sequence of the β -subunit. After the stop codon of the β -subunit, a 69 base pair spacer region between the β and α gene sequence was introduced, which again comprised the same ribosomal binding site and a TATA box in front of the ATG start codon of the α -subunit. The designed gene sequence was flanked by an *Xba*I and an *Xho*I restriction site and cloned for expression into a pET-28a+ vector (Thermo Fisher Scientific). In accordance with Herrick *et al.* [23], the α -subunit started with the first amino acid of the mature α ETF (α Gln20). For protein purification, a hexa-histidine tag was added to the N-terminus of the β -subunit. The recombinant plasmid was transformed to *E. coli* BL21 (DE3) cells. Positive clones were selected by kanamycin resistance. Correct cloning and potent expression colonies were verified by automated sequencing. All investigated enzyme variants of hETF-WT (β Y16F, α T266M, α N259A, α R249C, α Q285A, β E165A) were constructed by two-step site directed mutagenesis with Phusion DNA polymerase and the mutation primers shown in Table 2 (The altered codon is highlighted in bold).

Table 3 – Primer sequences used for site-directed mutagenesis. All primers were ordered purified salt free.

Primer	DNA Sequence 5' – 3'	T _m
α N259A_fw	GCAGGTTTTGTTCCG G CTGATATGCAGGTTGG	64.0 °C
α N259A_rev	CCAACCTGCATATC A GCCGGAACAAAACCTGC	64.0 °C
α R249C_fw	GCAGTTGGTGCAAGCT G CGCAGCAGTTGATGC	67.3 °C
α R249C_rev	GCATCAACTGCT G CGCAGCTTGACCAACTGC	67.3 °C
α T266M_fw	GATATGCAGGTTGGTCAGAT G GGCAAAATTGTTGCAC	64.8 °C
α T266M_rev	GTGCAACAATTTT G CCCATCTGACCAACCTGCATATC	64.8 °C
α Q285A_fw	GTATTAGCGGTGCAATT G CGCATCTGGCAGGCATG	67.7 °C
α Q285A_rev	CATGCCTGCCAGAT G CGCAATTGCACCGCTAATAC	67.7 °C
β Y16F_fw	GTTAAACGTGTTATTGATTT T GCCGTGAAAATTCGTG	60.0 °C
β Y16F_rev	CACGAATTTT C ACGGCAAAATCAATAACACGTTTAA	60.0 °C
β E165A_fw	CTGAAAGTTGAACGT G CGATTGATGGTGGTCTG	63.6 °C
β E165A_rev	CAGACCACCATCAAT C GCACGTTCAACTTTCAG	63.6 °C

First, two separate PCR reactions using either forward or reverse primer with 10 ng hETF-WT template DNA, 1x Phusion HF buffer, 200 μ M dNTPs, 3% DMSO, 1 unit of Phusion DNA polymerase and 0.5 μ M of each primer were run in 50 μ L volumes with (98 °C (2 min) – [98 °C (50 sec) – 60 °C (20 sec) – 68 °C (16.5 min)] x 5 – 4 °C ∞). Afterwards, the separated PCR reactions were combined and the same PCR program was further employed for another 20 cycles. The PCR was followed by a 2 h *DpnI* digestion step, the plasmid afterwards transformed to *E. coli* BL21 (DE3) cells and the strain selection done as above using the pET28a+ kanamycin resistance.

hETF Enzyme Expression – hETF expression was carried out in shake flasks in an HT Multitron Standard shaking system (Infors AG, Basel, Switzerland) at 150 rpm. In short, O/N LB medium cultures of *E. coli* BL21 (DE3) cells with the desired hETF variant were used to inoculate 1 L main cultures in baffled shake flasks to an OD₆₀₀ of 0.1. After reaching an OD₆₀₀ of 0.6-0.8, the enzyme expression was started by induction with 0.1 mM IPTG and expression took place O/N at 25 °C. The cell pellet was collected by centrifugation (2 704 g, 15 min, RT) and stored at -20 °C until further use.

hETF Enzyme Purification – In general, enzyme purification was done with the following protocol. If changes were done according buffers and pH it is stated directly in the Results section. Cell lysates were prepared by 4 times 3 min sonication, 3 min cooling steps using a Labsonic® L sonication probe (B. Braun Biotech, Berlin, Germany) in a Sonopuls® rosett cell RZ (Bandelin, Berlin, Germany). To every 1 g harvested wet cell pellet, 3 mL cell lysis buffer (50 mM HEPES/NaOH, 15 mM imidazole, pH 7.0) and a spatula tip of FAD were added before sonication. The lysates were cleared by centrifugation (38 720 g, 45 min, 4°C) and filtration through a paper filter. Nickel ion affinity chromatography was done by applying the cell lysates onto 5 mL HisTrap HP columns (GE Healthcare). Afterwards, the columns were washed with at least 10 column volumes lysis buffer and the enzyme stripped off with elution buffer (50 mM HEPES/NaOH, 200 mM imidazole, pH 7.0). The purification was monitored by SDS-PAGE and fractions containing hETF were concentrated using Amicon® ultracentrifugal filter units (10 kDa cut-off, Merck-Milipore, Darmstadt, Germany) and rebuffered to storage buffer (50 mM HEPES/NaOH, pH 7.0) using Sephadex G-25 PD10 desalting columns (GE Healthcare). After rebuffering, the enzyme solution was incubated at 37 °C for 30 min and afterwards cleared by centrifugation in order to get rid of misfolded protein and excessive hETF β -subunits. The obtained enzyme purity was sufficient for all kinetic and spectrophotometric studies.

hDMGDH Expression and Purification – hDMGDH expression and purification for use in interaction studies for steady-state kinetic analyses was done as previously reported by Augustin *et al.* [37].

SDS-PAGE – Enzyme samples were separated by SDS-PAGE with 12.5% separation and 5% stacking gels and reducing conditions (100 mM DTT in the sample buffer) basically as first described by Laemmli [38]. Gels were stained with Coomassie Brilliant Blue R-250 for purification control and as protein standard a PageRuler® Prestained protein ladder (Thermo Fisher Scientific) was employed.

UV/Vis Absorption Spectroscopy – UV/Vis absorption spectra to assess protein concentration, activity, purity and quality as well as for steady-state kinetic measurements and photoreduction were recorded with a Specord 210 spectrophotometer (Analytik Jena, Jena, Germany).

Enzyme Quantification and Calculation of the Extinction Coefficient – Protein concentrations of purified hETF enzymes were determined according the characteristic absorption of protein bound FAD at 469 nm. The molar extinction coefficient (ϵ) for hETF was calculated using an ϵ of free FAD at 469 nm of $9910 \text{ M}^{-1} \text{ cm}^{-1}$, to $9900 \pm 700 \text{ M}^{-1} \text{ cm}^{-1}$ for hETF-WT and all variants at 469 nm with the method described by Macheroux [39].

Extraction and Purification of 8f-FAD – hETF- α N259A variant or hETF-WT purified in 50 mM HEPES/NaOH buffer at pH 8.5 were denatured by two times treatment at $70 \text{ }^\circ\text{C}$ for 10 min and centrifugation at $18\,500 \text{ g}$ for 10 min. The supernatant was concentrated using Amicon[®] ultracentrifugal filter units (10 kDa cut-off) to approximately $300 \text{ }\mu\text{M}$, using the molar extinction coefficient of free FAD at 450 nm of $11\,300 \text{ L M}^{-1} \text{ cm}^{-1}$ [39]. HPLC purification was done on a Dionex UltiMate 3000 HPLC (Thermo Fisher Scientific) equipped with an Atlantis[®] dC18 column ($5 \text{ }\mu\text{m}$, $4.6 \times 250 \text{ mm}$, Waters, Milford, MA, USA) equilibrated with $\text{H}_2\text{O}/0.1\% \text{ TFA}$, $7\% \text{ ACN}$ and a diode array detector for UV/Vis monitoring ($\lambda = 280, 370, 450 \text{ nm}$). An injection volume of $40 \text{ }\mu\text{L}$, a temperature of $25 \text{ }^\circ\text{C}$ and a flow rate of 1 mL min^{-1} were used. 8f-FAD was separated from residual free FAD and other impurities for subsequent photo spectroscopic, NMR and HPLC/MS analyses using the following program: 0-25 min: 7-12% ACN, 25-30 min: 95% ACN, 30-35 min: 7% ACN. $200 \text{ }\mu\text{L}$ fractions were collected between 12.0 and 18.0 min and fractions with a pure and typical 8f-FAD UV/Vis spectrum were combined. The combined fractions were dried using an ISS110 Savant SpeedVac System at $45 \text{ }^\circ\text{C}$, $< 10 \text{ mbar}$ vacuum and an RH64-11 rotor (Thermo Fisher Scientific), and were afterwards stored at $-20 \text{ }^\circ\text{C}$ until further use. Purity of the cofactor was controlled by HPLC measurements using the same conditions as above.

Analysis of 8f-FAD by HPLC/ESI-MS - For HPLC/MS measurements, an Agilent Technologies 1200 Series (Santa Clara, CA, USA) equipped with a G1379B degasser, G1312B binary pump SL, G1367C HiP-ALS SL autosampler, a G1314C VWD SL UV detector, G1316B TCC SL column oven and a G1956B MSD mass selective detector was used. The mass spectrometer was operated in positive electro spray ionization mode. The analytes were separated on an Atlantis[®] dC18 column ($5 \text{ }\mu\text{m}$, $4.6 \times 250 \text{ mm}$, Waters) at $25 \text{ }^\circ\text{C}$ by using aqueous eluent (0.1% formic acid) and ACN at a flow of 1.0 mL min^{-1} . The column was equilibrated with 7% ACN in water (0.1% formic acid) and following gradient was used for analysis: 0-2 min: 7% ACN, 2-10 min: 7-100% ACN, 10-12 min: 100% ACN, 12-14 min: 7% ACN. $10 \text{ }\mu\text{L}$ of $300 \text{ }\mu\text{M}$ HPLC purified 8f-FAD or $300 \text{ }\mu\text{M}$ FAD solution for control, dissolved in water, were injected for each run.

Measurement of ¹H-NMR – 4 mM solutions of purified 8f-FAD or FAD dissolved in 20% D_2O in water (v/v) were subjected to ¹H-NMR analysis using a Varian INOVA 500 (499.82 MHz , Agilent)

spectrometer. $^1\text{H-NMR}$ spectra were recorded at 500 MHz at 30 °C. The signal of water protons (δ_{H} 4.75 ppm) was used as the reference for the observed chemical shifts.

EPR Spectroscopy – Electron paramagnetic resonance experiments were performed with 150 μM hETF- αN259A and hETF- βY16F purified in 50 mM HEPES/NaOH, pH 8.5 and with 150 μM hETF-WT purified in 50 mM HEPES/NaOH, pH 7.0 on an X-band ECS 106 spectrometer (Bruker, Billerica, MA, USA) with 9.45 GHz microwave frequency. A microwave power of 2 mW was used, with a modulation amplitude of 2.0 G at a modulation frequency of 50 kHz. Samples were run at 295 K in 100 μL glass capillaries and 10 scans with a conversion time of 5.12 ms, a time constant of 10.24 ms and a sweep time of 20.97 s. The magnetic field was scanned for 100 G from 3340 to 3440 G. The magnetic phase and field modulation amplitude of the signal channel of the EPR machine was calibrated with solid DPPH (α, α' - diphenyl- β -picryl hydrazyl) according to the manual to a g factor of 2.0036.

Steady-state Kinetics – Steady-state kinetic parameters were determined using 2,6-dichlorophenol-indophenol (DCPIP) according to Okamura-Ikeda *et al.* [40] as terminal electron acceptor and measurable dimension in the spectrophotometer. For the assays, 125 μM DCPIP, 100 nM hDMGDH and 0-100 μM hETF in 50 mM HEPES/NaOH were incubated at 25 °C for 10 min before initiation of the reaction. The reaction was started by addition of 25 mM dimethylglycine (DMG) and the change of absorption was monitored spectrophotometrically at 600 nm over 3 min. For each concentration, at least a triplicate measurement was performed, the initial velocities determined and K_{M} and k_{cat} assessed by non-linear hyperbolic fit in Origin 8.6 (OriginLab Corp., Northampton, MA, USA).

Anaerobic Photoreduction – Photoreduction of hETF-WT and variant αN259A was done according to the method reported by Massey and Hemmerich [41]. The experimental procedure of photoreduction and reoxidation was performed as described by Augustin *et al.* [37]. Approximately 20 μM purified enzyme in 50 mM HEPES/NaOH, pH 7.0 was reduced at 15 °C. Further reduction of hETF-WT was achieved by using a 10-fold excess of sodium dithionite in the solution.

Thermo FAD Temperature Stability – The temperature stability of the enzymes was determined by monitoring the change in the intrinsic protein fluorescence of FAD in a ThermoFluor[®] assay [42]. Thermo FAD measurements were carried out in an FX Connect real time PCR system (Bio-Rad) in 25 μL of 50 mM HEPES/NaOH, pH 7.0 and 30 μM enzyme. The samples were pre-heated to 25 °C and then the temperature was increased in 0.5 °C/min steps to 95 °C. Fluorescence data were collected using the FRET channel. Melting temperatures (T_{m}) were determined using the CFX Manager 3.0 software (Bio-Rad, Hercules, CA, USA).

AUTHOR CONTRIBUTIONS

PA and ECG executed all experiments. They expressed, purified and characterized the enzymes and all variants; RP conducted and interpreted all EPR spectroscopy experiments. PA and PM designed the biochemical experiments and interpreted the data; PA and PM wrote the manuscript.

ACKNOWLEDGMENTS

We would like to thank Dr. Hansjörg Weber for his help to perform NMR spectroscopy and Thorsten Bachler to set up the HPLC/MS method. Furthermore, Dr. Andreas Winkler performed the preliminary experiments on HDX/MS in Heidelberg, Germany. This work was supported by a grant from the Austrian Science Foundation (FWF) to PM (Doctoral program “Molecular Enzymology” W901).

ADDITIONAL OBSERVATIONS

Apart from all experiments described above, we obtained several other interesting results and observations during our study which are listed below. These experiments are not included in the main part of the paper draft because they lack accuracy, reproducibility or the outcome was not considered trustworthy. Nevertheless, some experiments might be useful for the paper, but will have to be repeated.

Additional Observation 1 - Kinetic investigation of 8f-FAD formation in hETF-WT and hETF- α N259A.

The *in vitro* conversion of FAD to 8f-FAD can be achieved by diluting hETF purified at pH 7.0 with basic buffers (i.e. pH 7.8 or 8.5) or by basic titration of the protein solution with high concentrated Na_2CO_3 . This conversion showed several distinct isosbestic points (Figure 8A) and a major increase in absorption around 415 nm. Therefore, this change in absorption at 415 nm as well as the change of the $\text{Abs}_{415/469}$ ratio was used to follow the formylation reaction.

8f-FAD formation velocities were examined for hETF-WT and hETF- α N259A at different temperatures and pH values. Both proteins, purified in HEPES buffer at pH 7.0, were diluted with HEPES buffers pH 7.8 and 8.5 and the change in absorption was followed spectrophotometrically. This simple assay suffers severely from precipitation effects especially of the WT protein at high temperatures. In order to overcome or minimize precipitation effects, the incubated proteins were centrifuged before each measurement and spectra were normalized to the absorption of 469 nm to balance the protein loss. The resulting measurements clearly showed that (1) the higher the temperature the faster 8f-FAD was built, (2) hETF variant α N259A was able to create 8f-FAD much faster than the WT protein and (3) that at physiological pH and temperature of 7.8 and 37 °C hETF-WT was able to form 8f-FAD, but so slow that neogenesis of 8f-FAD without further triggering factors is most likely not physiologically relevant (Additional Table 1). Notably, variant α N259A already showed slow conversion of FAD at pH 7.0 and 4 °C which was not observed for hETF-WT or any other variant, also upon long time storage. Formation of 8f-FAD was found to be buffer independent, but the conversion velocity in sodium phosphate buffer pH 8.5 was significant slower than in HEPES buffer. Precipitation of the protein at higher temperatures was less pronounced for the variant α N259A. Therefore, we assume that the open, flexible form also enhances protein stability.

Additional Table 1 – Reaction velocities of 8f-FAD formation in hETF-WT and α N259A variant at different temperatures and pH values. The velocities are shown as change in protein absorption at 415 nm per minute and are only for comparison.

	pH 7.0			pH 7.8			pH 8.5		
	4 °C	25 °C	37 °C	4 °C	25 °C	37 °C	4 °C	25 °C	37 °C
WT	no fFAD	n.d.*	n.d.	0.0026	0.00432	0.0021**	0.0106	0.0213	0.0339**
N259A	0.0035	n.d.	n.d.	n.d.	n.d.	0.217	0.0271	0.15	0.513

*n.d. – not determined

**measurements of the hETF-WT at 37 °C were severely disturbed by protein precipitation events and therefore these values are only rough estimations.

Additional Observation 2 - Alternative reactions and triggering factors leading to 8f-FAD formation.

Additionally to different pH, buffer and temperature conditions (Additional Observation 1), also the influence of light on the formation of 8f-FAD in WT samples incubated at pH 7.8 and 8.5 was investigated. Although, here again, the assay suffered from precipitation problems it can definitely be concluded that the exposure to a strong light source significantly increased the velocity of 8f-FAD formation at pH 7.8 and pH 8.5. Apart from light, also frequent freezing and thawing cycles lead to faster formation of 8f-FAD. Furthermore, it is yet not completely undoubtedly experimentally confirmed whether the His-tag or Ni-NTA affinity chromatography with imidazole can definitely be excluded as influencing factors (Missing Experiment 10).

Additionally, in Figure 13, we formulated a reaction mechanism, which is based on the availability of oxygen during the conversion. In contrast to this, we have seen in several occasions a formation and emerging of a distinct 415 nm peak although working in an oxygen free environment in the glovebox. These observations included photoreduction, kinetic experiments in the glovebox at 37 °C with air free buffers, dithionite reductions and interaction studies with hDMGDH. The collective property of all those experiments was that there was always a small but detectable portion of 8f-FAD already present as seen in the spectrum with a slightly increased peak at 415 nm and with small occurring peaks between 600 and 800 nm. Therefore, we hypothesize that maybe also a radical reaction mechanism upon reduction of the protein and transfer of the radicals could be a possibility to form 8f-FAD. Especially the influence of light is particularly evident which easily forms FAD or 8f-FAD semiquinone radicals also without the addition of EDTA or reduction enhancer like 5-diaza FMN or methylviologen. Furthermore, the reactions described above always seemed pH independent as the effect was also present in photoreduction at pH 7.0. In literature a radical mechanism that could add a formyl group to the 8α methyl group of the isoalloxazine was described in experiments with diphenyliodonium chloride and different flavins [43].

Additional Observation 3 – Characterization of further variants α R249A and α R249K.

Apart from the naturally occurring variation of arginine α 249 to cysteine [32,34], we also replaced the arginine with the uncharged, small amino acid alanine and the charged, bulky amino acid lysine. The primers used for site-directed mutagenesis as described in the Experimental Procedures are listed in Additional Table 2. Variant hETF- α R249A showed a very similar behavior as hETF- α R249C. The protein temperature stability was slightly reduced (Additional Table 3) and the variant was also not capable of 8f-FAD formation. On the other hand, variant hETF- α R249K, which retains the positive charge of arginine in the active site, was still able to catalyze 8f-FAD formation and also the protein stability was surprisingly increased to 65 °C (Additional Table 3). The results of these two variants emphasized the importance of the positive, stabilizing charge of arginine next to the isoalloxazine ring to neutralize negatively charged intermediates during 8f-FAD formation as well as to stabilize the final 8f-FAD semiquinone.

Additional Table 2 – Mutagenesis primer used to generate hETF variants α R249A and α R249K.

Primer	DNA Sequence 5' – 3'	T _m
α R249A_fw	GCAGTTGGTGCAAGCGCGGCAGCAGTTGATGC	67.3 °C
α R249A_rev	GCATCAACTGCTGCCGCGCTTGCACCAACTGC	67.3 °C
α R249K_fw	GCAGTTGGTGCAAGCAAAGCAGCAGTTGATGCAG	67.3 °C
α R249K_rev	CTGCATCAACTGCTGCTTTGCTTGCACCAACTGC	67.3 °C

Additional Observation 4 – Thermo FAD measurements of all related variants.

Variants not able to form 8f-FAD apparently also showed decreased stability in Thermo FAD measurements (Additional Table 3). All proteins were purified in 50 mM HEPES/NaOH, pH 7.0 and measured at a final concentration of 30 μ M protein at least in triplicates. Additional Table 3 shows that except for variant α R249A, all other variants that are not able to form 8f-FAD showed lower temperature stability. On the other hand, the variants that show higher flexibility of the protein and faster 8f-FAD formation had constant or increased melting temperatures. The naturally occurring variants in glutaric aciduria type II disease, α R249C and α T266M both had a significantly reduced temperature stability.

Additional Table 3 – Temperature stability of hETF-WT in comparison with various variants. The temperature stability was measured in Thermo FAD assays and the melting temperature (T_m) is shown in °C. Triplicates were done.

hETF	WT	α N259A	β E165A	α R249A	α R249C	α R249K	α T266M	α Q285A	β Y16F
T_m [°C]	60.5	60.0	59.0	62.0	57.3	65.0	55.2	57.5	58.0*

* T_m of variant β Y16F could only be measured when SYPRO-Orange was added, Thermo FAD measurements did not give any results. It seems that the tyrosine to phenylalanine variation somehow trapped the cofactor in the protein and/or quenched its fluorescence.

Additional Observation 5 – Stopped flow interaction measurements of hETF-WT and hDMGDH.

Stopped flow measurements to study the interaction of hETF-WT with hDMGDH were mainly done to determine binding affinity (K_D) of the proteins and to determine reductive half-reaction kinetics of hETF-WT. Both aspects will be treated in detail in Chapter IV of this thesis. For the experiments on 8f-FAD it is important to note that during these interaction studies, a rise of the hETF peak around 415 nm prior to the actual hETF-reduction as seen in photoreduction sometimes appeared but could not always be reproduced, quantified or characterized. These observations add to similar observations made during protein photoreduction and conversion of FAD to 8f-FAD in the glovebox and suggest additional factors influencing 8f-FAD formation velocity (Additional Experiment 2). Furthermore, this observation led to the question if 8f-FAD is also built upon protein-hETF interaction (Missing Experiment 5).

Additional Observation 6 – HDX/MS measurements of hETF-WT and hETF- α N259A.

Hydrogen/Deuterium exchange mass spectrometry (HDX/MS) is a new method to determine protein flexibility and protein dynamics as can be reviewed in [44]. Thankfully, Dr. Andreas Winkler measured our hETF-WT protein, purified at pH 7.0 (0% 8f-FAD) and pH 8.5 (~30% 8f-FAD) as well as hETF- α N259A purified at pH 8.5 (100% 8f-FAD) and found out that the higher the formylation of the protein, the more flexible the proteins get. For instance, partly formylated hETF-WT showed a much higher flexibility and tendency to occur in its open form in solution than unformylated hETF-WT. Although these results are preliminary this could be an explanation why formylated protein showed higher protein affinity than unformylated one.

Additional Observation 7 – Interaction studies of hETF with hDMGDH and other dehydrogenases.

The characterization of the interaction between hDMGDH and hETF was investigated in detail and will be provided as a separate paper draft (Chapter IV). The interaction of hETF with the other flavin dehydrogenases isobutyryl-CoA dehydrogenase, medium chain acyl-CoA dehydrogenase and acyl-CoA dehydrogenase family member 9 (ACAD-9) are currently planned and will be done during the PhD thesis of Sami Ullah Khan with help of Wolf-Dieter Lienhart in the group of Peter Macheroux.

MISSING EXPERIMENTS

Additionally to the “Additional Experiments”, there are several important data in the paper draft missing to complete the study. The following section provides ideas of missing experiments that would help to complete the paper draft to a final publication.

Missing Experiment 2 - Redoxpotentials of unformylated hETF-WT in comparison with highly formylated hETF-N259A variant.

The formylation of FAD in hETF not only massively influences the UV/Vis spectrum, protein affinity and protein stability, but above all alters the redoxpotential of the cofactor and subsequently of the protein. The method of choice to investigate the redox potentials of flavoprotein is the xanthine/xanthine oxidase method established by Vincent Massey [45]. The drawback of this method for our investigations is that it is very difficult to separate the redox potential of the one electron transfer of hETF-WT from the oxidized to the red anionic semiquinone, which unfortunately is not stabilized enough during xanthine oxidase reduction. Nevertheless, redox potentials of hETF-WT have been already determined in literature by use of gallocyanine and pyocyanine as redox dyes which could serve as references [34]. Furthermore, it has to be kept in mind that with 8f-FAD the stable state is the semiquinone and it is more difficult to compare the redox potentials of hETF-WT with the variant. The redox potential of the variant from oxidized to semiquinone state cannot be measured because the oxidized form was not seen or obtained yet.

Additional to the spectroscopic method using xanthine and xanthine oxidase, we are currently setting up a collaboration with Dr. Roland Ludwig from the Department of Food Sciences and Technology from the BOKU Vienna, who is able to measure redox potentials potentiometrically and therefore could be able to efficiently separate one electron transfer redox potentials. This was already performed and described for ETF from *Methylophilus methylotrophus* [46] or nearly 40 years ago for hETF-WT [47].

Missing Experiment 3 and 4 - Time-dependent formation of 8f-FAD in hETF- β E165A purified at pH 7.0 in comparison with variant α N259A, repeat of steady-state kinetics with variant hETF- β E165A in comparison with variant α N259A.

Steady-state kinetic experiments provided us with one of the most important results of this paper draft, the decrease of the Michaelis-Menten constant while maintaining the reaction velocity the higher the fraction of formylated cofactor in the protein (Figure 10, Table 1). This was especially obvious for hETF variant α N259A which lacks the salt bridge formed between α N259 and β E165 in the protein. The consequence of the variation is a higher flexibility of the protein, higher exposure of the bound cofactor to the solvent and higher tendency of the protein to exist in its open and thus more reactive form in solution [6]. For our studies we focused on variant α N259A as this variant provided us with better protein yields and overall more reproducible results. Nevertheless, also variant β E165A forms 8f-FAD

significantly faster than the WT, already at low pH, and it would be a good idea to repeat our experiments (i.e. steady-state kinetics, formylation grade, redoxpotential) with this variant. Furthermore, during the investigations of hMCAD-hETF interaction by Toogood *et al.* [5,6], variant β E165A was used for hMCAD-hETF co-crystallization and also some kinetic investigations with rat DMGDH was done. Similar to our results, also Toogood *et al.* observe a decreased K_M value with protein variant hETF- β E165A in the interaction with rat DMGDH and human MCAD [6].

We have already constructed an *E. coli* expression strain for hETF- β E165A expression, hETF- β E165A protein was already expressed and showed in its unformylated form at pH 7.0 a very similar kinetic and spectroscopic results compared to hETF-WT enzyme (Figure 11, Table 2).

Kinetic experiments and Thermo FAD measurements with hETF variant β E165A purified at higher pH and therefore with a higher formylation grade were not conducted. It is expected that the experiments resemble the results obtained for the sister variant α N259A and hence shows greater affinity to partner dehydrogenases.

Missing Experiment 5 - Does the interaction of hETF with hDMGDH form 8f-FAD?

In our experiments, we established the fact that 8-formyl FAD can be formed in hETF-WT and it can be formed at physiological pH of 7.8. The presence of the formyl group is thought to change the redoxpotential of the protein and also change the protein affinity. Nevertheless, we have not been able to tell yet whether its formation is physiologically relevant, if the protein exists *in vivo* in the cells as a mixture of unformylated and formylated form or whether it is formed spontaneously at cell stress, higher metabolic pressure due to increased β -oxidation or amino acid metabolism. Also other beneficial effects of 8f-FAD, as higher protein lifetime or the recruitment of new interaction partners cannot be excluded. One of the questions still to be answered is if 8f-FAD formation is necessary or increased upon hETF – protein interaction, in our case during the interaction with the human dimethylglycine dehydrogenase.

We conducted our steady-state experiments at pH 7.0 where 8f-FAD formation has not been observed in solution for hETF-WT and therefore a stable FAD content in the protein during the reaction was guaranteed. Also in the experiments with 8f-FAD fractions in hETF-WT and hETF- α N259A variant, the formylation grade of the proteins should stay constant during the reaction due to the low pH. Nevertheless, this scenario is still an assumption and therefore it cannot be excluded that additional 8f-FAD is formed during the interaction of hETF with hDMGDH not only at physiological pH of 7.8, and higher, but also already at pH 7.0.

In order to investigate a possible 8f-FAD formation during the reaction of hETF with hDMGDH, two easy experiments could be conducted. First, hETF and hDMGDH are incubated together in assay conditions for several minutes until most of the hETF is reduced and/or has taken part at the reaction at different pH values (pH 7.0, pH 7.8 and pH 8.5). Afterwards, the assay mixture is separated by size

exclusion chromatography and the obtained hETF fraction analyzed spectrophotometrically for 8f-FAD containing protein. Negative controls without the addition of hDMGDH to the mixture have to be conducted separately to show that “inter-reacted” hETF fractions contain a higher formylation grade than unreacted ones.

As already discussed in Additional Observation 2” faster and spontaneous 8f-FAD formation in the protein was already observed during the interaction of hDMGDH and hETF at stopped flow measurements (Additional Observation 5). The problem was that a fast emerge of a peak at 415 nm was not seen all the time and therefore the experiments were not reproducible. Furthermore, the resolution of the stopped flow device in the range of 415 nm often was too low to quantify small changes in absorption.

Missing Experiment 6 - Photoreduction of non 8f-FAD producing variants. Are these variants still able to stabilize semiquinones?

One assumption why some of our hETF variants lost their ability to build 8f-FAD could be that they lost the ability to stabilize semiquinones, especially important for variants α T266M and α R249C. This hypothesis could be easily confirmed by photoreduction of these variants and comparison with the wild-type enzyme. Full reduction of hETF-WT to the hydroquinone can only be achieved with high sodium dithionite concentrations and oxygen exclusion as the semiquinone is considerably stabilized in the wild-type protein. It has to be noted that hETF can be easily photoreduced and addition of methylviologen and 5-deaza-FMN is not necessary. In fact, hETF was shown to be photoreduced even without the addition of EDTA to the solution.

Missing Experiment 7 – Test of additional variants α Q262A and α H286A for 8f-FAD formation.

The alignment of the crystal structures of hETF-WT and three bacterial analogues in Figure 12C, as well as the sequence alignment of several proteins from the ETF-family [5] showed that there are additional amino acids in proximity to the active site that are strictly conserved in all shown proteins. Among them, most interestingly the role of amino acid residues α Q262 and α H286 should be investigated, above all, concerning their ability to form 8f-FAD. The expected role of both amino acids is to stabilize negative charges during the reaction as well as the semiquinone in the end, very similar to residues α T266 and α R249.

The construction of the variants, the design of the mutagenesis primers and the protein expression and purification can be easily done as described in the Experimental Procedures. The protein characterization would include the spectrophotometrical characterization as done for all other variants, purification at different pH values, Thermo FAD measurements as well as investigation of the interaction behavior with hDMGDH.

Additional missing experiments not included in Peters paper draft:**Missing Experiment 8** - Reoxidation velocities of reduced hETF-WT and hETF-N259A

The conversion of FAD to 8f-FAD in hETF not only influences the reduction behavior of the protein (to be seen with Missing Experiment 2) by expectedly making the redox potential more positive, but also will affect the reoxidation of the protein *in vivo* by the electron transferring flavoprotein dehydrogenase (hETF-QO) and *in vitro* by air oxygen. In order to investigate the reoxidation, photoreduced protein has to be exposed to either air oxygen and investigated spectrophotometrically or reoxidized by air-saturated buffer in a stopped flow device. Consequently, it would be expected that oxygen reactivity of the formylated α N259A variant is decreased compared to unformylated hETF-WT.

Missing Experiment 9 - Further oxidation of protein bound 8f-FAD semiquinone.

During our investigations of free 8f-FAD in solution and bound to the protein, it was striking that the cofactor does not occur in a fully oxidized form but as stable semiquinone when bound to the protein. During the interaction with partner dehydrogenases, 8f-FAD semiquinone gets fully reduced to its hydroquinone form and is re-oxidized to a mixture of anionic and neutral semiquinones afterwards. A further oxidized 8f-FAD never has been observed.

In order to test whether 8f-FAD can be further oxidized in the protein environment the reaction of formylated protein with strong oxidating reagents such as H₂O₂, DCPIP or ferrocene should be investigated. A probable oxidation can be observed spectrophotometrically, in difference titration experiments or by means of the stopped flow device. It has to be noted that only very little amounts of the oxidizing reagents should be used in order to avoid protein denaturation as has been seen in quick and dirty experiments before.

Missing Experiment 10 - Does the N-terminal His-tag or imidazole influence the protein activity and 8f-FAD formation?

In this paper draft, we show that the N-terminal His-tag did not influence protein stability, formation of 8f-FAD and the protein showed a similar activity as reported for rat DMGDH – human ETF interaction [6]. Nevertheless, in order to get a definite picture, it would be favorable to prove that the kinetic parameters for hETF-WT with cleaved off His-tag resemble the data obtained for hETF-WT with an N-terminal His-tag. Furthermore, it cannot be excluded yet that residual imidazole in the buffers or impurities of His-tagged hETF-WT proteins in the cleaved off fraction influenced the obtained results in Figure 6D.

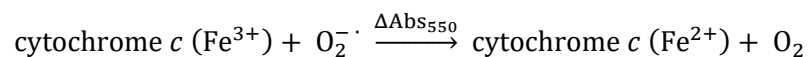
We have already constructed an *E. coli* expression strain for hETF-WT expression with TEV protease cleavable His-tag. The protein was expressed and purified and showed the same spectroscopic behavior as the WT, before and after cleavage of the His-tag (Figure 6D). Furthermore, protein stability determined with Thermo FAD also was not influenced by the His-tag and determined to be 60 °C for

the His-tagged and untagged protein respectively. The only experiments missing are the complete steady-state characterization to get K_M , k_{cat} and catalytic efficiency of the untagged protein and to exclude an influence of imidazole. Furthermore, it would also be profitable to repeat the 8f-FAD formation experiments with higher amounts of His-tag free protein.

It has to be noted that a very high amount of TEV protease will be needed in order to get enough untagged protein to conduct this experiment. In order to get rid of the cleaved off His-tag and the TEV protease, the available TEV protease in our laboratory is also tagged with a His-tag and can be efficiently removed by a second His-trap affinity chromatography.

Missing Experiment 11 - Superoxide detection by reduction of ferricytochrome *c* during the formation of 8f-FAD.

The reaction mechanism we formulated in Figure 13 involves the formation of the radical oxygen superoxide species ($O_2^{\cdot -}$) during two reaction steps. In order to strengthen our reaction mechanism and to prove the formation of $O_2^{\cdot -}$ a cytochrome *c* / superoxide dismutase coupled assay could be employed. In this assay ferricytochrome *c* is reduced to ferrocyanochrome *c* (see equation) and the change in absorption can be followed spectrophotometrically at 550 nm [48].



In order to demonstrate the specificity of the reaction during the assay, the inhibition of ferricytochrome *c* reduction has to be proven by exogenous superoxide-dismutase [49]. An example for an assay setup can be found in the publication by Barbacanne *et al.* [50]. This assay is the most common one to detect superoxide species but there are also several other simple assays established; inhibition of aconitase, oxidation of hydroethidine or also several luminescence based methods could be used alternatively [48,51].

There exist previous studies reporting that at elevated pH levels, reactive oxygen species formation in mitochondria is severely increased [52] and more importantly, it has been shown that purified hETF already produces considerable amounts of superoxide [53]. In the study by Rodrigues and Gomes, especially the interaction of the protein with hMCAD produced considerable amounts of reactive oxygen species and it has to be clarified if this is solely because of the formation of the hETF semiquinone during the reaction or also because of the formation of 8f-FAD.

Missing Experiment 12– Protein crystallization.

Literature provides several structures of ETF wild-type and variants from bacterial and mammalian origin, but there is no structure yet with a bound 8f-FAD as cofactor. Although some of the deposited electron densities would allow to fit an 8f-FAD instead of the present FAD into the structure, one of the

most important experiments to be conducted in future would be the crystallization of hETF-WT or variant α N259A with a bound formylated 8f-FAD. The crystal structure of bound 8f-FAD could also show the impact of the formyl group onto the surrounding amino acids and the binding mode of the cofactor itself. In the crystal structure for formate oxidase, the 8f-FAD cofactor is significantly bent, which could be a direct effect of the formylation. Protein crystallization was already tried but unfortunately, all crystallization tryouts with hETF-WT (formylated and unformylated) and variants α N259A and β E165A have not been successful so far. For previous protein crystallization tryouts, a second purification step was done by size exclusion chromatography on an ÄKTA FPLC system (GE Healthcare) at 4 °C in 50 mM HEPES/NaOH, pH 7.0 to get rid of residual impurities and protein aggregates. Chromatography was controlled by SDS-PAGE and fractions containing hETF were collected and concentrated. All purifications were done identically for the wild-type and all variant enzymes. Afterwards crystallization screens were done at different concentrations of the proteins (5 – 15 mg/mL = 80-250 μ M) with the crystallization conditions used by Roberts *et al.* [7] and by Toogood *et al.* [5,6]. For future experiments also the conditions used to crystallize the bacterial ETF enzymes could be used for screening. Furthermore, crystallization tryouts with hETF with cleaved off His-tag by TEV protease should be used.

Missing Experiment 13 - Determination of formylation grade by HPLC purification.

During the investigation of hETF-WT and its variants purified at different pH values, we came up with the idea to estimate the formylation grade of the protein by using the absorption ratio of 415 nm and 469 nm ($Abs_{415/469}$). Nevertheless, this concept never has been experimentally proven and also the basis values for 0% 8f-FAD, hETF-WT purified at pH 7.0 and 100% 8f-FAD, hETF- α N259A purified at pH 8.5 and incubated O/N at 25 °C, have never been verified and quantified.

In order to experimentally confirm our $Abs_{415/469}$ concept, we would have to express the concerned proteins, extract the cofactor mixture as described in Experimental Procedures, concentrate the solution to approximately 300 μ M and analyze the cofactor composition with our established HPLC purification protocol. As we were able to efficiently separate FAD from open and hemiacetal form of 8f-FAD, the formylation grade of the protein could be calculated by simply comparing the obtained peak areas after HPLC purification.

The possibility to quantify the formylation grade of FAD in hETF would make kinetic and spectroscopic experiments more accurate and could better relate observations like decreasing K_M and k_{cat} values to actual formylation grades of the proteins.

REFERENCES

- 1 Crane FL, Mii S, Hauge JG, Green DE & Beinert H (1956) On the mechanism of dehydrogenation of fatty acyl derivatives of coenzyme A. I. The general fatty acyl coenzyme A dehydrogenase. *J. Biol. Chem.* **218**, 701–6.
- 2 Toogood HS, Leys D & Scrutton NS (2007) Dynamics driving function – new insights from electron transferring flavoproteins and partner complexes. *FEBS J.* **274**, 5481–5504.
- 3 Ghisla S & Thorpe C (2004) Acyl-CoA dehydrogenases. A mechanistic overview. *Eur. J. Biochem.* **271**, 494–508.
- 4 He M, Pei Z, Mohsen A-W, Watkins P, Murdoch G, Van Veldhoven PP, Ensenaer R & Vockley J (2011) Identification and characterization of new long chain acyl-CoA dehydrogenases. *Mol. Genet. Metab.* **102**, 418–29.
- 5 Toogood HS, van Thiel A, Basran J, Sutcliffe MJ, Scrutton NS & Leys D (2004) Extensive domain motion and electron transfer in the human electron transferring flavoprotein.medium chain Acyl-CoA dehydrogenase complex. *J. Biol. Chem.* **279**, 32904–12.
- 6 Toogood HS, van Thiel A, Scrutton NS & Leys D (2005) Stabilization of non-productive conformations underpins rapid electron transfer to electron-transferring flavoprotein. *J. Biol. Chem.* **280**, 30361–6.
- 7 Roberts DL, Frerman FE & Kim J-JP (1996) Three-dimensional structure of human electron transfer flavoprotein to 2.1-Å resolution. *Proc. Natl. Acad. Sci.* **93**, 14355–14360.
- 8 Roberts DL, Salazar D, Fulmer JP, Frerman FE & Kim J-JP (1999) Crystal structure of *Paracoccus denitrificans* electron transfer flavoprotein: structural and electrostatic analysis of a conserved flavin binding domain. *Biochemistry* **38**, 1977–89.
- 9 Burgess SG, Messiha HL, Katona G, Rigby SEJ, Leys D & Scrutton NS (2008) Probing the dynamic interface between trimethylamine dehydrogenase (TMADH) and electron transferring flavoprotein (ETF) in the TMADH-2ETF complex: role of the Arg- α 237 (ETF) and Tyr-442 (TMADH) residue pair. *Biochemistry* **47**, 5168–81.
- 10 Chowdhury NP, Mowafy AM, Demmer JK, Upadhyay V, Koelzer S, Jayamani E, Kahnt J, Hornung M, Demmer U, Ermler U & Buckel W (2014) Studies on the Mechanism of Electron Bifurcation Catalyzed by Electron Transferring Flavoprotein (Etf) and Butyryl-CoA Dehydrogenase (Bcd) of *Acidaminococcus fermentans*. *J. Biol. Chem.* **289**, 5145–5157.
- 11 Watmough NJ, Kiss J & Frerman FE (1992) Structural and redox relationships between *Paracoccus denitrificans*, porcine and human electron-transferring flavoproteins. *Eur. J. Biochem.* **205**, 1089–1097.
- 12 Mewies M, McIntire WS & Scrutton NS (1998) Covalent attachment of flavin adenine dinucleotide (FAD) and flavin mononucleotide (FMN) to enzymes: The current state of affairs. *Protein Sci.* **7**, 7–21.

- 13 Edmondson DE & Singer TP (1976) 8 α -substituted flavins of biological importance: an updating. *FEBS Lett.* **64**, 255–65.
- 14 Singer TP & Edmondson DE (1974) 8 α -Substituted flavins of biological importance. *FEBS Lett.* **42**, 1–14.
- 15 Macheroux P, Kappes B & Ealick SE (2011) Flavogenomics - a genomic and structural view of flavin-dependent proteins. *FEBS J.* **278**, 2625–2634.
- 16 Jhulki I, Chanani PK, Abdelwahed SH & Begley TP (2016) A Remarkable Oxidative Cascade That Replaces the Riboflavin C8 Methyl with an Amino Group during Roseoflavin Biosynthesis. *J. Am. Chem. Soc.* **138**, 8324–8327.
- 17 Maeda Y, Doubayashi D, Oki M, Nose H, Sakurai A, Isa K, Fujii Y & Uchida H (2009) Expression in *Escherichia coli* of an unnamed protein gene from *Aspergillus oryzae* RIB40 and cofactor analyses of the gene product as formate oxidase. *Biosci. Biotechnol. Biochem.* **73**, 2645–9.
- 18 Doubayashi D, Ootake T, Maeda Y, Oki M, Tokunaga Y, Sakurai A, Nagaosa Y, Mikami B & Uchida H (2011) Formate oxidase, an enzyme of the glucose-methanol-choline oxidoreductase family, has a His-Arg pair and 8-formyl-FAD at the catalytic site. *Biosci. Biotechnol. Biochem.* **75**, 1662–7.
- 19 Edmondson DE (1974) Intramolecular hemiacetal formation in 8-formylriboflavine. *Biochemistry* **13**, 2817–21.
- 20 Yorita K, Matsuoka T, Misaki H & Massey V (2000) Interaction of two arginine residues in lactate oxidase with the enzyme flavin: Conversion of FMN to 8-formyl-FMN. *Proc. Natl. Acad. Sci.* **97**, 13039–13044.
- 21 Porcelli AM, Ghelli A, Zanna C, Pinton P, Rizzuto R & Rugolo M (2005) pH difference across the outer mitochondrial membrane measured with a green fluorescent protein mutant. *Biochem. Biophys. Res. Commun.* **326**, 799–804.
- 22 Llopis J, McCaffery JM, Miyawaki A, Farquhar MG & Tsien RY (1998) Measurement of cytosolic, mitochondrial, and Golgi pH in single living cells with green fluorescent proteins. *Proc. Natl. Acad. Sci.* **95**, 6803–6808.
- 23 Herrick KR, Salazar D, Goodman SI, Finocchiaro G, Bedzyk LA & Frerman FE (1994) Expression and characterization of human and chimeric human-*Paracoccus denitrificans* electron transfer flavoproteins. *J. Biol. Chem.* **269**, 32239–45.
- 24 Husain M & Steenkamp DJ (1983) Electron transfer flavoprotein from pig liver mitochondria. A simple purification and re-evaluation of some of the molecular properties. *Biochem. J.* **209**, 541–545.
- 25 Horai H, Arita M, Kanaya S, Nihei Y, Ikeda T, Suwa K, Ojima Y, Tanaka K, Tanaka S, Aoshima K, Akimoto N, Maoka T, Sakurai N, Suzuki H, Shibata D, Neumann S, Iida T, Tanaka K, Funatsu K, Matsuura F, Soga T, Taguchi R, Saito K & Nishioka T (2010) MassBank: a public repository for sharing mass spectral data for life sciences. *J. Mass Spectrom.* **45**, 703–714.

- 26 Schleicher E, Bittl R & Weber S (2009) New roles of flavoproteins in molecular cell biology: Blue-light active flavoproteins studied by electron paramagnetic resonance. *FEBS J.* **276**, 4290–4303.
- 27 Massey V & Palmer G (1966) On the Existence of Spectrally Distinct Classes of Flavoprotein Semiquinones. A New Method for the Quantitative Production of Flavoprotein Semiquinones *. *Biochemistry* **5**, 3181–3189.
- 28 Christensen E, Kølvrå S & Gregersen N (1984) Glutaric Aciduria Type II: Evidence for a Defect Related to the Electron Transfer Flavoprotein or Its Dehydrogenase. *Pediatr. Res.* **18**, 663–667.
- 29 Frerman FE & Goodman SI (2001) Defects of electron transfer flavoprotein and electron transfer flavoprotein-ubiquinone oxidoreductase: glutaric acidemia type II. In *The Metabolic and Molecular Bases of Inherited Disease. (8th ed.)* (Scriver CR, Beaudet AL, Sly WS, & Valle D, eds), 8th editio, pp. 2357–2365. McGraw-Hill, New York.
- 30 Schiff M, Froissart R, Olsen RKJ, Acquaviva C & Vianey-Saban C (2006) Electron transfer flavoprotein deficiency: Functional and molecular aspects. *Mol. Genet. Metab.* **88**, 153–158.
- 31 Salazar D, Zhang L, DeGala GD & Frerman FE (1997) Expression and Characterization of Two Pathogenic Mutations in Human Electron Transfer Flavoprotein. *J. Biol. Chem.* **272**, 26425–26433.
- 32 Henriques BJ, Bross P & Gomes CM (2010) Mutational hotspots in electron transfer flavoprotein underlie defective folding and function in multiple acyl-CoA dehydrogenase deficiency. *Biochim. Biophys. Acta - Mol. Basis Dis.* **1802**, 1070–1077.
- 33 Lehman TC & Thorpe C (1992) A new form of mammalian electron-transferring flavoprotein. *Arch. Biochem. Biophys.* **292**, 594–599.
- 34 Dwyer TM, Zhang L, Muller M, Marrugo F & Frerman F (1999) The functions of the flavin contact residues, α Arg249 and β Tyr16, in human electron transfer flavoprotein. *Biochim. Biophys. Acta - Protein Struct. Mol. Enzymol.* **1433**, 139–152.
- 35 John P & Whatley FR (1975) *Paracoccus denitrificans* and the evolutionary origin of the mitochondrion. *Nature* **254**, 495–498.
- 36 Bross P, Pedersen P, Winter V, Nyholm M, Johansen BN, Olsen RKJ, Corydon MJ, Andresen BS, Eiberg H, Kølvrå S & Gregersen N (1999) A Polymorphic Variant in the Human Electron Transfer Flavoprotein α -Chain (α -T171) Displays Decreased Thermal Stability and Is Overrepresented in Very-Long-Chain acyl-CoA Dehydrogenase-Deficient Patients with Mild Childhood Presentation. *Mol. Genet. Metab.* **67**, 138–147.
- 37 Augustin P, Hromic A, Pavkov-Keller T, Gruber K & Macheroux P (2016) Structure and biochemical properties of recombinant human dimethylglycine dehydrogenase and comparison to the disease-related H109R variant. *FEBS J.* **283**, 3587–3603.
- 38 Laemmli UK (1970) Cleavage of Structural Proteins during the Assembly of the Head of Bacteriophage T4. *Nature* **227**, 680–685.

- 39 Macheroux P (1999) UV-visible spectroscopy as a tool to study flavoproteins. *Methods Mol. Biol.* **131**, 1–7.
- 40 Okamura-Ikeda K, Ikeda Y & Tanaka K (1985) An essential cysteine residue located in the vicinity of the FAD-binding site in short-chain, medium-chain, and long-chain acyl-CoA dehydrogenases from rat liver mitochondria. *J. Biol. Chem.* **260**, 1338–45.
- 41 Massey V, Hemmerich P, Knappe WR, Duchstein HJ & Fenner H (1978) Photoreduction of flavoproteins and other biological compounds catalyzed by deazaflavins. Appendix: photochemical formation of deazaflavin dimers. *Biochemistry* **17**, 9–17.
- 42 Forneris F, Orru R, Bonivento D, Chiarelli LR & Mattevi A (2009) Thermo FAD, a ThermoFluor®-adapted flavin ad hoc detection system for protein folding and ligand binding. *FEBS J.* **276**, 2833–2840.
- 43 Chakraborty S & Massey V (2002) Reaction of Reduced Flavins and Flavoproteins with Diphenyliodonium Chloride. *J. Biol. Chem.* **277**, 41507–41516.
- 44 Konermann L, Pan J & Liu Y-H (2011) Hydrogen exchange mass spectrometry for studying protein structure and dynamics. *Chem. Soc. Rev.* **40**, 1224–1234.
- 45 Massey V (1991) A simple method for the determination of redox potentials. In *Flavins and Flavoproteins* (Curti B, Zanetti G, & Ronchi S, eds), pp. 59–66. Walter de Gruyter, Como, Italy.
- 46 Byron CM, Stankovich MT, Husain M & Davidson VL (1989) Unusual redox properties of electron-transfer flavoprotein from *Methylophilus methylotrophus*. *Biochemistry* **28**, 8582–7.
- 47 Voltti H & Hassinen IE (1978) Oxidation-reduction midpoint potentials of mitochondrial flavoproteins and their intramitochondrial localization. *J. Bioenerg. Biomembr.* **10**, 45–58.
- 48 Tarpey MM (2004) Methods for detection of reactive metabolites of oxygen and nitrogen: in vitro and in vivo considerations. *AJP Regul. Integr. Comp. Physiol.* **286**, 431R–444.
- 49 Misra HP & Fridovich I (1972) The role of superoxide anion in the autoxidation of epinephrine and a simple assay for superoxide dismutase. *J. Biol. Chem.* **247**, 3170–5.
- 50 Barbacanne M-A, Souchard J-P, Darblade B, Iliou J-P, Nepveu F, Pipy B, Bayard F & Arnal J-F (2000) Detection of superoxide anion released extracellularly by endothelial cells using cytochrome c reduction, ESR, fluorescence and lucigenin-enhanced chemiluminescence techniques. *Free Radic. Biol. Med.* **29**, 388–396.
- 51 Georgiou CD, Papapostolou I & Grintzalis K (2008) Superoxide radical detection in cells, tissues, organisms (animals, plants, insects, microorganisms) and soils. *Nat. Protoc.* **3**, 1679–1692.
- 52 Selivanov VA, Zeak JA, Roca J, Cascante M, Trucco M & Votyakova T V. (2008) The Role of External and Matrix pH in Mitochondrial Reactive Oxygen Species Generation. *J. Biol. Chem.* **283**, 29292–29300.
- 53 Rodrigues J V. & Gomes CM (2012) Mechanism of superoxide and hydrogen peroxide generation by human electron-transfer flavoprotein and pathological variants. *Free Radic. Biol. Med.* **53**, 12–19.

CHAPTER IV

INSIGHTS INTO THE PROTEIN-PROTEIN INTERACTION OF HUMAN DIMETHYLGLYCINE DEHYDROGENASE AND HUMAN ELECTRON TRANSFERRING FLAVOPROTEIN

Peter Augustin, Eva Christine Gerstmann, Julia Messenlehner, Florian Wieser, Peter Macheroux

Institute of Biochemistry, Graz University of Technology, Graz, Austria

Running title

hETF-hDMGDH Protein-Protein Interaction

Keywords

Electron transfer, flavin adenine dinucleotide, microscale thermophoresis, recombinant protein expression, protein-protein interaction, transient protein complexes.

Abbreviations

DCPIP, 2,6-dichlorophenolindophenol; hDMGDH, human dimethylglycine dehydrogenase; hETF, human electron transferring flavoprotein; hMCAD, human medium chain acyl-CoA dehydrogenase; hETF-QO, human electron transferring flavoprotein ubiquinone oxidoreductase; ITC, isothermal titration calorimetry; MST, microscale thermophoresis; WT, wild-type.

ABSTRACT

The human electron transferring flavoprotein (hETF) is an extraordinary versatile and important electron carrier in mitochondria able to interact with up to thirteen structurally distinct flavin dehydrogenases. So far, only the interaction mechanism of hETF and one partner protein, the human medium chain acyl-CoA dehydrogenase (hMCAD), has been characterized in detail. Recently, we established a heterologous human dimethylglycine dehydrogenase (hDMGDH) expression system that produces enough enzyme to investigate the hETF-hDMGDH interaction mechanism in a greater context. The aim was to identify amino acids important for the interaction and eventually to evaluate whether the published interaction mechanism of hMCAD can be universally applied to all thirteen dehydrogenase partners. Additionally, we determined the dissociation constant for the hETF-hDMGDH complex with three independent methods and could confirm that hETF only weakly interacts with hDMGDH in a transient protein complex.

INTRODUCTION

The human electron transferring flavoprotein (hETF) catalyzes the electron transfer from at least thirteen flavodehydrogenases to the human electron transfer flavoprotein dehydrogenase (hETF-QO) in the mitochondrial matrix, lies at a key metabolic branch point of mitochondrial electron transfer and is an alternative path to feed electrons into the mitochondrial respiratory chain [1–3]. Primary flavoprotein partners are fatty acyl-CoA dehydrogenases from β -oxidation (short chain, medium chain, long chain, very long chain, ACAD9-11), CoA dehydrogenases involved in amino acid metabolism (iso-valeryl, short branched chain and iso-butyryl CoA dehydrogenase) as well as sarcosine and dimethylglycine dehydrogenase from one-carbon and folate metabolism. Despite a great structural diversity of the primary partner proteins and hETF-QO, hETF retains a surprisingly great specificity upon protein-protein interaction [4].

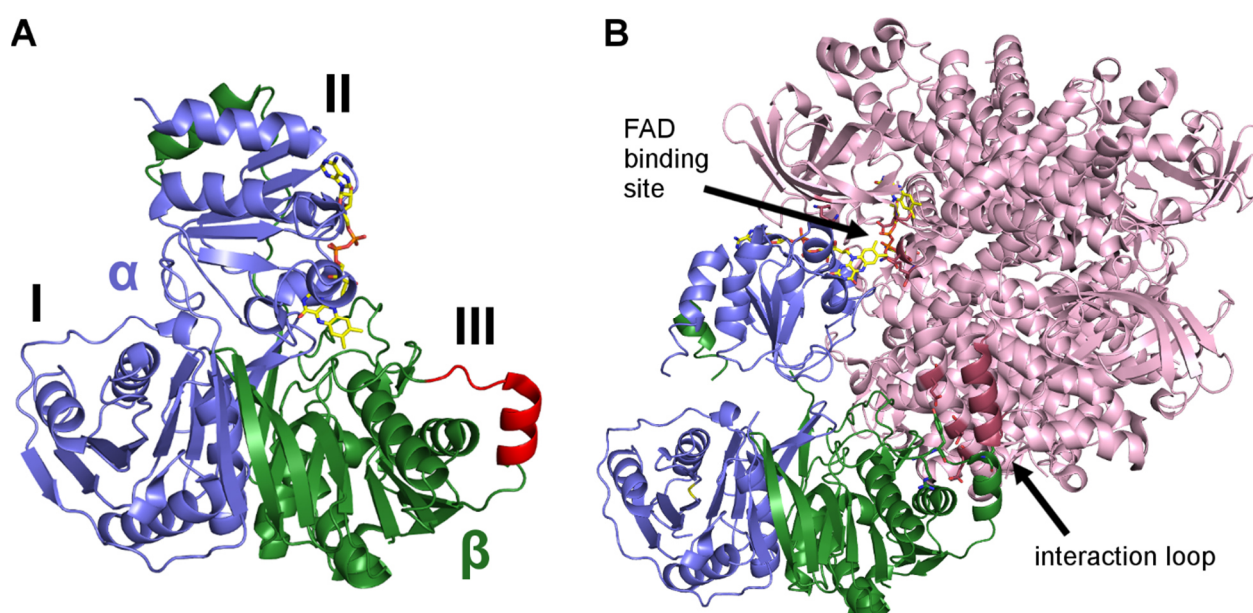


Figure 1 – hETF-WT (pdb: 1EFV) and hETF-hMCAD complex (pdb: 2A1T) crystal structures. (A) The heterodimeric hETF crystal structure (α -subunit shown in slate blue, β -subunit in forest green) can be divided into three domains (I-III). Domain III features the recognition loop important for protein-protein interaction (depicted in red, residues β 191- β 200). The arrows in (B) mark the two binding sites of hETF with hMCAD through the recognition loop and the FAD binding site. The homotetrameric hMCAD is shown in pink. A more detailed view of both interaction sites can be found in Figure 5.

hETF is a heterodimeric protein that folds into three distinct domains (Figure 1A). Domain II comprises a non-covalently bound FAD cofactor and is responsible for initiating electron transport. Protein-protein interaction is induced by domain III [5]. In 2005, the crystal structure of a hETF-hMCAD complex has been solved and the protein-protein interaction described in detail [4,5]. The specificity of the interaction by hETF is guaranteed by a dual interaction mechanism characterized by two interaction interfaces (Figure 1B). In a first step, hETF recruits partner proteins via the recognition loop centered around the

essential protein anchor β Leu195. The initial turn of an alpha helix preceding this region interacts with the hMCAD surface and extends an alpha helix of hMCAD with perfect alignment of the axes and the dipoles of both helices (Figure 1B and in more detail in Figure 5A). In a second step, the flexibility of hETF domain II enables an extensive motion to sample the available space within the different hETF-protein complexes to bring both FAD cofactors in close proximity to initiate electron transfer (Figure 5B), [5,6].

The hETF-hMCAD protein-protein interaction served as our model system to investigate the hETF-hDMGDH interaction. The crystal structure features different amino acids in the complex involved in hydrogen bonding and ionic and hydrophobic interactions that were investigated in the context of hETF-hDMGDH protein interaction. hETF variants characterized in this study are not only important for protein interaction but are also essential for the regulation of the redox behavior of the protein. Furthermore, several of the investigated hETF variants are also involved in the human inherited metabolic disease glutaric aciduria type II (OMIM: 231680), [7–9]. In this disease, the electron transfer from the primary flavoprotein dehydrogenases to the mitochondrial respiratory chain is impaired by an inactive hETF or hETF-QO leading to a severe nonketotic hypoglycemia, metabolic acidosis and excretion of large amounts of fatty acid and amino acid-derived metabolites [10,11].

We could identify several amino acids that impair not only the interaction with hMCAD but also with hDMGDH. Hence, our results suggest that hDMGDH shares a very similar interaction mechanism with hETF as described for hMCAD.[4,5] Furthermore, we determined the dissociation constant of hETF and hDMGDH with three independent methods and established the transient nature of the protein complex.

RESULTS

Protein Expression, Purification and Protein Stability

All nine investigated hETF protein variants (Table 1) could successfully be expressed in *Escherichia coli* and showed the same yield as obtained for hETF-WT in our previous study Chapter III. All proteins were purified at 50 mM HEPES, pH 7.0 to avoid 8f-FAD formation which has been observed at higher pH values (Chapter III). After purification, SDS-PAGE analysis indicated highly pure protein and the flavin spectra were highly similar to hETF-WT (data not shown). Only variant Q265A showed a minor fraction of aggregated and precipitated protein after His-trap affinity chromatography (GE Healthcare) and had to be additionally purified by size exclusion chromatography (Superdex 200 10/300 GL, GE Healthcare). Thermo FAD measurements revealed that especially variations around the FAD binding site (α R249C, α T266M, α Q265A, α Q285A) greatly influenced protein stability compared to the wild-type enzyme (Table 1). The variations in the interaction loop region of hETF (β R191C, β Y192A, β L195A) did not change the melting temperature. All melting curves showed a homogenous melting behavior and no signs of protein aggregates or impurities.

Table 1 – Thermal protein stability of hETF-variants determined by Thermo FAD measurements.

Variant	T _m [°C]	Variant	T _m [°C]
WT	60.5	α R249C	57.3
β R191C	59.5	α R249K	65.0
β Y192A	62.0	α T266M	55.2
β L195A	60.5	α Q265A	55.0
α R249A	62.0	α Q285A	57.5

NanoTemper Microscale Thermophoresis (MST)

MST uses the different thermal migration behavior of a fluorescently labelled protein in unbound and protein bound state in a heated spot in solution to determine protein-protein interactions [12]. Red fluorescently labelled hDMGDH was incubated with different concentration of hETF and measured in a NanoTemper Monolith NT.115 device (Figure 2). With an initial hETF concentrations of 250 μ M a dissociation constant (K_D) of 15 ± 6 μ M was determined. Measurements at very low hETF concentrations (< 1 μ M) showed false positive signals due to photo bleaching effects and were handled as outliers (Figure 2, grey dots). For the sigmoid curve fit (Hill equation) a non-bound state (fraction bound = 0) at concentrations lower than 1 μ M were assumed.

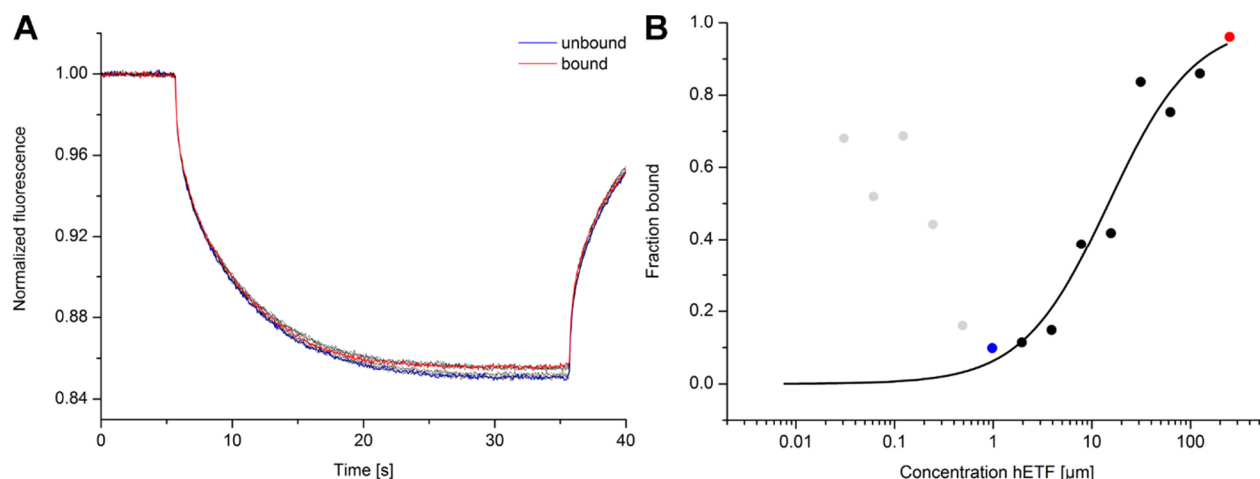


Figure 2 – Determination of dissociation constants by NanoTemper microscale thermophoresis. Panel A features the initial normalized MST traces measured. In blue and red, the unbound and bound traces are indicated. Panel B shows the sigmoid fit of the measured binding states and a K_D of $15 \pm 6 \mu\text{M}$ was obtained. Again, in blue and red, the unbound and bound traces are displayed. The grey dots represent outliers due to photo bleaching effects at very low hETF concentrations.

Presteady-State Kinetics

Anoxic presteady-state measurements were used to determine the re-oxidation rate of substrate reduced hDMGDH by hETF (k_{ox}) and the K_D of hDMGDH and hETF protein complex (Figure 3). The change of absorption during the redox reaction of hDMGDH was investigated at 482 nm as hETF holds an isosbestic point at that wavelength upon reduction (Chapter III, Figure . A K_D of $16 \pm 10 \mu\text{M}$ and a k_{ox} of $0.28 \pm 0.06 \text{ s}^{-1}$ were determined by the hyperbolic fit of the apparent re-oxidative rates.

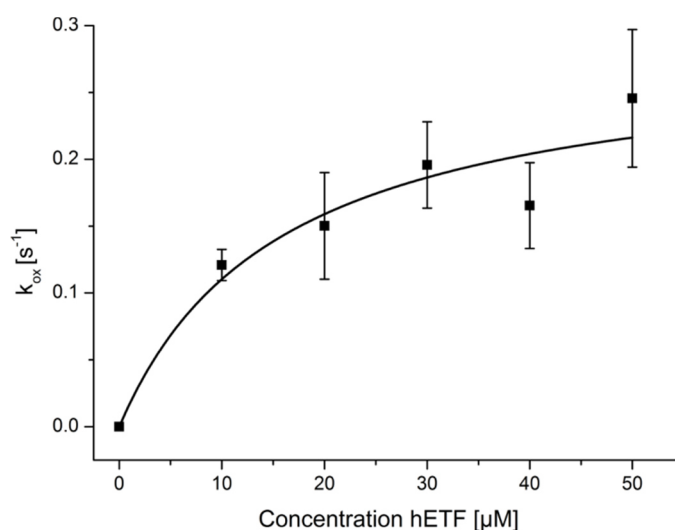


Figure 3 – Determination of the dissociation constant by pre-steady state kinetics using stopped-flow. All hETF concentrations were measured at least in triplicates at $25 \text{ }^\circ\text{C}$. The errors are displayed as standard deviations.

Isothermal Titration Calorimetry (ITC)

Protein-protein interaction affinity of hDMGDH and hETF with ITC was done by titrating 20 μM hDMGDH in the measurement cell with a 20 fold excess of hETF (Figure 3). After subtraction of the blank run (435 μM hETF titrated against 50 mM HEPES, pH 7.8) and assuming a molar binding ratio of 1, a K_D of $30 \pm 7 \mu\text{M}$ was determined.

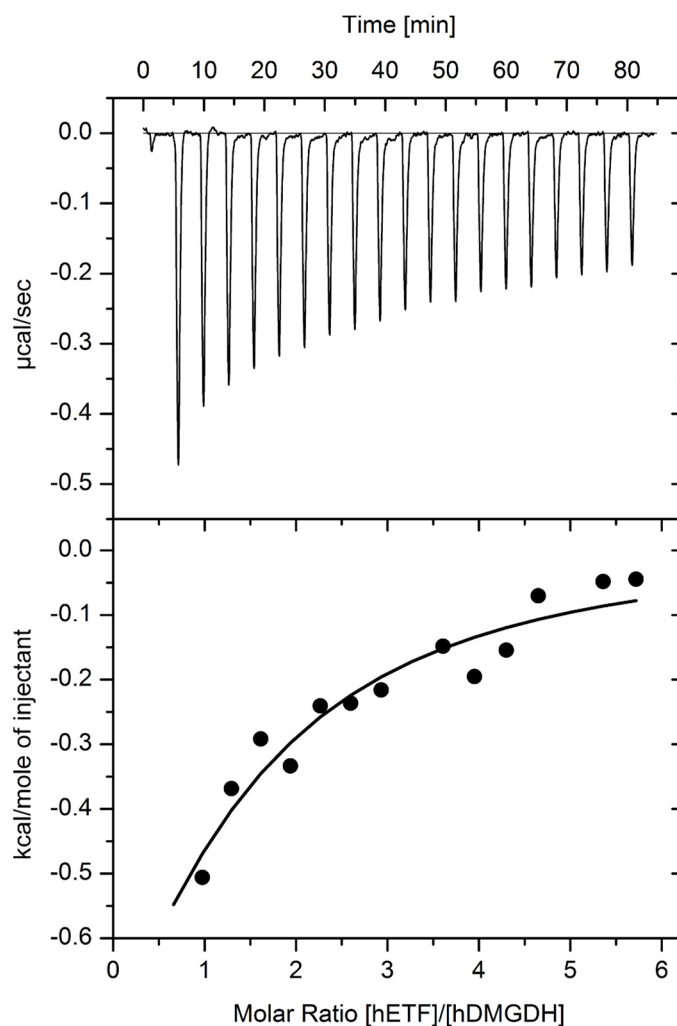


Figure 4 – Determination of the dissociation constant by isothermal titration calorimetry. 20 μM hDMGDH was titrated with 435 μM hETF. Both proteins were dissolved in 50 mM HEPES, 100 mM NaCl, pH 7.8 at 25 $^{\circ}\text{C}$.

Characterization of hETF-hDMGDH Interaction by Steady-state Kinetics

The importance of various amino acid sidechains on the hETF-hDMGDH interaction was studied using steady-state kinetics in a DCPIP based protein assay. Table 2 shows that several variations not only influence protein stability (Table 1) but also severely disturb activity and affinity of the two proteins. Variants β R191C and β L195A located on the interaction loop completely lost their ability to interact with hDMGDH and no K_M or k_{cat} values could be measured. Variants α R249C, α T266M and β Y192A still showed a certain affinity to hDMGDH but also failed to transfer electrons in the assay. On the other hand, variants α Q265A and α Q285A showed similar activities as the wild-type and surprisingly even a greater protein affinity.

Table 2 – Steady state parameters of hETF-WT in comparison with seven variants. All assays were performed in 50 mM HEPES, pH 7.0 at 25 °C at least in triplicates. The errors are shown as standard deviations.

	Variant	K_M	k_{cat}	k_1
		μM	min^{-1}	$L mol^{-1} min^{-1}$
	WT	80 ± 7	10.5 ± 0.5	$1\ 300 \pm 100$
FAD binding site	α R249A	-	-	-
	α R249C	36 ± 3	0.4 ± 0.3	100 ± 40
	α R249K	190 ± 56	1.0 ± 0.2	50 ± 30
	α T266M	16 ± 5	0.3 ± 0.1	200 ± 60
	α Q265A	6 ± 1	5.6 ± 0.1	$9\ 800 \pm 700$
	α Q285A	31 ± 3	6.7 ± 0.2	$2\ 200 \pm 200$
recognition loop	β R191C	-	-	-
	β Y192A	96 ± 71	0.3 ± 0.1	30 ± 20
	β L195A	-	-	-

DISCUSSION

The hETF-hDMGDH Protein Complex Shows a Transient Nature

hETF-hDMGDH protein affinity was estimated using three independent methods, microscale thermophoresis (MST, Figure 2), stopped-flow spectroscopy (Figure 3) and isothermal titration calorimetry (ITC; Figure 4). All three methods provided similar K_D values between 15 and 30 μM indicating a weak, transient protein interaction. The only other affinity constant reported so far for hETF-hDMGDH interaction was 2 μM and determined by plasmon resonance [13]. Previous studies on hETF-acyl-CoA dehydrogenase complexes also reported a limp protein interaction and an unusual small interaction interface of only 3.2% of the available protein surface [4,5,7,14,15]. The fact that the first complete hETF-hMCAD crystal structure could only be obtained with hETF variant βE165A , which stabilizes nonproductive, thus, longer interacting conformational states of hETF that lead to more stable protein complexes, additionally emphasizes the transient nature of hETF complexes (**pdb: 2A1T**), [4].

Using stopped-flow spectroscopy, we additionally determined the oxidative rate (k_{ox}) of reduced hDMGDH by hETF-WT to $0.28 \pm 0.06 \text{ s}^{-1}$ (Figure 3). Compared to the k_{cat} obtained in steady-state kinetics, which nearly reached a similar value of $0.2 \pm 0.01 \text{ s}^{-1}$, it can be assumed that the re-oxidation is the rate limiting step in the assay and most likely also in the electron transfer from hDMGDH to the respiratory chain. Previous studies showed that the reduction of hDMGDH by its natural substrate DMG proceeds much faster with a rate of $17 \pm 0.3 \text{ s}^{-1}$ [16]. The turnover numbers for the disproportionation of hETF semiquinone by hETF-QO of $81.4 \pm 3.3 \text{ s}^{-1}$ (i.e. the re-oxidation of hETF) are also considerably faster [17] and therefore presumably also the electron transfer to DCPIP.

Methodological Limits in the Determination of the hETF-hDMGDH Dissociation Constant

All three methods described above suffered from methodological drawbacks. In general, all shown non-linear fits (Figure 2-4) had to be extrapolated to obtain the needed slopes because of lacking results especially at very low and very high hETF concentrations. Nevertheless, the consistent K_D values suggest correct and reasonable measurements.

To our view, the most reliable results could be obtained using MST. Unfortunately, the concentration of hETF was too little to obtain a good fit at saturating protein concentrations (bound fraction = 1), (Figure 2). Another problem of the measurement were false positive signals at very little concentrations (Figure 2, grey dots) due to photo bleaching of the labeled protein by the laser [18]. A decrease of the laser intensity did lead to better results at low concentrations but resulted in higher noise ratios (data not shown). The addition of Tween[®] 20 to avoid protein aggregation and protein adhesion to the capillary walls and the screen of different capillary types improved the measurements. A rerun of the MST measurements with higher hETF concentrations up to 600-800 μM and the use of the NanoTemper Anti Photo bleaching Kit could give better results concerning high and low concentrations. As a rule of a

thumb, ligand concentrations for NanoTemper MST should be used in concentrations 10-20 times the concentration of K_D (personal communication), which was obviously not reached with the present experiments.

With stopped-flow spectroscopy, the greatest problem were the measurements at very high hETF concentrations which showed very large standard deviations (Figure 3). The flavin spectrum of high concentrated hETF completely overlapped the spectrum of the significantly lower concentrated hDMGDH and thus small changes at 482 nm were difficult to assess. It cannot be excluded that absorption changes caused by hDMGDH reoxidation at 482 nm was not overlaid by the other factors like hETF photoreduction, hETF protein precipitation or wavelength inaccuracies during the fast measurement. Due to the concentration limitations also saturating conditions of hETF binding to hDMGDH could not be reached; only measurements up to 50 μM hETF were reasonably possible. Furthermore, the stopped-flow measurements suffered from low reproducibility with different hETF protein batches further leading to high standard deviations. Altogether, the results obtained by stopped-flow spectroscopy gave the least trustworthy values.

In ITC measurements, the classical sigmoid shape of the nonlinear least squares fitting curve in Figure 4 was not received and therefore it was difficult to correctly determine the slope. Especially, the reference plateau at the beginning of the unbound protein complex was missing. In general, the enthalpy changes during the injections were very little because of the weak protein-protein binding and only slightly differed from the blank measurements, but was negative indicating favorable binding. Very small changes in the binding enthalpy increase the error of the measurement. Nevertheless, with increasing ligand concentration in the measure cell, less heat was produced and a saturation can be observed. ITC was only successfully measured once and variations in hETF and hDMGDH concentrations did not produce any further analyzable results.

Impaired Protein Affinity by Variation of the hETF Recognition Loop Region

All three variants with mutations in the recognition loop of the protein (βR191C , βY192A , βL195A ; Figure 5A) showed dramatically reduced protein-protein affinity and thus impaired electron transfer in our assay (Table 2). These effects can directly be related to a disturbed protein-protein interaction mechanism between hETF and hDMGDH. Cross-linking experiments by Steenkamp *et al.* indicated that hETF interacts with its primary protein partners as well as with hETF-QO through the recognition loop region [19,20]. In a study by Hoard-Fruchey *et al.* it was revealed with microelectrospray ionization-mass spectrometry and surface plasmon resonance that human short chain acyl-CoA dehydrogenase, which is structurally related to hMCAD, and hDMGDH share the same or closely overlapping binding motifs on hETF [13].

As all three variations are located on the surface of the hETF protein and additional effects on the protein structure are unlikely. We also did not observe a changed thermal protein stability (Table 1). The sterical separation from the FAD binding site should also not influence the redox behavior of the cofactor.

Protein-protein contact between the hETF recognition loop and hMCAD is mainly established by hydrogen bonds of β Y192 and the backbone nitrogen of β L195 with hMCAD (Figure 5A), (pdb: 2A1T, 1T9G), [4,5]. β L195 additionally serves as hydrophobic protein anchor in a hydrophobic patch of hMCAD. Similar to the results published for hMCAD, hETF variant β L195A also was completely inactive in our steady-state assays with hDMGDH (Table 2). Also the loss of the hydrogen bond in variant β Y192A led to a 30 fold decrease in activity. The third variant investigated, the naturally occurring β R191C variation, again resulted in a complete loss of activity. It has been demonstrated before that hETF variant β R191C leads to ETF deficiency and a 90% loss of ETF activity in fibroblast tissue samples [9]. In the hETF-hMCAD crystal structure, β R191 is not directly involved in complex formation (Figure 5A) and a possible effect of the mutation on the protein structure was not investigated so far. Yet, the variant can be expressed as stable protein in *E. coli* as well as in human fibroblast tissue [9]. Also its thermal stability is the same as the wild-type (Table 1).

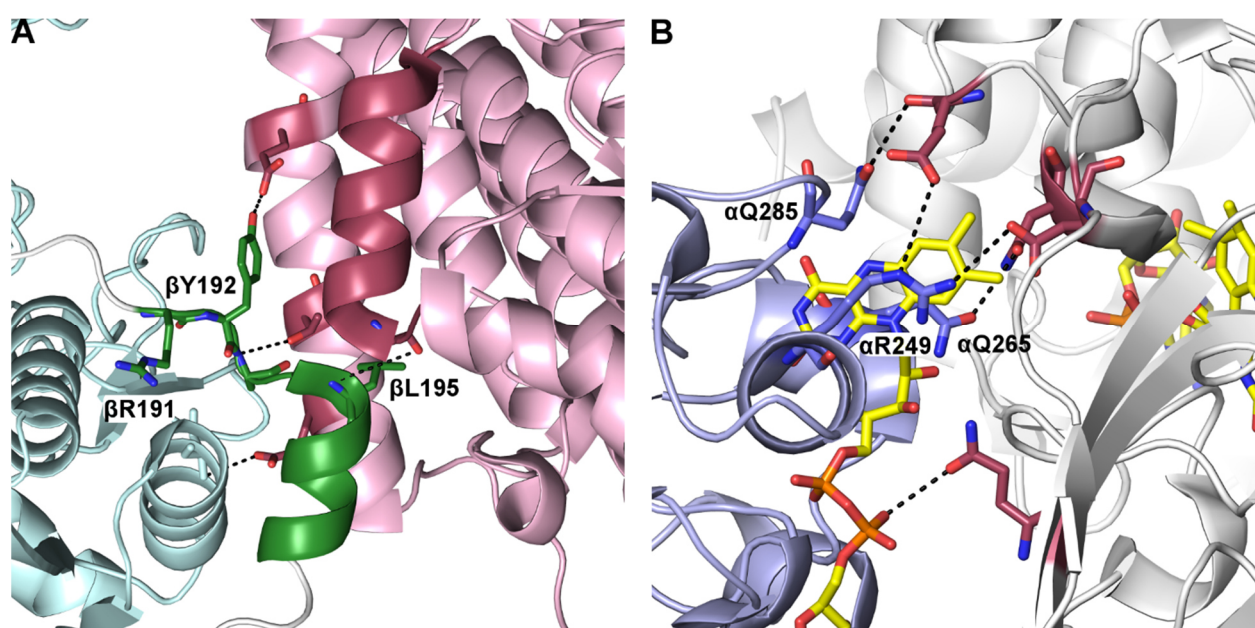


Figure 5 – Close up view of hETF-hMCAD interaction sites (pdb:2A1T), [4]. Panel A shows the recognition loop of hETF in forest green and the three amino acids mutated in our study. While residue β Y192 forms a direct hydrogen bond with hMCAD and β L195 functions as hydrophobic protein anchor, a direct interaction of β R191 with hMCAD cannot be derived from the crystal structure. The interaction interface of the hETF FAD binding site with hMCAD displayed in panel B is mainly formed by direct hydrogen bonds of residues α R249, α Q265 and α Q285. The investigated residue α T266 does not form a hydrogen bond with hMCAD and is not displayed in panel B. The hETF β -subunit is shown in forest green, the α -subunit in slate blue and interacting hMCAD residues in raspberry.

Impaired Electron Transfer by Variation of the hETF FAD Binding Site

Protein variants in the surrounding of the non-covalently bound FAD not only affect protein-protein interaction by the loss of intermolecular hydrogen or salt bridge bonds, but also change the redox-potential of the bound cofactor and decrease the protein stability [7,21]. hETF-variants α T266M and α R249C are the most common natural occurring missense mutations in the glutaric aciduria type II disease [7–9].

The investigated variants α R249A, α R249C and α R249K all showed a complete loss of protein activity in the steady-state assays (Table 2). Interestingly, in contrast to the non-natural variants α R249A and α R249K, the natural occurring α R249C variation did not affect hETF-hDMGDH affinity and also showed a decreased thermostability (Tables 1 and 2). Similar to our results, Dwyer *et al.* reported a 90% decreased activity of variant α R249K with porcine MCAD in stopped-flow experiments [21]. Toogood *et al.* found a complete loss of activity of variant α R249A with hMCAD [4], variant α R249C was not kinetically investigated so far. α R249 lies in close proximity to the FAD cofactor (Figure 5B), neutralizes the anionic semiquinone state of the protein and thus stabilizes productive conformational states of hETF for electron transfer [9,21]. The globally conserved residue in the hETF protein family [2] also serves as kinetic block on the full reduction of the FAD to the dihydroquinone [22]. Furthermore, the residue modulates the redox potential of the bound flavin by a hydrogen bond with the carbonyl oxygen at C(2) of the isoalloxazine ring [21]. The redox potential measured for protein variant α R249K is 60 mV decreased compared to the wild-type [21]. Additionally, in hETF-hMCAD complexes, α R249 forms an ionic bond with glutamic acid 212 of hMCAD [4]. Our results showed that in variants α R249A and α R249K, not only the alteration of the redox potential but also the loss of this ionic bond is responsible for lost protein activity. On the other hand, variant α R249C was able to retain a certain affinity to hDMGDH but also failed to catalyze an electron transport to DCPIP.

Only 6 Å away from α R249 another key residue of hETF, α T266, was investigated. Similar to α R249, α T266 forms a hydrogen bond with N(5) of the flavin isoalloxazine ring and also decreases the redox potential of hETF by approximately 50 mV [7]. It has been shown that the loss of this isoalloxazine bond leads to an increase of the flavin semiquinone stability upon its disproportionation catalyzed by hETF-QO [7]. In our steady-state assays, variant α T266M lost its activity while maintaining its affinity to hDMGDH, but also showed a decreased thermostability in Thermo FAD (Table 1 and 2). Salazar *et al.* reported that the reductive half reaction of hETF- α T266M variant with porcine sarcosine dehydrogenase and MCAD was not influenced by the variation, but instead the electron transfer and disproportionation of FAD by ETF-QO. In this context, we assume that the observed loss of activity with hDMGDH is caused by an impaired reoxidation mechanism of hETF. Obviously, the loss of the N(5) hydrogen bond not only impairs re-oxidation with ETF-QO but also with DCPIP. A similar behavior is also imaginable for hETF variant α R249C but has not been described so far.

Situated around 5 Å away from the N(5) of the isoalloxazine ring, the last investigated residues, α Q265 and α Q285 also form direct hydrogen bonds to hMCAD in the hETF-hMCAD crystal structure (Figure 5B), [4]. Both variants should lack the ability to form these hydrogen bonds but surprisingly showed an even greater affinity to hDMGDH than the wild-type while maintaining the enzyme activity. It seems that the exchange to the small alanine leads to less electrostatic repulsion between the proteins and a stabilization of the protein complex.

The DCPIP assay we used for the determination of steady-state kinetics suffered from irregularities as already discussed in Chapter III. In short, we observed that already hETF together with DCPIP causes the reduction of DCPIP and thus a change in absorption. We observed that this change was linear and always constant after 5 to 10 min. In order to better compare our obtained results from the different variants, we introduced a 10 min incubation step before starting the assay with dimethylglycine as described in the Experimental Procedures. For future experiments, we recommend to use a higher concentration of DCPIP in the assays, at least 200 μ M, to avoid limiting DCPIP concentrations during the assay.

CONCLUSION

The observation that almost all amino acids of hETF involved in hMCAD binding are also important to interact with the structurally unrelated hDMGDH prompted us to the conclusion that all thirteen flavin partner dehydrogenases of hETF not only share the same dual interaction mechanism through recognition loop and FAD binding site, but also involve the same, conserved amino acids. Yet it is still unclear if hETF involves the same binding mechanism to interact with hETF-QO. Nonetheless, our studies indicated that especially the natural occurring hETF variants β R191C affecting the recognition loop as well as α R249C and α T266M which influence the redox potential and the semiquinone stability of the FAD cofactor are also involved in hETF-QO binding. The exact mechanism of hETF binding to hDMGDH awaits further studies and especially a crystal structure of the protein complex would be of utmost importance. However, the transient nature of the protein complex, which we could confirm with different experiments, makes the growth of complex crystals and the elucidation of the crystal structure a difficult task to be addressed in future.

EXPERIMENTAL PROCEDURES

Most of the methods listed below were already used in our previous study and described in the Experimental Procedures section in Chapter III.

Enzymes and Reagents– All chemicals used were ordered from Carl Roth GmbH (Karlsruhe, Germany) or Sigma-Aldrich (St. Louis, MO, USA) and were of the highest purification grade available.

Expression and Purification of hETF-WT and Variants – Design of the hETF-WT expression plasmid, the protein expression and the purification of hETF-WT were done as described in detail in the Experimental Procedures section of Chapter III. The investigated hETF variants α R249C, α T266M and α Q285A as well as the wild-type were already constructed, expressed and purified in our previous study (Chapter III). Variants β R191C, β Y192A, β L195A, α R249A, α R249K and α Q265A were newly created in this study with the mutagenesis primers listed in Table 3. After purification, the proteins were flash-frozen and stored at $-80\text{ }^{\circ}\text{C}$ in 50 mM HEPES/NaOH, pH 7.0 until further use. Variant α Q265A formed precipitates after His-trap purification and was further purified by size-exclusion chromatography (Superdex 200 GL 10/300, GE Healthcare, Chalfont St Giles, UK) with 50 mM HEPES, pH 7.0 as running buffer. Yellow colored fractions were combined and concentrated with Amicon ultracentrifugal filter units (30 kDa cut-off, Merck-Milipore, Darmstadt, Germany) as described in Chapter III.

Table 3 – Primers used for site-directed mutagenesis of hETF-WT plasmid to obtain hETF variants. The exchanged codons are highlighted in bold.

Primer	DNA Sequence 5' – 3'	T _m
β R191C_fw	GCGCCTGAATGAACCGT GT TTATGCAACCCTGCCG	69.1 °C
β R191C_rev	CGGCAGGGTTGCATAACACGGTTCATTCAGGCGC	69.1 °C
β Y192A_fw	CTGAATGAACCGCGT GC GGCAACCCTGCCGAATAT	69.9 °C
β Y192A_rev	ATATTCGGCAGGGTTGCC GC CACGCGTTCATTCAG	69.9 °C
β L195A_fw	CCGCGTTATGCAACCG CG CCGAATATTATGAAAG	61.0 °C
β L195A_rev	CTTTCATAATATTCGG CG CGGTTGCATAACGCGG	61.0 °C
α Q265A_fw	GATATGCAGGTTGGT GC GACCGGCAAAATTGTTG	64.1 °C
α Q265A_rev	CAACAATTTTCCGGT CG CACCAACCTGCATATC	64.1 °C
α R249A_fw	GCAGTTGGTGAAG CG CGGCAGCAGTTGATGC	67.3 °C
α R249A_rev	GCATCAACTGCTGCC CG GCTTGCACCAACTGC	67.3 °C
α R249K_fw	GCAGTTGGTGAAG CAA AGCAGCAGTTGATGCAG	67.3 °C
α R249K_rev	CTGCATCAACTGCTG CTT TGCTTGCACCAACTGC	67.3 °C

hDMGDH Gene Expression and Purification – hDMGDH expression plasmid was designed and the protein expressed and purified as described in detail by Augustin *et al.* [16]. After purification the protein was flash-frozen and stored at -80 °C in 50 mM HEPES/NaOH, 100 mM NaCl, pH 7.8 until further use.

UV/Vis Absorption Spectroscopy – UV/Vis absorption measurements were used to determine protein concentrations, protein quality and steady-state kinetics with a Specord 210 spectrophotometer (Analytik Jena, Jena, Germany). The extinction coefficients were determined according the method previously described by Macheroux [23] to 11 600 M⁻¹ cm⁻¹ for hDMGDH at 450 nm [16] and to 9 900 M⁻¹ cm⁻¹ for hETF and all its variants at 469 nm (Chapter III).

Steady-state Kinetics – The assay used to study the steady-state kinetic interaction parameters was modified from Okamura-Ikeda *et al.* [15]. 100 nM hDMGDH, 3-100 µM hETF-WT and variants and 135 µM DCPIP, as terminal electron acceptor and measurable dimension, were incubated for 10 min at 25 °C in 50 mM HEPES/NaOH pH 7.0. The reaction was started by addition of 25 mM dimethylglycine and the change in absorption at 600 nm was followed spectrophotometrically over 3 min. For each hETF concentration at least a triplicate measurement was performed, the initial velocities determined and K_M and k_{cat} assessed by non-linear hyperbolic fit in Origin 8.6 software (OriginLab Corp, Northampton, MA, USA).

NanoTemper Microscale Thermophoresis (MST) – MST experiments were performed on a NanoTemper Monolith NT.115 (Munich, Germany) during a two day work-shop of Peter Augustin in Munich in February 2016. For the interaction experiments, 100 µL 18 µM purified hDMGDH was fluorescently labeled with the RED-NHS protein labeling kit (MO-L001, NanoTemper) and used in a final concentration of approximately 100 nM in 50 mM HEPES pH 7.8, 100 mM NaCl and 0.05% Tween[®] 20. 435 µM purified hETF in 50 mM HEPES, pH 7.8 containing 0.05% Tween[®] 20 was used in a concentration range of 250 µM – 1 nM in 14 glass capillaries. The addition of 0.05% Tween[®] 20 and the use of premium coated capillaries (MO-AK005, NanoTemper) reduced the binding of the protein to the capillary wall especially critical at low protein concentrations. Thermophoresis was performed at 25 °C with an excitation power of 20% and an MST laser power of 40%. The fluorescence changes during thermophoresis were converted into the fraction of hETF bound to hDMGDH and fitted using a sigmoid Hill curve with the NanoTemper evaluation software.

Presteady-state kinetics – Presteady-state reaction kinetics were measured anaerobically with a Hi-Tech stopped flow instrument (SF-61DX2, TgK Scientific Limited, Bradford-on-Avon, UK) in a glove box (Belle Technology, Weymouth, UK) at 25 °C. For the determination of the oxidative rate of hDMGDH bound FAD, 20 µM, DMG reduced, hDMGDH in 50 mM HEPES/NaOH, 100 mM NaCl pH 7.8 was shot against different concentrations of hETF (20-100 µM) dissolved in 50 mM HEPES/NaOH pH 7.0.

The change in absorption was monitored at 482 nm with a KinetaScanT diode array detector (MG-6560, TgK Scientific Limited). Each ETF concentration was measured at least in triplicates and the apparent rate constants (k_{app}) for different concentrations were determined using an exponential fitting function in Kinetic Studio software (TgK Scientific Limited). The dissociation constant (K_D) was determined by a hyperbolic fit of all measured k_{app} employing Origin 8.6 software (OriginLab Corp).

Isothermal Titration Calorimetry (ITC) – Microcalorimetric data for the binding of hDMGDH to hETF were measured at 25 °C with a VP-ITC microcalorimeter (MicroCal, Northampton, MA, USA). A 17 μ M solution of hDMGDH in the sample cell was titrated with 435 μ M hETF. Both enzymes were dissolved in 50 mM HEPES buffer pH 7.8, 100 mM NaCl and degassed directly before the measurement. The titration experiment consisted of 20 injections and a total of 20 aliquots (one aliquot 2 μ L and 19 aliquots 15 μ L) hETF solution were injected with a rate of 0.5 μ L/s into 1.42 mL of the hDMGDH solution and constant stirring at 270 rpm. After an initial delay of 60 s, every injection was carried out over a period of 30 s with a spacing of 250 s between each injection. The heat of binding was calculated by integration of the area under each peak in the thermogram. A reference measurement was made by injecting the hETF solution into only 50 mM HEPES, 100 mM NaCl, pH 7.8 buffer the same way which was subtracted afterwards from the interaction experiment to correct for the heat of dilution of the enzyme. Corrected values were plotted against the molar ratio of hDMGDH vs. hETF concentration in the cell to obtain a binding isotherm. The binding affinity (K_a), the binding enthalpy (ΔH) were obtained by a nonlinear least squares fitting curve generated in Origin 7.0 (MicroCal). The dissociation constant (K_D) is the reciprocal value of K_a . A binding molarity between hDMGDH and hETF of 1 was assumed.

AUTHOR CONTRIBUTIONS

PA, ECG, JM and FW executed all experiments. They expressed, purified and characterized the enzymes and all variants. PA, ECG and PM designed the biochemical experiments and interpreted the data. PA and PM wrote the manuscript.

ACKNOWLEDGEMENT

We would like to thank Dr. Silvia Wallner for introducing us into ITC measurements. This work was supported by a grant from the Austrian Science Foundation (FWF) to Peter Macheroux (Doctoral program “Molecular Enzymology” W901).

REFERENCES

- 1 Ghisla S & Thorpe C (2004) Acyl-CoA dehydrogenases. A mechanistic overview. *Eur. J. Biochem.* **271**, 494–508.
- 2 Toogood HS, Leys D & Scrutton NS (2007) Dynamics driving function – new insights from electron transferring flavoproteins and partner complexes. *FEBS J.* **274**, 5481–5504.
- 3 He M, Pei Z, Mohsen A-W, Watkins P, Murdoch G, Van Veldhoven PP, Ensenaer R & Vockley J (2011) Identification and characterization of new long chain acyl-CoA dehydrogenases. *Mol. Genet. Metab.* **102**, 418–29.
- 4 Toogood HS, van Thiel A, Scrutton NS & Leys D (2005) Stabilization of non-productive conformations underpins rapid electron transfer to electron-transferring flavoprotein. *J. Biol. Chem.* **280**, 30361–6.
- 5 Toogood HS, van Thiel A, Basran J, Sutcliffe MJ, Scrutton NS & Leys D (2004) Extensive domain motion and electron transfer in the human electron transferring flavoprotein.medium chain Acyl-CoA dehydrogenase complex. *J. Biol. Chem.* **279**, 32904–12.
- 6 Leys D, Basran J, Talfournier F, Sutcliffe MJ & Scrutton NS (2003) Extensive conformational sampling in a ternary electron transfer complex. *Nat. Struct. Biol.* **10**, 219–25.
- 7 Salazar D, Zhang L, DeGala GD & Frerman FE (1997) Expression and Characterization of Two Pathogenic Mutations in Human Electron Transfer Flavoprotein. *J. Biol. Chem.* **272**, 26425–26433.
- 8 Henriques BJ, Bross P & Gomes CM (2010) Mutational hotspots in electron transfer flavoprotein underlie defective folding and function in multiple acyl-CoA dehydrogenase deficiency. *Biochim. Biophys. Acta - Mol. Basis Dis.* **1802**, 1070–1077.
- 9 Schiff M, Froissart R, Olsen RKJ, Acquaviva C & Vianey-Saban C (2006) Electron transfer flavoprotein deficiency: Functional and molecular aspects. *Mol. Genet. Metab.* **88**, 153–158.
- 10 Christensen E, Kølvrå S & Gregersen N (1984) Glutaric Aciduria Type II: Evidence for a Defect Related to the Electron Transfer Flavoprotein or Its Dehydrogenase. *Pediatr. Res.* **18**, 663–667.
- 11 Frerman FE & Goodman SI (2001) Defects of electron transfer flavoprotein and electron transfer flavoprotein-ubiquinone oxidoreductase: glutaric acidemia type II. In *The Metabolic and Molecular Bases of Inherited Disease. (8th ed.)* (Scriver CR, Beaudet AL, Sly WS, & Valle D, eds), 8th ed., pp. 2357–2365. McGraw-Hill, New York.
- 12 Jerabek-Willemsen M, Wienken CJ, Braun D, Baaske P & Duhr S (2011) Molecular Interaction Studies Using Microscale Thermophoresis. *Assay Drug Dev. Technol.* **9**, 342–353.
- 13 Hoard-Fruchey HM, Goetzman E, Benson L, Naylor S & Vockley J (2004) Mammalian electron transferring flavoprotein.flavoprotein dehydrogenase complexes observed by microelectrospray ionization-mass spectrometry and surface plasmon resonance. *J. Biol. Chem.* **279**, 13786–91.
- 14 Beckmann JD & Frerman FE (1985) Reaction of electron-transfer flavoprotein with electron-transfer flavoprotein-ubiquinone oxidoreductase. *Biochemistry* **24**, 3922–5.

- 15 Okamura-Ikeda K, Ikeda Y & Tanaka K (1985) An essential cysteine residue located in the vicinity of the FAD-binding site in short-chain, medium-chain, and long-chain acyl-CoA dehydrogenases from rat liver mitochondria. *J. Biol. Chem.* **260**, 1338–45.
- 16 Augustin P, Hromic A, Pavkov-Keller T, Gruber K & Macheroux P (2016) Structure and biochemical properties of recombinant human dimethylglycine dehydrogenase and comparison to the disease-related H109R variant. *FEBS J.* **283**, 3587–3603.
- 17 Simkovic M, Degala GD, Eaton SS & Frerman FE (2002) Expression of human electron transfer flavoprotein-ubiquinone oxidoreductase from a baculovirus vector: kinetic and spectral characterization of the human protein. *Biochem. J.* **364**, 659–67.
- 18 Breitsprecher D, Schlinck N, Witte D, Duhr S, Baaske P & Schubert T (2016) Nucleic Acid Aptamers. **1380**, 99–111.
- 19 Steenkamp DJ (1988) Cross-linking of the electron-transfer flavoprotein to electron-transfer flavoprotein-ubiquinone oxidoreductase with heterobifunctional reagents. **255**, 869–876.
- 20 Steenkamp DJ (1987) Preferential cross-linking of the small subunit of the electron-transfer flavoprotein to general acyl-CoA dehydrogenase. *Biochem J* **243**, 519–524.
- 21 Dwyer TM, Zhang L, Muller M, Marrugo F & Frerman F (1999) The functions of the flavin contact residues, α Arg249 and β Tyr16, in human electron transfer flavoprotein. *Biochim. Biophys. Acta - Protein Struct. Mol. Enzymol.* **1433**, 139–152.
- 22 Talfournier F, Munro AW, Basran J, Sutcliffe MJ, Daff S, Chapman SK & Scrutton NS (2001) α Arg-237 in *Methylophilus methylotrophus* (sp. W 3 A 1) Electron-transferring Flavoprotein Affords ~200-Millivolt Stabilization of the FAD Anionic Semiquinone and a Kinetic Block on Full Reduction to the Dihydroquinone. *J. Biol. Chem.* **276**, 20190–20196.
- 23 Macheroux P (1999) UV-visible spectroscopy as a tool to study flavoproteins. *Methods Mol. Biol.* **131**, 1–7.

CHAPTER V

CHARACTERIZATION OF THE FUNCTION OF DIMETHYLGLYCINE DEHYDROGENASE IN THE SARCOSINE-METABOLISM OF HUMAN PROSTATE CANCER CELLS

*Michael Haider[§], Anika Stracke[§], Nathalie Meier-Allard[§], Peter Augustin[‡], Peter Macheroux[‡],
Andreas Meinitzer[‡] and Robert Fuchs[§]*

[§]Institute of Pathophysiology and Immunology, Medical University of Graz, Graz, Austria

[‡]Institute of Biochemistry, Graz University of Technology, Graz, Austria

[‡]Clinical Institute of Medical and Chemical Laboratory Diagnostics, Graz, Austria

Abbreviations

AR, androgen receptor; CAM-assay, chicken chorioallantoic membrane assay, DMG, dimethylglycine; HCC, hepatocellular carcinoma; hDMGDH, human dimethylglycine dehydrogenase; hETF, human electron transferring flavoprotein; hGNMT, human glycine-N-methyltransferase; hPIPOX, human L-pipecolate oxidase; hSARDH, human sarcosine dehydrogenase; PCa, prostate cancer; qRT-PCR, quantitative real-time polymerase chain-reaction; shRNA, small hairpin RNA.

PREFACE

In the previous chapters, the human dimethylglycine dehydrogenase (hDMGDH) was extensively characterized *in vitro* with a variety of biophysical methods. In Chapter II, new aspects concerning its reaction mechanism and the influence of the natural occurring H109R variant are discussed. In Chapters III and IV, hDMGDH was used to characterize novel features concerning the human electron transferring flavoprotein (hETF) and to elucidate the protein-protein interaction mechanism of hDMGDH and hETF. So far, mammalian DMGDH was mainly characterized *in vitro* and a profound biomedical study of the human enzyme and investigations in a physiological context, for instance in human cell lines or tissue, are missing. In collaboration with the Medical University of Graz (MUG) we tried to determine the importance of DMGDH in human cells. The following chapter is a summary of the experiments and results concerning our characterization of DMGDH in three different human prostate cancer cell lines.

The experiments presented were mainly done by Michael Haider during his Master's Thesis, Anika Stracke and Robert Fuchs at the Institute of Pathophysiology and Immunology, MUG. Western blotting was performed by Michael Haider and Peter Augustin at Graz University of Technology. Michael Haider was supervised by Robert Fuchs. Robert Fuchs and Peter Augustin designed and planned all experiments. Andreas Meinitzer established the method to measure sarcosine concentrations in prostate cancer cells by means of HPLC. Nathalie Meier-Allard assisted in quantitative real-time PCR measurements. The financing of the project was shared between the Institute of Pathophysiology and Immunology, MUG and the Institute of Biochemistry, TU Graz. Furthermore, Robert Fuchs and Peter Augustin received a funding of 1 500 € by the science resort of the City of Graz (Sub A16-40-2015).

All results are presented in more detail and with the addition of all necessary Data and Figures in the Master's Thesis of Michael Haider entitled "Charakterisierung der Rolle des Enzyms Dimethylglycindehydrogenase im Sarkosinmetabolismus von humanen Prostatakarzinomzellen".

INTRODUCTION

The human dimethylglycine dehydrogenase (hDMGDH, EC 1.5.8.4.) catalyzes the oxidative demethylation of dimethylglycine to sarcosine as part of the choline degradation pathway (Chapter II). Furthermore, the enzyme is involved in one-carbon metabolism via its tetrahydrofolate cofactor and in electron transport to the mitochondrial electron transport chain via its covalently bound FAD cofactor. A malfunctioning hDMGDH, mainly caused by a histidine to arginine variation in the proximity of the FAD binding site of the protein (Chapter II), causes DMGDH deficiency (OMIM: 605850), resulting in an accumulation of DMG and a 4-fold higher plasma creatinine level [1,2]. People affected from this inborn error of metabolism mainly suffer from severe muscle fatigue and a fish like body odor.

In recent years, sarcosine, a metabolite of hDMGDH (Chapter II), gained public attention as a possible biomarker for aggressive prostate cancer [3]. Investigations on the regulation of sarcosine and the proteins involved in sarcosine metabolism are in the focus of present research. Together with the human enzymes glycine-N-methyltransferase (hGNMT, EC 2.1.1.20.), sarcosine dehydrogenase (hSARDH, EC 1.5.8.3.) and L-pipecolate oxidase (hPIPOX, EC 1.5.3.7.), hDMGDH is the fourth enzyme involved in sarcosine metabolism (Figure 1). Conversion of dimethylglycine or glycine by hDMGDH or hGNMT are the only known pathways leading to sarcosine in the human body.

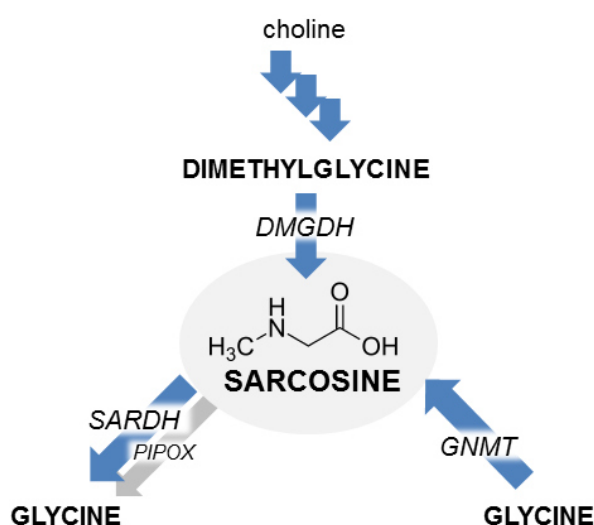


Figure 1 – Scheme of human sarcosine metabolism. The enzymes dimethylglycine dehydrogenase (hDMGDH) and glycine-N-methyltransferase (hGNMT) are the only known routes to sarcosine in human cells. The catabolism of sarcosine is done by sarcosine dehydrogenase (hSARDH) and to a much lesser extent by L-pipecolate oxidase (hPIPOX).

Sarcosine in Prostate Cancer

Since 1994, prostate cancer (PCa) has been the most diagnosed cancer within Austrian men. In 2011, 4 722 men were newly diagnosed with PCa and 1 146 men died, making it the third deadliest cancer after lung and colorectal cancer [4]. Globally, the International Agency for Research on Cancer (IARC)

estimates the numbers to 1 112 000 incidences and approximately 307 000 cases of death in the year 2012 [5].

In 2009, Sreekumar *et al.* linked the metabolite sarcosine for the first time with prostate cancer progression and aggressiveness [3]. Upon a general increase in amino acid metabolism and nitrogen breakdown, metastatic PCa samples had increased levels of sarcosine in 79% of the samples analyzed. Strikingly, none of the analyzed benign samples showed detectable amounts of sarcosine. Sreekumar *et al.* further demonstrated that external addition of sarcosine to cultures of malign prostate cells increased invasiveness and cell motility. Based on these findings, the possibility of monitoring PCa progression by analysis of sarcosine levels, as well as its use as a predictor for aggressiveness was suggested [3]. On the other hand, some subsequent publications, especially by Jentzmik *et al.*, denied any diagnostic significance of sarcosine in prostate cancer and the identification of aggressive tumors [6,7]. In 2010, they claimed that the results obtained by Sreekumar *et al.* were likely biased by choosing poor-defined patient cohorts for their metabolomic profiling studies. However, at the moment, the overall consensus of the research community is that sarcosine alone cannot be used as a new universal biomarker for prostate cancer, but that the enzymes involved in its metabolism definitely can play a role in prostate cancer development, progression, motility and aggressiveness [7–11].

In follow up studies, the group around Sreekumar *et al.* also investigated functional mechanisms behind the stimulatory role of sarcosine on prostate cancer. The investigation of the transcriptional regulation of sarcosine related enzymes was done on the basis of androgen receptor (AR) signaling and the ETS transcription factors ERG and ETV1. Dysregulated androgen signaling and gene fusions of the ETS family are known driving forces for prostate cancer development [12]. Sreekumar *et al.* came to the conclusion that hGNMT and hSARDH are regulated on the transcriptional level upon binding of AR and ERG transcription factors to the promoter regions of hGNMT and hSARDH respectively [3]. A similar study concerning AR and ETS gene fusion transcriptional regulation of hDMGDH was not described or published.

Investigations on Enzymes Related to Sarcosine Metabolism

As shown in Figure 1, sarcosine amounts in humans are mainly regulated by three enzymes, glycine N-methyltransferase, sarcosine dehydrogenase and dimethylglycine dehydrogenase. Furthermore, Dodt *et al.* reported in 2000 sarcosine metabolizing activity for the enzyme L-pipecolic acid oxidase (hPIPOX), which is similar to mammalian sarcosine dehydrogenases and bacterial sarcosine oxidases [13].

In 2003, Khan *et al.* investigated the role of sarcosine metabolism in prostate cancer progression in more detail. The consequences of the silencing and overexpression of hSARDH, hGNMT and hPIPOX in PCa cells (mainly DU145) and benign prostate cells (RWPE) were investigated *in vitro* and *in vivo* using chicken chorioallantoic membrane (CAM) assays and mouse xenograft models. Consistent with earlier findings, an elevated expression of hGNMT and knockdown of hSARDH and hPIPOX respectively

enhanced the sarcosine pool in PCa cells and as a consequence prostate cancer cell invasiveness and motility. Knockdown of hGNMT promoted expression of hSARDH and hPIPOX and inhibited tumor growth. Furthermore, hGNMT was found to be overexpressed in cancer tissue, whereas hSARDH and hPIPOX were downregulated as confirmed by qRT-PCR. This study strengthened the evidence that sarcosine is an onco-metabolite in PCa [8]. Furthermore, knockdown of hGNMT resulted in 70% reduction of hGNMT expression and subsequently in reduction of cell proliferation, a greater percentage of cell death and hampered invasion and anchorage-dependent growth due to phenotypes with lower levels of sarcosine. External addition of sarcosine to the cells could only partly reverse these effects, mainly because of the present activities of hSARDH and hPIPOX, which readily convert sarcosine to glycine.

Similar knock-down and overexpression experiments were also done with hSARDH and hPIPOX. The results were as expected: overexpression of hSARDH reduced sarcosine levels, invasion potential and proliferation, whereas knock-down increased invasion and anchorage independent growth of the cells [8]. These effects also occurred with overexpression and silencing of hPIPOX, but in a less pronounced manner.

In order to prove these *in vitro* findings *in vivo*, CAM assays and mouse xenograft models were used. Analogous to the *in vitro* results, DU145 and PC3 PCa cells with hGNMT knock-down as well as hSARDH overexpression resulted in decreased ability of the cells to metastasize compared to wild-type cells. In the mouse model, implanted DU145 cells with hGNMT knock-down or hSARDH overexpression formed significantly smaller tumors (75% reduction). The publication by Khan *et al.* intensively focused on the enzymes hGNMT, hSARDH and hPIPOX but interestingly completely left out the fourth key enzyme involved in sarcosine homeostasis, hDMGDH.

Involvement of hDMGDH in Other Diseases

Apart from prostate cancer, sarcosine and dimethylglycine have also been mentioned in connection with breast cancer and hepatocellular carcinoma (HCC), respectively. Yoon *et al.* described that HER2/TNBC type tumors of breast cancer show several similarities to prostate cancer behavior, which also might be caused by an altered sarcosine metabolism in these cells [14]. hDMGDH was investigated as diagnostic and prognostic marker in HCC and was shown to suppress cancer metastasis *in vitro* [15]. However, it has to be mentioned that the methodological and experimental quality of the article published by Liu *et al.* in *Oncotarget* 2016 is poor. Therefore, we doubt whether all reported results are valid. A further hint about a role of hDMGDH in liver cancer is found in a patent of 2003 as a possible liver cancer marker protein, but no further information has been published as yet [16].

Lastly, an epidemiological study by Magnusson *et al.* in 2015 suggested a protective role of dimethylglycine on human glucose metabolism and therefore connects the activity of hDMGDH with

diabetes mellitus type II [17]. In fact, it was shown that SNPs located in the promotor region of hDMGDH causes a higher protein expression and activity, leading to lower DMG levels in the cells and subsequently to increased insulin resistance. Therefore, the supplementary intake of DMG or the inhibition of hDMGDH in order to prevent diabetes type II was discussed. However, so far, no biochemical proves for these hypotheses have been published.

Aim of the Project

The main goals of the project were to evaluate the significance of hDMGDH activity and expression levels regarding sarcosine metabolism in prostate cancer cell lines. In addition, possible regulatory mechanisms and a better understanding of the overall physiological importance of hDMGDH were sought. Current publications dealing with sarcosine metabolism in prostate cancer [3,8] only characterized the influence of hSARDH, hGNMT and hPIPOX on intracellular sarcosine levels and completely omitted this forth important enzyme leading to sarcosine *in vivo*.

RESULTS AND DISCUSSION

In our first experiments, we determined the expression level of hDMGDH in comparison to hSARDH and hGNMT in the three prostate cancer cell lines DU145, PC3 and LNCaP by quantitative real-time PCR (qRT-PCR) and indirect immunofluorescence. The cell line DU145 was also mainly used by Sreekumar *et al.* and Khan *et al.* in their studies [3,8] and is together with PC3 and LNCaP the most widely used PCa cell line in research [18]. Immunofluorescence analysis only was done for hDMGDH and hGNMT using mouse anti-hDMGDH or anti-GNMT antibodies provided by Santa Cruz Biotechnology. The immobilized cells showed bright fluorescent signals with both antibodies compared to the negative controls (secondary antibody only), indicating expression of both enzymes. With qRT-PCR we only found a very low expression level of all three proteins with dC_q values around 20 related to the expression of 18S rRNA. Cultivation of androgen receptor expressing LNCaP cells in the presence of testosterone or dihydrotestosterone significantly increased the expression of hGNMT and that of hSARDH slightly, whereas hDMGDH expression was not influenced as determined with qRT-PCR. This confirmed previous reports that hGNMT and hSARDH expression is influenced by androgens [3,19].

After confirmation of hDMGDH expression in the investigated PCa cell lines, we established stable DU145 hDMGDH knock-out cell clones by silencing the enzyme expression by means of small hairpin (sh) RNA using a lentiviral vector system. Stable clones were identified by limiting dilution and resistance towards puromycin. As negative control we transfected cells with scrambled, random shRNA which is not targeted towards any RNA sequence in the cells. In individual hDMGDHsh clones an approximate 10-fold decrease of hDMGDH expression at mRNA level was observed in comparison to the wild type. Also the immunofluorescence screening of selected knock-down clones showed a significantly decreased fluorescence signal compared to the respective wild-type. Furthermore, the clones also exhibited a 10-fold decreased hGNMT and a 3-fold decreased hSARDH mRNA expression. Nevertheless, the determined intracellular sarcosine levels measured with HPLC were not influenced by hDMGDH silencing and showed no correlation with the protein expression pattern. In general, we found approximately $\sim 200\text{-}300$ pmol sarcosine/ 10^6 DU145 cells, in wild-type and hDMGDH silenced clones, which was 2-fold more than previously reported using isotope dilution GC-MS with selected ion monitoring [3,8]. Furthermore, the knock-down clones did not show altered behavior regarding proliferation and migration compared to the wild-type cell line as investigated with WST-1[®] and wound healing assays, respectively.

Taken together, we could not show in any of the experiments performed that the knock-down of hDMGDH in prostate cancer cell lines had an effect on the intracellular sarcosine concentration respectively growth and migration behavior. Unfortunately, we also failed to confirm the protein expression of hDMGDH or the knock-down of hDMGDH with Western blotting. In detail, all signals obtained in PCa cell lysates by Western blotting with our used anti-hDMGDH antibody were of wrong

size (approximately 40 kDa). Natural full length hDMGDH which was used as positive control in the Western blotting assay showed signals at approximately 100 kDa which corresponds to the molecular weight of hDMGDH. Although the obviously wrong 40 kDa signals appeared in wild-type PCa cell lysates and disappeared in the DMGDHsh clones, the results are inconclusive because the negative control with scrambled shRNA also lost this signal. We believe that these signals were caused by an unspecific cross reaction of our used DMGDH antibody which was further influenced by the lentiviral transfection. Furthermore, the signals obtained by Western blotting also questioned our results obtained by immunofluorescence stated above, which also could be the result of unspecific antibody binding.

CONCLUSION AND OUTLOOK

In our study we did not find a significant role of hDMGDH in the sarcosine metabolism of prostate cancer cell lines. Sarcosine levels as well as proliferation and cell migration were not changed in hDMGDHsh clones compared to the wild-type cells. Furthermore, in contrast to hGNMT and to a lower level also hSARDH, we could not find that hDMGDH expression was androgen regulated. The most interesting result we got was that the knock-down of hDMGDH simultaneously negatively affected the expression of hSARDH and hGNMT. This could be interpreted that in the case of downregulated hDMGDH expression, less sarcosine is produced in the cells and therefore less hSARDH has to be expressed to maintain a stable sarcosine level. However, in contrary to this hypothesis, hGNMT was not upregulated in order to maintain the homeostasis of sarcosine in the cells. A possible explanation could be that hGNMT has a much greater activity *in vivo* compared to hSARDH that already small amounts of the protein are able to maintain the needed sarcosine levels. In fact, *in vitro* studies of both enzymes isolated from the liver of *Rattus norvegicus*, which are highly (>95%) identical with the human enzyme, showed a 10 times higher turnover number for GNMT compared to SARDH of 0.7 s^{-1} and 0.065 s^{-1} respectively [20,21].

At the moment, no further experiments are planned concerning the role of hDMGDH in PCa cell lines, because we think that based on our obtained results hDMGDH only plays an insignificant role in sarcosine metabolism, growth and migration behavior in these cell lines. In retrospective, we think that using the CRISPR/Cas9 technique to silence hDMGDH expression would have been a better way to completely reduce hDMGDH protein expression and to get rid of a residual protein expression [22]. Furthermore, the investigation of solid tumors *in vivo* would be a good addition and would perhaps bring different results. Our inability to show and determine hDMGDH expression on protein level at the right size by Western blotting could either be the result of an unspecific antibody or may be a hint that hDMGDH is not stable and gets degraded during the preparation of cell lysates. Therefore, testing alternative antibodies or the method to prepare the cell lysates might have improved our results. Last but not least, a detailed investigation of other human cells apart from PCa, for instance hepatocellular carcinoma cells or benign liver cells, would have been a good addition to our experiments. Results of immunohistochemistry experiments presented in the Human Protein Atlas show that hDMGDH is only very low expressed in prostate cancer tissue but to a much greater extent in malignant liver tissue [23].

REFERENCES

- 1 Binzak B a, Wevers R a, Moolenaar SH, Lee YM, Hwu WL, Poggi-Bach J, Engelke UF, Hoard HM, Vockley JG & Vockley J (2001) Cloning of dimethylglycine dehydrogenase and a new human inborn error of metabolism, dimethylglycine dehydrogenase deficiency. *Am. J. Hum. Genet.* **68**, 839–47.
- 2 Moolenaar SH, Poggi-Bach J, Engelke UFH, Corstiaensen JMB, Heerschap A, De Jong JGN, Binzak BA, Vockley J & Wevers RA (1999) Defect in dimethylglycine dehydrogenase, a new inborn error of metabolism: NMR spectroscopy study. *Clin. Chem.* **45**, 459–464.
- 3 Sreekumar A, Poisson LM, Rajendiran TM, Khan AP, Cao Q, Yu J, Laxman B, Mehra R, Lonigro RJ, Li Y, Nyati MK, Ahsan A, Kalyana-Sundaram S, Han B, Cao X, Byun J, Omenn GS, Ghosh D, Pennathur S, Alexander DC, Berger A, Shuster JR, Wei JT, Varambally S, Beecher C & Chinnaiyan AM (2009) Metabolomic profiles delineate potential role for sarcosine in prostate cancer progression. *Nature* **457**, 910–4.
- 4 Statistik Austria (2011)
http://www.statistik.at/web_de/statistiken/gesundheit/krebskrankungen/prostata/index.html.
- 5 International Agency for Research on Cancer: GLOBOCAN (2012)
http://globocan.iarc.fr/Pages/fact_sheets_cancer.aspx.
- 6 Jentzmik F, Stephan C, Miller K, Schrader M, Erbersdobler A, Kristiansen G, Lein M & Jung K (2010) Sarcosine in urine after digital rectal examination fails as a marker in prostate cancer detection and identification of aggressive tumours. *Eur. Urol.* **58**, 12-8–1.
- 7 Pavlou M & Diamandis EP (2009) The search for new prostate cancer biomarkers continues. *Clin. Chem.* **55**, 1277–9.
- 8 Khan AP, Rajendiran TM, Ateeq B, Asangani IA, Athanikar JN, Yocum AK, Mehra R, Siddiqui J, Palapattu G, Wei JT, Michailidis G, Sreekumar A & Chinnaiyan AM (2013) The role of sarcosine metabolism in prostate cancer progression. *Neoplasia* **15**, 491–501.
- 9 Song YH, Shiota M, Kuroiwa K, Naito S & Oda Y (2011) The important role of glycine N-methyltransferase in the carcinogenesis and progression of prostate cancer. *Mod. Pathol.* **24**, 1272–80.
- 10 Chen X, Overcash R, Green T, Hoffman D, Asch AS & Ruiz-Echevarría MJ (2011) The tumor suppressor activity of the transmembrane protein with epidermal growth factor and two follistatin motifs 2 (TMEFF2) correlates with its ability to modulate sarcosine levels. *J. Biol. Chem.* **286**, 16091–100.
- 11 Green T, Chen X, Ryan S, Asch AS & Ruiz-Echevarría MJ (2013) TMEFF2 and SARDH cooperate to modulate one-carbon metabolism and invasion of prostate cancer cells. *Prostate* **73**, 1561–75.

- 12 Tomlins S a, Rhodes DR, Perner S, Dhanasekaran SM, Mehra R, Sun X-W, Varambally S, Cao X, Tchinda J, Kuefer R, Lee C, Montie JE, Shah RB, Pienta KJ, Rubin M a & Chinnaiyan AM (2005) Recurrent fusion of TMPRSS2 and ETS transcription factor genes in prostate cancer. *Science* **310**, 644–8.
- 13 Dodt G, Kim D, Reimann S, McCabe K, Gould SJ & Mihalik SJ (2000) The human L-pipecolic acid oxidase is similar to bacterial monomeric sarcosine oxidases rather than D-amino acid oxidases. *Cell Biochem. Biophys.* **32 Spring**, 313–6.
- 14 Yoon JK, Kim DH & Koo JS (2014) Implications of differences in expression of sarcosine metabolism-related proteins according to the molecular subtype of breast cancer. *J. Transl. Med.* **12**, 149.
- 15 Liu G, Hou G, Li L, Li Y, Zhou W & Liu L (2016) Potential diagnostic and prognostic marker dimethylglycine dehydrogenase (DMGDH) suppresses hepatocellular carcinoma metastasis in vitro and in vivo. *Oncotarget*.
- 16 Borlak J (2013) Novel Biomarkers of Liver Cancer - US Patent 2013/0183737 A1. .
- 17 Magnusson M, Wang TJ, Clish C, Engström G, Nilsson P, Gerszten RE & Melander O (2015) Dimethylglycine Deficiency and the Development of Diabetes. *Diabetes* **64**, 3010–6.
- 18 Sobel R & Sadar M (2005) Cell Lines Used in Prostate Cancer Research: A Compendium of Old and New Lines - Part 2. *J. Urol.* **173**, 360–372.
- 19 Ottaviani S, Brooke GN, O’Hanlon-Brown C, Waxman J, Ali S & Buluwela L (2013) Characterisation of the androgen regulation of glycine N-methyltransferase in prostate cancer cells. *J. Mol. Endocrinol.* **51**, 301–12.
- 20 Porter DH, Cook RJ & Wagner C (1985) Enzymatic properties of dimethylglycine dehydrogenase and sarcosine dehydrogenase from rat liver. *Arch. Biochem. Biophys.* **243**, 396–407.
- 21 Luka Z, Mudd SH & Wagner C (2009) Glycine N-methyltransferase and regulation of S-adenosylmethionine levels. *J. Biol. Chem.* **284**, 22507–11.
- 22 Cong L, Ran FA, Cox D, Lin S, Barretto R, Hsu PD, Wu X, Jiang W & Marraffini LA (2013) Multiplex Genome Engineering Using CRISPR/VCas Systems. *Science (80-.)*. **339**, 819–823.
- 23 Uhlen M, Fagerberg L, Hallstrom BM, Lindskog C, Oksvold P, Mardinoglu A, Sivertsson A, Kampf C, Sjostedt E, Asplund A, Olsson I, Edlund K, Lundberg E, Navani S, Szigartyo CA-K, Odeberg J, Djureinovic D, Takanen JO, Hober S, Alm T, Edqvist P-H, Berling H, Tegel H, Mulder J, Rockberg J, Nilsson P, Schwenk JM, Hamsten M, von Feilitzen K, Forsberg M, Persson L, Johansson F, Zwahlen M, von Heijne G, Nielsen J & Ponten F (2015) Tissue-based map of the human proteome. *Science (80-.)*. **347**, 1260419–1260419.

CURRICULUM VITAE

Name Dipl.-Ing. Peter Augustin
Address Josef-Hubergasse 28/2/5, 8020 Graz
Date of Birth 4th of February 1986; Tamsweg, Austria
Telephone +43 650 9704788
E-Mail p.augustin@gmx.at



Education

Oct 2012 – Mar 2017 **PhD in Enzymology and Biochemistry**
Extensive biochemical investigations on the human dimethylglycine dehydrogenase
Supervisor - Dr. Peter Macheroux, Institute of Biochemistry
Graz University of Technology

Nov 2011 – Nov 2012 **Master of Science in Molecular Biotechnology**, passed with excellence
Improving the application of recombinant membrane proteins in Komagataella pastoris
Supervisor - Dr. Harald Pichler; Institute of Molecular Biotechnology
Graz University of Technology

Nov 2008 – Nov 2012 **Masters studies in Biotechnology**
Main focus - Molecular biotechnology and biocatalysis
Graz University of Technology

Oct 2005 – Nov 2008 **Bachelor of Science, Technical Chemistry**
Main focus - Biotechnology and organic chemistry
Graz University of Technology

Sep 1996 – Jun 2004 **Matura (A-levels)**, passed with excellence
Bundesgymnasium Tamsweg

Internships and job employments

Oct 2012 – Oct 2016 Graz University of Technology, Institute of Biochemistry
University assistant, PhD position

Jan 2012 – Oct 2012 ACIB, Haus der Biokatalyse (TU Graz)
Scientific researcher

Apr 2010 – June 2010 Graz University of Technology, Haus der Biokatalyse (TU Graz)
Scientific coworker

Summer 2011 University of Novi Sad, Serbia - Department of Biology
Research Internship (Sommerprogramm Chemie, TU Graz)

Summer 2010 Syracuse University, USA - Department of Chemistry
Research Internship (REU program)

Summer 2007 & 2008 Graz University of Technology, Institute of Material Sciences
Summer jobs and project laboratory

Additional qualifications

Laboratory skills

- Advanced experience in cloning strategies and heterologous protein expression in *E. coli* and *K. pastoris*: Design and optimization of expression vectors, expression upscaling, expression in biofermenters, process optimization, protein purification techniques and Western blot analysis.
- Advanced experience in protein biochemistry: Establishment of enzymatic assays, spectroscopy, stopped flow, ITC, ThermoFluor® and enzyme kinetics (steady-state, pre-steady-state).
- Basic skills in protein crystallization, HPLC, HPLC/MS and NMR.

Soft skills

- **Languages** - German (mother tongue), English (fluent in written and spoken), French (Level B2), Spanish (Level A2), Croatian (Level A1).
- **IT-skills** - Windows system, Ubuntu system, Microsoft Office, Basics in Bioinformatics, PyMol.
- Lecturer and supervising tutor in various lab courses, supervision of bachelor and master students.
- Experienced in data presentation: Talks and poster presentations on a regular basis at conferences, team meetings with cooperation partners and similar.

Publications

Papers

Augustin P, Hromic A, Pavkov-Keller T, Gruber K, Macheroux P. (2016). **Structure and Biochemical Properties of Recombinant Human Dimethylglycine Dehydrogenase and Comparison to the Disease-Related H109R Variant.** *FEBSJ*, 283(19), 3587-3603

Ribitsch, D, Zitzenbacher, S, Augustin P *et al.* (2014). **High-quality production of human α -2, 6-sialyltransferase in *Pichia pastoris* requires control over N-terminal truncations by host-inherent protease activities.** *Microbial cell factories*, 13(1), 138.

Wriessnegger, T, Augustin, P *et al.* (2014). **Production of the sesquiterpenoid (+)-nootkatone by metabolic engineering of *Pichia pastoris*.** *Metabolic engineering*, 24, 18-29.

Lectures

Augustin P, Hromic A, Gruber K, Macheroux P. – **Biochemical investigations on the human dimethylglycine dehydrogenase** – *DocDay, TU Graz*, 2016 – Best Talk Award

Augustin P, Gerstmann E, Hromic A, Gruber K, Macheroux P. – **Extensive biochemical investigations on the human dimethylglycine dehydrogenase** – *ÖGMBT Meeting. Salzburg*, 2015.

Augustin P, Emmerstorfer A, Wriessnegger T - **Expression of membrane attached enzymes in yeast.** – *DSM Meeting. Kaiseraugst, Switzerland*, 2011